THE ROLE OF MATRIX COMPOSITION AND AGE IN SOLUTE DIFFUSION WITHIN ARTICULAR CARTILAGE

A Dissertation
Presented to
The Academic Faculty

by

Onyi Nonye Irrechukwu

In Partial Fulfillment
of the Requirements for the Degree
Doctor of Philosophy in Bioengineering

Georgia Institute of Technology
December, 2007

THE ROLE OF MATRIX COMPOSITION AND AGE IN SOLUTE DIFFUSION WITHIN ARTICULAR CARTILAGE

Approved by:

Dr. Marc E Levenston, Advisor
School of Biomechanical Engineering
Stanford University

Dr. Athanassios Sambanis
School of Chemical & Biomolecular Engineering
Georgia Institute of Technology

Dr. Andrés J. García
School of Mechanical Engineering
Georgia Institute of Technology

Dr. Johnna Temenoff
School of Biomedical Engineering
Georgia Institute of Technology

Dr. William Koros
School of Chemical & Biomolecular Engineering
Georgia Institute of Technology

Dr. Brani Vidakovic
School of Biomedical Engineering
Georgia Institute of Technology

Date Approved: November 2, 2007

To my parents and siblings,

ACKNOWLEDGEMENTS

Samuel Johnson famously wrote, “Our brightest blazes of gladness are commonly kindled by unexpected sparks”. Ending up at Georgia Tech was indeed an unexpected delight. No doubt it has been a long and arduous journey but alas, even roses have thorns.

I would like to thank my advisor, Dr. Marc Levenston, for his guidance and insightful perspectives. I would also like to express my gratitude to committee members – Dr. Andrés Garcia, Dr. William Koros, Dr. Athanassios Sambanis, Dr Johnna Temenoff and Dr Brani Vidakovic – for their guidance and support during this research undertaking. Each one of them had an open door and a welcoming smile.

A journey of a thousand miles begins with one step. I would like to thank Professor Charles Ume for helping me begin this journey.

I wish to thank all of the ex-members of the Levenston lab: Dr. Valerie Sitterle, Dr. Stacy Imler, Dr. Janna Mouw, Dr. Eric Vanderploeg, Dr. Ashley Palmer, Dr. Chris Wilson, Dr. John Connelly, Dr Wei Sun, Crystal Hsu, Sarah West, James Nishimuta (well, James is still slaving out there in sunny CA!!!), Elyse Baum, Marine Amouroux, Bao To, for their helpful tidbits along the way. They made the lab a pleasant place to work in. Their humor and wit made it easier to deal with the daily grind of graduate school.

It would be thoughtless of me if I forget to thank Johnafel Crowe who helped me with all my confocal microscopy experiments. I also wish to thank Aqua Asberry who has helped me in the last few months with histology. I have not met more dedicated people, always willing and glad to be called upon. I wish to thank Chris Ruffin, Steve

Woodard, Sally Gerrish, Vivian Johnson, and all the IBB staff. They have been great! I have loved every minute of my stay in that building – where everybody knows your name!!! I cannot forget Wing 2D, 1D, 2A and 1B. I have never met more friendly people who really cared about you. I am going to miss them all. And of course, special thanks goes to the guys and gals of the Neuro-Labs especially Edgar Brown (a modeling genius!). They always (and I mean always!) had food.

One of the very few reasons I would miss harvesting cartilage is the opportunity it afforded me to meet friends that I will forever cherish. I would like to thank my gal pals: Dr. Lori Lowder, soon-to-be Dr. Josette Broiles, Ify Ofoma, Dr. Gelsy Oviedo, Dr. Suchirita Shankar and Dr. Bina Rai. They sang with me, laughed with me, lived with me, ate with me, danced with me and yet they like me! It is still a wonder!! They made this entire experience worth my while. I also want to thank the lads that I have met who always lent a helping hand and listened to my cries of woe: William Wan, Choon Yap, Dr. Uzoma Onunkwo, Yash Kolambkar, Dave Muir, Dr. Patricio Vela, Dr. Massimiliano Pezzoli, Banji Oladeji, Sanjeev Dwivedi, Dr. Harvinder Singh Gill, Veer Mahajan and so many others who I cannot mention for the sake of brevity.

I wish to thank Dr. Federico Bonetto for his illuminating discussions and explications. He was a tremendous help. I would also like to thank my undergraduate mentor, Dr Tony Farquhar, from the bottom of my heart for his insightful analysis of issues. He has been unwavering in his support and in his faith in me and my abilities. He has been both a friend and a teacher, I could not possibly ask for more.

They say a prophet is not acclaimed in his own country. I guess they were wrong because my home is my throne. I would not be here today if it were not for the love of

my parents (Chris and Mary Irrechukwu) and my siblings, Uchey, Eby and Ogbo. They have been the oases in my wilderness, my Rock of Gibraltar. They are the smartest, kindest, funniest and most-loving people in the world! They make me smile even amidst my tears. They believed even when I lost faith. This diploma is really and truly theirs!

I also want to thank my beautiful extended family – my grandma, uncles, aunts, cousins and in-laws – from the bottom of my heart. Your prayers have been answered: one less liability, one more asset. I would like to thank my pastor and church members for their unrelenting prayers. Finally, I thank God for making all this possible. A Bible verse comes to my mind: "Those who wait upon the Lord shall renew their strength. They shall mount up with wings like eagles. They shall run and not be weary. They shall walk and not faint". Thank you Lord, for making me soar.

TABLE OF CONTENTS

		Page
ACKNOWLEDGEMENTS		iv
LIST OF TABLES		ix
LIST OF FIGURES		x
LIST OF SYMBOLS AND ABBREVIATIONS		xiv
SUMMARY		xvi
CHAPTER		
1	**INTRODUCTION**	1
	Motivation	1
	Research Objectives	4
	Significance and Contributions	10
2	**BACKGROUND AND LITERATURE REVIEW**	12
	Articular Cartilage	12
	The Role of Solute Transport in Articular Cartilage	24
3	**IMPROVED ESTIMATION OF SOLUTE DIFFUSIVITY THROUGH NUMERICAL ANALYSIS OF FRAP EXPERIMENTS**	32
	Introduction	32
	Model Development	38
	Model Validation	41
	Results	50
	Discussion	61
4	**DIFFUSIVE PROPERTIES OF IMMATURE ARTICULAR CARTILAGE: THE ROLE OF MATRIX COMPONENTS**	69
	Introduction	69

Materials and Methods 72

Results 82

Discussion 109

Limitations 121

5 **SOLUTE DIFFUSION IN CARTILAGE SUPERFICIAL ZONE: DIFFERENCES BETWEEN IMMATURE AND MATURE TISSUE** 123

Introduction 123

Materials and Methods 125

Results 128

Discussion 135

6 **CONCLUSIONS AND FUTURE WORK** 141

Conclusions 141

Modeling Challenges 146

Future Work 158

APPENDIX A: MATLAB CODE 161

APPENDIX B: HISTOGRAM OF NORMALIZED LEAST SQUARE ERRORS FOR 1-D DDSPE METHOD 191

REFERENCES 192

VITA 201

LIST OF TABLES

Page

Table 1: Zone and orientation dependence of 2D model diffusivity estimates <1$\mu m^2/s$ 151

Table 2: Mean cell number, mean cell radius and % area fraction of cells in zones. 152

Table 3: Influence of cells on the accurate estimation of matrix diffusivities using the 2D DDSPE method: effect of filtering.. 153

Table 4: Comparison of 1D and 2D DDSPE methods using simulated concentration profiles. 158

LIST OF FIGURES

Page

Figure 1: Anatomy of the Knee Joint..... 12

Figure 2: Zonal organization of articular cartilage 21

Figure 3: Schematic representation of FRAP 30

Figure 4: Comparison of initial conditions for different approaches to FRAP analysis... 35

Figure 5: Flowchart describing the DDSPE method for numerical analysis of FRAP experiments. Estimates for the solute diffusivity D and scan photobleaching rate constant k_s are produced by minimizing the objective function Φ. ..... …41

Figure 6: Comparison of the three methods for analysis of simulated FRAP experiments over a range of conditions. The estimated diffusivity is presented as a fraction of the diffusivity prescribed for each simulation. The sensitivity of the estimated diffusivities to spot radius is determined and compared to the DDSPE method for (A) Axelrod model, (B) modified Axelrod model and (C) Endress model. For all spot sizes and diffusivities, the DDSPE method exactly identified the prescribed diffusivity. 51

Figure 7: Effects of time-varying boundary concentrations on the accuracy of DDSPE diffusivity estimates for simulated FRAP experiments. (A) Concentration variation at the truncated boundary for a range of prescribed diffusivities. (B) Failing to account for the time-varying boundary concentration produces substantial errors in the estimated diffusivity. 53

Figure 8: Effects of photobleaching during image acquisition scanning on the accuracy of DDSPE, modified Axelrod, and Endress diffusivity estimates for simulated FRAP experiments. 55

Figure 9: Effect of varying the photobleached spot radius on the estimated diffusivity of 10.5kda fitc in 2% agarose determined with (A) the DDSPE method, (B) the Axelrod analytical model, (C) the modified Axelrod analytical model and (D) the Endress analytical model.
..... 58

Figure 10: Comparison of the diffusivities of dextrans in agarose gels estimated using the DDSPE method with those calculated with an empirical model from the literature. (A) Variations in DDSPE and theoretically estimated diffusivity with gel density and solute size. (B) Relationship between the DDSPE and theoretical diffusivities across experimental conditions. 60

Figure 11: Tissue harvest and Sample preparation.. 74

Figure 12: Light micrographs of H&E stained 8 week-old cartilage sample (10X) depicting the various cartilage zones: A) Superficial, B) middle and C) deep zones..... 83

Figure 13: Distribution of sGAG contents, expressed per wet mass (mg/mg) in immature bovine cartilage. Cartilage samples were from 6-8 week old calves. A) sGAG/wet mass measurements from 3 sample explants as a function of distance from the articular surface. B) sGAG/wet mass averaged over all animals. 85

Figure 14: Zonal dependence of sGAG/wet mass contents in the six immature bovines (Leg 1-VI). (i)-(v) mean sGAG/wet mass for each animal..... 86

Figure 15: Distribution of collagen contents, expressed per wet mass (mg/mg) in immature bovine cartilage. Cartilage samples were from stifle joints of 6-8 week old calves. A) collagen/wet mass measurements from 3 sample explants as a function of distance from the articular surface. B) Collagen/wet mass of the different cartilage zones averaged over all animals..... 88

Figure 16: Collagen contents of the different cartilage zones expressed per wet mass. (i)-(vi) are mean values in each animal..... 89

Figure 17: Distribution of water, expressed per wet mass (mg/mg), as in immature bovine cartilage.. A) Water fraction measurements from 3 sample explants as a function of distance from the articular surface. B) Water contents of the different cartilage zones averaged over 3 animals..... 91

Figure 18: Fractional water content of the different cartilage zones. (i)-(iii) Mean water fractions of each animal. 92

Figure 19: Confocal micrographs of fluorescently-labeled cartilage sample at different time points during a FRAP experiment (100X). 93

Figure 20: Effect of freezing on estimated diffusivities. 95

Figure 21: Diffusivity profiles of 4kDa dextran within articular cartilage**.** A) Transverse diffusivities measured in sample explants as functions of normalized depth from the articular surface. B) Radial and transverse diffusivities in the different cartilage zones (superficial (SZ), middle (MZ) and deep (DZ)) averaged over all six animals. 97

Figure 22: Diffusivity of 4kda FITC-dextran in the different cartilage zones (superficial (SZ), middle (MZ) and deep (DZ)) and in radial and transverse orientations. radial D and transverse D represent radial and transverse diffusivities respectively. (i)-(vi) Mean diffusivities normalized to transverse diffusivity in the MZ for each animal..... 98

Figure 23: The ratio of radial to transverse diffusivities (diffusional anisotropy) of each cartilage zone expressed as mean ± SD. 100

Figure 24: Diffusivity as a function of collagen per wet mass in immature cartilage. A) Radial diffusivity values are plotted against corresponding collagen per wet mass values for the same cartilage explants. B) Transverse diffusivities as a function of collagen content... 102

Figure 25: Diffusivity as a function of sGAG content in immature cartilage. A) Radial diffusivity values are plotted against corresponding sGAG per wet mass values for the same cartilage explants. B) Transverse diffusivities as a function of sGAG content... 103

Figure 26: Diffusivity as a function of the water content of immature cartilage explants. A) Variations in radial diffusivity as a function of cartilage water fraction and B) Transverse diffusivity as a function of water fraction. . 104

Figure 27: Relationship between the biochemical components. A) Correlation between fractional water content and sGAG/dry mass; B) Correlation between fractional water content and collagen/dry mass; C) Correlation between collagen/dry mass and sGAG/dry mass... 105

Figure 28: Diffusivities as a function of sGAG per dry mass (mg/mg). A) Variation in radial diffusivity as a function of sGAG per dry mass. B) Dependence of transverse diffusivity on sGAG per dry mass.. 107

Figure 29: Diffusivities as a function of collagen per dry mass (mg/mg). A) Variation in radial diffusivity as a function of collagen per dry mass. B) Dependence of transverse diffusivity on collagen per dry mass. 108

Figure 30: Light micrographs of H&E stained 2 year-old bovine cartilage sample (10X) depicting the various cartilage zones. Depicted are A) Superficial, B) middle and C) deep zones.. 128

Figure 31: Zonal variation of sGAG (expressed per wet mass) in mature (2 year-old) bovine articular cartilage... 130

Figure 32: Comparison between sGAG contents in immature (8 week-old) and mature (2year-old) bovine articular cartilage... 130

Figure 33: Zonal variation of collagen content (expressed per wet mass) in mature bovine articular cartilage... 131

Figure 34: Comparison between collagen contents in immature (8 week-old) and mature (2year-old) bovine articular cartilage... 131

Figure 35: Fractional water content of the different zones (superficial, middle and deep) in mature (2 year-old) bovine articular cartilage. 132

Figure 36: Comparison between water contents in immature (8 week-old) and mature (2year-old) bovine articular cartilage. 132

Figure 37: Diffusivity of 4kda fitc-dextran in immature and mature cartilage superficial zone: Effects of orientation and age. Diffusivity values are plotted on a log scale. radial D and transverse D represent radial and transverse diffusivities respectively. 134

Figure 38: Diffusional anisotropy in the cartilage superficial zone: Influence of age.... 134

Figure 39: 2D analytical results of the diffusivity of 4kda fitc-dextran in the different cartilage zones (superficial (SZ), middle (MZ) and deep (DZ)) and in radial and transverse orientations. radial D and transverse D are radial and transverse diffusivities respectively. 150

Figure 40: Diffusivity estimates from filtered (f) and unfiltered images from the superficial (SZ), middle (MZ) and deep (DZ) zones using both 1D and 2D DDSPE models.. 156

Figure 41: Representative experimental and simulated fractional fluorescence profiles of 10kDa dextran in 2% agarose gels.....15662

Figure 42: Representative experimental and simulated fractional fluorescence profiles of 4kDa dextran in cartilage samples……...162

Figure 43: Histogram of the normalized least square error values obtained during from the analyses of the FRAP experimental data using the 1D-DDSPE method……...195

LIST OF ABBREVIATIONS

1D	one dimensional
2D	two dimensional
3D	three dimensional
CLSM	confocal laser scanning microscope
DDSPE	Direct Diffusion Parameter Estimation
DMMB	Dimethylene methyl blue
DTI	Diffusion tensor imaging
DZ	Deep zone
ECM	Extracellular matrix
FCD	Fixed charge density
FE	Finite Element
FITC	fluorescein isothiocyanate
FRAP	Fluorescence Recovery after Photobleaching
GAG	glycosaminoglycan
H&E	Haematoxylin and Eosin
kDa	kilo Daltons
LMP	low melting point
MZ	middle zone
N.A.	numerical aperture
MRI	magnetic resonance imaging
NMR	nuclear magnetic resonance
OA	osteoarthritis
PBS	phosphate buffered saline

PG	proteoglycan
ROI	region of interest
SD	standard deviation
SEM	standard error of measurement
sGAG	sulphated glycosaminoglycan
SZ	superficial zone

SUMMARY

Solute diffusion is critical to maintenance of cellular function and matrix integrity in articular cartilage. Nutrient deficiency due to transport limitations is thought to be one of the causes of the pathological degeneration of the cartilage tissue. The matrix ultrastructure and composition of cartilage are thought to mediate its resistance to the diffusive movement of water and solutes. Thus, it follows that a careful study of diffusion within cartilage as outlined in this project will lead to a better understanding of the causes of cartilage degeneration.

To accurately estimate diffusion coefficients in articular cartilage and other hydrated medium, we developed a finite-element based method, the Direct Diffusion Simulation Parameter Estimation method (DDSPE), to be used for quantitative determination of solute diffusivities from Fluorescence Recovery After Photobleaching data. Analyses of simulated and experimental FRAP data demonstrated that this method was more accurate than existing analytical methods, including having a low sensitivity to variations in the spot radius.

Subsequently, the roles of extracellular matrix composition and tissue orientation in solute diffusion within immature bovine articular cartilage were explored. Diffusivities were measured through the articular cartilage depth and in two different orientations (radial and transverse). Diffusivities were then correlated with extracellular matrix components. Matrix water content was found to be the best predictor of solute diffusion rates in immature cartilage. Although no specific experiments were done to measure the effect of structure, our results suggested that matrix structure did indeed modulate

transport. Diffusional anisotropy, defined as the ratio of the diffusivities in both orientations, was observed to be significant in all the immature cartilage zones although it was highest in the superficial zone.

As a consequence, the differences in solute diffusion between immature and mature bovine articular cartilage were investigated. Diffusion rates and diffusional anisotropy decreased in the mature cartilage superficial zone. The decrease in diffusivities observed in mature cartilage suggests that there may be a reduction in nutrient and growth factor supply to the cells. Nevertheless, healthy adult cartilage can still maintain its normal function even with a reduction in solute diffusion rates as nutrient diffusion distances are shorter in mature cartilage. However, any disruption in the mechanical or biological environment could cause an imbalance in tissue homeostasis, which when combined with decreased diffusivities, could trigger catastrophic matrix degeneration. Thus, decreased diffusivity may be a necessary but not a sufficient prerequisite of matrix degeneration. Such a finding could provide insight into the mechanisms and causes of age-related cartilage degeneration.

CHAPTER 1

INTRODUCTION

1.1 MOTIVATION

Osteoarthritis (OA) is a debilitating joint disease and the most common cause of pain and disability among middle aged and older people(1). It is characterized by the gradual erosion and breakdown of articular cartilage, the connective tissue coating the articulating surfaces of bones in diarthrodial joints. Recent reports show that arthritis costs industrialized nations 1-2.5% of their gross national product, with osteoarthritis accounting for a major share of these costs(2). While the risk of OA is known to increase with age and excessive loading of the joint surface, the cause of this disease is not well understood (1) frustrating attempts to prevent and retard its progression.

However, reduction in nutrient transport to chondrocytes is thought to be one of the possible causes of cartilage degeneration. Thus, the motivation for the present investigation was to characterize the transport mechanisms of immature and mature cartilage and consequently, identify transport parameters that could be age-dependent as well as possible early indicators of degeneration. This may provide insight into the pathogenesis of joint degenerative diseases

Early intervention strategies have been proven to be critical to the successful management of arthritic joints. Effective diagnostic tools and strategies will ensure the early detection of disease and may result in successful treatments. The ultrastructure and

composition of the cartilage matrix is dependent on tissue maturity or age. Transport pathways within cartilage and indeed any tissue are modulated and determined by its matrix composition and structure and thus could serve as a window into the healthy and diseased cartilage matrix micro-architecture. These studies will provide baseline transport parameters characteristic of healthy articular cartilage. Subsequent changes in these local transport parameters could be indicators of matrix degeneration.

Furthermore, one of the current therapies for the treatment of OA is the surgical replacement of the diseased tissue using non-biologic materials. However, joint replacements have also been shown to fail rapidly after the first ten years of implantation(3). Hence, there is a need for the development of tissue engineered constructs for joint replacements. To design and fabricate superior constructs, it is necessary to characterize the properties of healthy native cartilage, including its transport properties and elucidate the relationship between the matrix structure and its transport parameters. These will be used as a baseline for the development of scaffolds that retain the quality and function of the native tissue.

In addition, intra-articular drug delivery is fast becoming an attractive therapeutic strategy for arthritic joints. One of the challenges of intra-articular drug delivery is the short residence times of the drugs within the joint space(4). In order to overcome this problem, the transport mechanisms of these therapeutic agents in articular cartilage including the limits of their penetration distance within the matrix need to be studied and characterized. Furthermore, based on the results of such transport studies, better drug

delivery strategies might be developed to decrease the clearance rates of these therapeutic agents from the joint cavity.

1.2 RESEARCH OBJECTIVES

The overall goal of this project is to investigate the roles of extracellular matrix (ECM) composition, tissue orientation and age on solute diffusion in bovine articular cartilage. The contributions of matrix proteoglycan, collagen and water contents to diffusion were assessed by measuring the correlation coefficient between each matrix component and the measured diffusivities. Furthermore, the variation of diffusion rates with orientation of the tissue sample was investigated by measuring the diffusivity of a fluorescent solute in the radial and transverse orientations. In addition, the solute diffusivities in the superficial zone of immature and mature cartilage were compared to probe the role of age in cartilage transport.

Age-dependent changes in matrix ultrastructure and composition has been investigated in articular cartilage. Adult cartilage is reported to have smaller sized proteoglycan (PG) aggregates, decreased PG content and a stiffer collagen network than juvenile cartilage. With smaller and fewer PG aggregates, there are likely to be fewer obstructions to the transport routes within the matrix.

At its core, this study seeks to illustrate the relationship between structure, composition and solute transport. Thus, three specific aims were pursued to achieve this objective.

1.2.1 Specific Aim 1

Develop a numerical technique to accurately estimate diffusivities from data obtained from fluorescence recovery after photobleaching (FRAP) experiments and benchmark the results obtained using this new technique against results obtained using existing analytical methods.

FRAP is one of the techniques used to quantitatively estimate the transport rates of solutes within native and engineered tissues as well as in polymer hydrogels. Some advantages of FRAP over other diffusion measurement techniques include ease of use, use of minute samples, localized diffusion measurements and fast (short duration) experiments. However, accurate determination of solute diffusivities from FRAP experiments is often hindered by limitations of existing analytical models.

In this research work, a new model was developed that incorporated more realistic experimental conditions. The DDSPE (Direct Diffusion Simulation Parameter Estimation) finite element model was developed using finite-element analysis software, COMSOL, in combination with MATLAB. Diffusivities were quantified from confocal microscope images obtained from FRAP experiments and the model was validated using both theoretical and experimental means. The theoretical robustness of the DDSPE method was determined by testing, over a range of conditions, its ability to predict a known diffusivity from simulated data. As further validation of the model, FRAP experiments were performed on agarose gels labeled with fluorescent dextrans. The effects of bleach radius, molecular weight of the solute and gel concentration on the estimated diffusivities were investigated. Results obtained from data analyses verified the dependency of diffusivity on solute size and gel density and demonstrated that the

DDSPE method was insensitive to bleach spot size. Finally, to test the DDSPE model's superiority over other methods, results obtained from simulated and experimental FRAP data using this new model was compared with results using existing analytical methods.

1.2.2 Specific Aim II

Determine the solute diffusivity profiles through immature articular cartilage and investigate the effects of tissue orientation on diffusion within immature cartilage.

The *working hypothesis* is that solute diffusivity will be negatively correlated with matrix proteoglycan concentration. In addition, solute diffusion rates will vary with the orientation of the tissue sample and this measured diffusional anisotropy will be zone-dependent.

The concentration of aggrecan (the major PG in articular cartilage) has been reported to increase from the superficial zone to the deep zone. Furthermore, the intermolecular PG spacing is thought to regulate solute transport within the cartilage matrix via steric hindrance of these solute molecules. Hence, solute mobility rates should be inversely related to PG concentration.

Collagen fiber alignment is zone-dependent: parallel to the articular surface in the superficial zone, randomly oriented in the middle zone and perpendicular to the articular surface in the deep zone. The organization of these fibers confers stronger anisotropic properties on the superficial and deep zones relative to the middle zone. Previous studies

have shown that cartilage mechanical properties (shear and tensile modulus) are depth-dependent and the alignment of the collagen fibers may modulate these properties, resulting in mechanical anisotropy across these zones(5). Hitherto, investigations on diffusional anisotropy within cartilage have been limited to anisotropic proton diffusion. To the best of our knowledge, there has been no research on anisotropic diffusion using a solute of physiologically-relevant size. Consequently, these studies were designed to determine the influence of anisotropy on diffusive resistance by comparing diffusivities measured in cartilage samples cut from two different orientations.

Radial (cut perpendicular to the articular surface) and transverse (cut parallel to the articular surface) slices were obtained from full thickness articular cartilage plugs. The transverse and radial diffusivity profiles of a 4kDa-fluorescently-tagged solute within articular cartilage were determined from the tissue samples using fluorescence recovery after photobleaching (FRAP) experiments. The concentration of the matrix components (sulfated glycosaminoglycans, collagen and water contents) were measured throughout the articular cartilage depth (i.e. surface to deep layers) using standard biochemical assays and the correlations between matrix components and diffusivity measurements were determined.

1.2.3 Specific Aim III

Evaluate the effects of tissue orientation and age on the diffusive resistance of superficial zone articular cartilage.

The *working hypothesis* is that solute diffusivity in the superficial zone of mature bovine cartilage will be higher than in the immature cartilage. In addition, we hypothesize that diffusional anisotropy within this layer will increase as the cartilage ECM matures.

As chondrocytes age, both the size and the number of proteoglycan aggregates produced by these cells lessen making it easier for solutes to diffuse through the matrix. In addition, collagen fiber organization within articular cartilage is thought to become more ordered as the animal matures. Magnetic resonance imaging studies on the effect of maturation on porcine articular cartilage collagen architecture concluded that the collagen fibers become more ordered and dense as the cartilage matures(6, 7). Thus as material anisotropy appears to increase with maturity, it is probable that diffusional anisotropy in adult cartilage may be higher than in juvenile cartilage.

Furthermore, initial ECM modifications associated with OA occur at the cartilage superficial zone(1). Furthermore, the superficial zone (SZ) is believed to play a critical role in articular cartilage function as the removal of the SZ from normal cartilage has been reported to decrease its ability to bear and distribute loads and retain matrix fluids(8). The superficial zone also serves a barrier between the synovial fluid and the underlying cartilage zones. Therefore, it could play a significant role in the transport of molecules into the cartilage matrix. Given its clinical relevance, it is necessary to

compare the transport properties of the superficial zone in immature and mature articular cartilage.

FRAP experiments were performed on tissue samples obtained from immature (8-week old) and mature (2-year old) bovine knees using the method detailed in Specific Aim II. In this case, however, samples were taken only from the superficial zone (~100μm thick). The numerical model developed in Specific Aim I was used to calculate the diffusivities from the FRAP data and correlations between the diffusivities and the experimentally measured ECM components were calculated.

Thus, this study investigated the influences of tissue orientation and matrix composition on solute diffusion within articular cartilage.

1.3 SIGNIFICANCE AND CONTRIBUTIONS

In this research work, solute diffusion coefficients in the different cartilage zones and in the radial and transverse orientations were measured via FRAP. In characterizing the diffusive properties of articular cartilage via the studies done in this research project, part of the groundwork has been laid for the design and subsequent fabrication of tissue engineered constructs for cartilage repair and replacement. The transport parameters (specifically solute diffusivities) of engineered constructs can be compared with that measured in normal articular cartilage to validate and ensure their similitude. The inter-relationship between cartilage zone, matrix composition, matrix structure and diffusivity will help identify key zonal features that need to be replicated during the fabrication of and tissue constructs.

In addition, investigations into the transport mechanisms within cartilage will lead to insight into the pathogenesis and progression of cartilage degenerative diseases and aid in early detection of disease. These studies provide a baseline for the transport parameters of normal healthy articular cartilage and any changes in these parameters would indicate matrix breakdown and initiation of disease. One school of thought asserts that degenerative diseases are initiated by a reduction in nutrient supply. Since diffusion is the primary means of nutrient transport in articular cartilage, it follows that a careful study of diffusion within cartilage as outlined in this project will lead to a better understanding of the etiology of diseases such as osteoarthritis.

As the risk of joint degenerative diseases increases with age, it is reasonable to assume that injured or diseased cartilage is likely to be mature or adult cartilage. In addition, degenerative diseases such as OA appear to initiate at the cartilage superficial

zone. Experiments measuring diffusion coefficients within the adult cartilage superficial layer will provide insight into the microstructure of the aging superficial zone. Furthermore, these solute transport studies may help estimate the residence time of macromolecules (e.g. intra-articular drugs, cytokines, proteins) within the synovial fluid (intra-articular joint space). These experiments may provide information that help in development of strategies which will ensure successful localized drug delivery to diseased or injured sites *in vivo*.

Finally, since the transport of metabolites regulates matrix biosynthesis and degradation, the study of solute diffusion is critical for understanding several physiological processes in cartilage. It is important to take solute transport into consideration when designing dose response experiments in order to distinguish between the effects due to mass transport limitations from those due solely to the concentration of the solute under investigation.

CHAPTER 2

BACKGROUND AND LITERATURE REVIEW

2.1 ARTICULAR CARTILAGE

Articular cartilage is the tissue that covers the ends of bones within diarthrodial joints. Its main functions are to lubricate the joints by providing a smooth and frictionless surface and to distribute loads to the underlying bone(9).

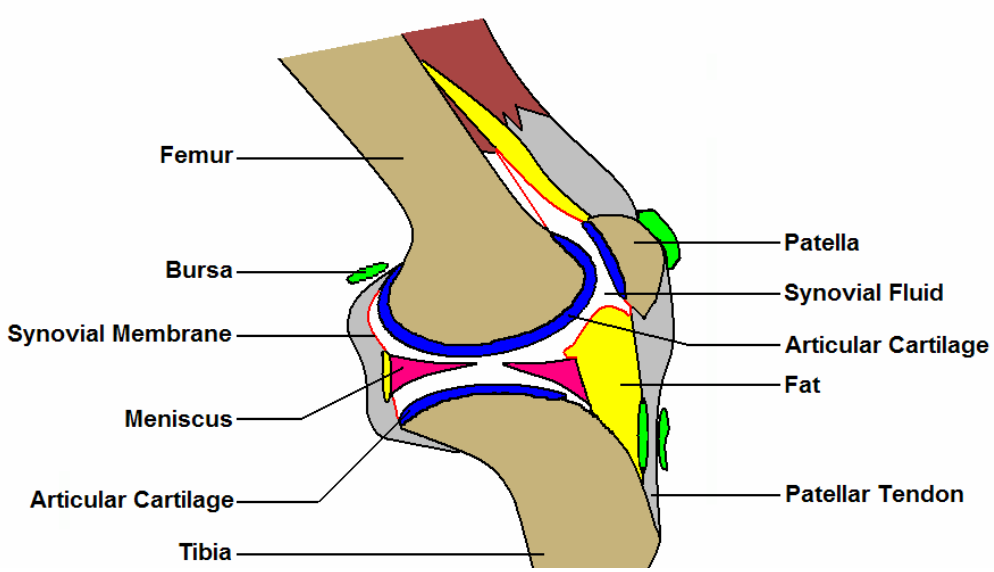

Figure 1: **Anatomy of the Knee Joint.** The articular cartilage lines the ends of the femur bone (femoral condyles) and the tibia (tibial plateau)
Adapted from http://images.main.uab.edu/healthsys/ei_0276.gif

2.1.1 Articular Cartilage Composition and Structure

The main components of articular cartilage are water (68-85% of the tissue volume), chondrocytes (~5%) (cells) and extracellular matrix (10). Adult articular cartilage has a very limited supply of blood vessels, hence, nutrients and cytokines need to diffuse through the ECM to get to the chondrocytes. As a result, the structure and composition of the ECM play a significant role in determining the transport properties of the tissue.

Chondrocytes

Articular cartilage is a unique tissue because, unlike most biological tissues, its cellular volume fraction is very low. Nevertheless, chondrocytes are pivotal to the maintenance of cartilage function as they control the synthesis and breakdown of the matrix molecules(11). Growth factors, nutrients and other signaling molecules diffuse to the chondrocytes and affect their metabolic function. Chondrocytes are known to be surrounded by a pericellular matrix (PCM) made up mainly of proteoglycans and some collagen molecules which separates the plasma membrane from the extracellular matrix(12). Although the role of the pericellular matrix is unclear, it is thought to be significant in matrix biomechanics and in the transport of molecules to and from the chondrocytes(13). Like other cell types, chondrocytes consist of cytoplasmic structures bounded by a semi-permeable plasma membrane. Within the cell cytoplasm are the cytoskeletal structures (actin, microtubules and intermediate filaments), the nucleus and other organelles which are also bounded by semi-permeable membranes. The limited

permeability of the membranes and the presence of the PCM might drastically reduce the solute flux in and out of cells. In addition, cytoskeletal and cytoplasmic structures may inhibit intracytoplasmic transport by binding to solutes or obstructing the transport pathway, further decreasing solute mobility within these cells(14).

Furthermore, the shape, size and density of the chondrocytes vary throughout the depth of the articular cartilage and aid in distinguishing the different cartilage zones from one another(10). Indeed, the deformation of these cells under mechanical loading is reported to be depth-dependent(15). Hence, it is reasonable to expect that the transport properties of the chondrocytes might vary with depth and be critical in modulating diffusion within the matrix.

Interstitial water

The interstitial fluid in cartilage consists mostly of water and electrolytes. Water makes up about 70-85% of the total tissue volume(10). Water content is known to be highest in surface layers, although it decreases with depth from the superficial to the deep cartilage layers(16). In the course of daily activity, articular cartilage (of the lower extremity) is subjected to loads far greater than the body weight. The tissue is able to sustain these loads by pressurizing its interstitial fluid. Interstitial fluid pressurization, in part, occurs as a result of the resistance imposed by the collagen fiber network on PG swelling (16). Thus, matrix water content also governs the mechanical properties of the tissue. Furthermore, interstitial water is necessary for the lubrication of the joint surfaces and the transport of nutrients to the cells.

Extracellular matrix

The cartilage extracellular matrix is composed primarily of proteoglycans enmeshed in a network of collagen fibers.

Collagen Network

Collagen fibrils form a dense network that pervades the cartilage extacellular matrix. Therefore, the matrix architecture/structure is to a large extent determined by the organization of the collagen fibrils. Articular cartilage is made up primarily of type II collagen (~90%) with the other collagens - collagen types VI, IX, X and XI – present in small amounts(17). Imaging-based techniques such as polarized light microscopy (PLM) and magnetic resonance imaging (MRI) have been used to visualize the collagen ultrastructure including fibril alignment, length and thickness; these techniques have been used to quantitatively estimate matrix anisotropy in cartilage, primarily a result of collagen fiber alignment(18).

Studies suggest that matrix microstructure influences cartilage material properties. Collagen fibril packing density (i.e. the spacing between the fibers) has been found to vary with depth in articular cartilage and to be correlated with fibril volume and fibrillar water content(19). Thus, solute mobility rates within the matrix can be affected by the tortuous transport routes prescribed by the fiber network.

Apart from its putative role in solute transport, the architecture and alignment of collagen fibers have been shown to determine both the tensile properties and anisotropy of the cartilage matrix(17, 20). Collagen molecules are cross-linked (i.e. covalently bonded) to each other to maintain the structural integrity of the fibrils. Some matrix

compounds, including proteoglycans, play a role in the cross-linking of collagen fibrils, and the degree of cross-linking of the collagen molecules is known to determine the tensile stiffness of the collagen fibers. It has also been reported that fibril stiffness may influence matrix permeability and anisotropy. As such, collagen cross-linking may modulate solute transport within the matrix.

Proteoglycans

Proteoglycans make up 5-10% of the cartilage extracellular matrix. Apart from the ECM, proteoglycans are also present on cell surfaces and have many biological functions including cell-cell signaling and collagen fibril formation. These molecules comprise of a protein backbone to which are attached unbranched polysaccharide chains known as glycosaminoglycans. Glycosaminoglycans (GAGs) are made of repeating disaccharide units which often times are sulfated. The predominant GAGs present in articular cartilage are hyaluronan, chondroitin sulfate, keratin sulfate, and dermatin sulfate(10). Glycosaminoglycans are negatively charged, hence, they confer a net negative charge on the cartilage matrix. Indeed studies have shown that the measured fixed negative charge density of cartilage is attributed to the negatively charged groups of the glycosaminoglycan(21, 22). To maintain ionic equilibrium, GAGs attract water and other electrolytes into the ECM causing the proteoglycan molecules to swell, forming a gel-like substance. The interplay between this swelling pressure, the repulsive forces between the PGs due to the negative charges and the restraining forces of the collagen network enables the cartilage matrix to resist high magnitude compressive loads(23)..

Several proteoglycans are present in articular cartilage including aggrecan, decorin, biglycan, fibromodulin, and perlecan. However, aggrecan is the most abundant PG in articular cartilage and is normally bound to hyaluronan forming large PG aggregates with molecular weights larger than 10^5 kDa(16). Indeed, studies have shown that no covalent bonds exist between the proteoglycans and collagen fibrils. Rather, the size of the PGs is key to their retention in the cartilage matrix (24). In the same vein, the spatial orientation and size of the proteoglycans are thought to regulate the mobility of solutes within the matrix.

2.1.2 Zonal and regional organization

Articular cartilage ultrastructure has been characterized using electron microscopy and histology. These studies revealed that cartilage can be subdivided into three distinct zones: the superficial, middle and deep zones. However, underneath the deep zone is a layer of calcified cartilage which separates the uncalcified cartilage from the underlying bony structure. The composition, structure and organization of the matrix components vary from zone to zone and these zonal features ensure the continued function of the cartilage tissue.

Superficial zone

The superficial zone is 10-20% of the total tissue thickness. Here, the chondrocytes are flat and aligned parallel to the articular surface. Cell density is at its highest in this zone. The collagen fibrils in this layer have the smallest diameter (~20nm) compared to the other zones and run parallel to the articular surface (10, 25). Aggrecan concentration is at its minimum in this zone while water content is highest in this zone (80% of the tissue volume) decreasing steadily through the depth to about 65% in the deep zone [9]

Middle zone

In the middle zone, which is 40-60% of the cartilage total thickness, the collagen fibrils have a larger diameter than the fibrils in the superficial zone and are randomly oriented making this zone relatively isotropic. The middle zone has spherical cells, a lower cell density than the superficial zone and a preponderance of the proteoglycan aggrecan in its extracellular matrix (10).

Deep zone

In the deep zone (about 30% of the total thickness), the fibrils are organized perpendicular to the joint surface [2]. The deep zone is situated between the middle zone and the calcified cartilage zone. In immature cartilage, the zone is highly vascularized but becomes increasingly avascular as the cartilage matrix matures. Although cell density is

at its lowest in this zone, the deep zone chondrocytes have the largest surface area compared to the other cartilage zones (25). In addition, these cells have a column-like shape and are arranged in vertical stacks Both aggrecan content and fibril diameter (70-120 nm), are at their peaks in this zone (10).

Calcified cartilage zone

The tidemark separates the deep zone from the layer of calcified cartilage, although it is sometimes regarded as being part of the calcified zone. The calcified cartilage layer has material properties that are in-between those of the uncalcified cartilage and the subchondral bone. There are large quantities of calcium salts and a network of blood vessels within this layer (26). The chondrocytes in this layer are small and exhibit the hypertrophic phenotype. These hypertrophic chondrocytes are different from the chondrocytes in the other regions as they synthesize Type X collagen and are able to calcify the extracellular matrix. This calcified zone ensures the structural and mechanical integration of the cartilage matrix with the underlying bone (10).

Both the composition and structure of the extracellular matrix result in material and mechanical properties which are indicative of, and tailored to the articular cartilage's physiological function.

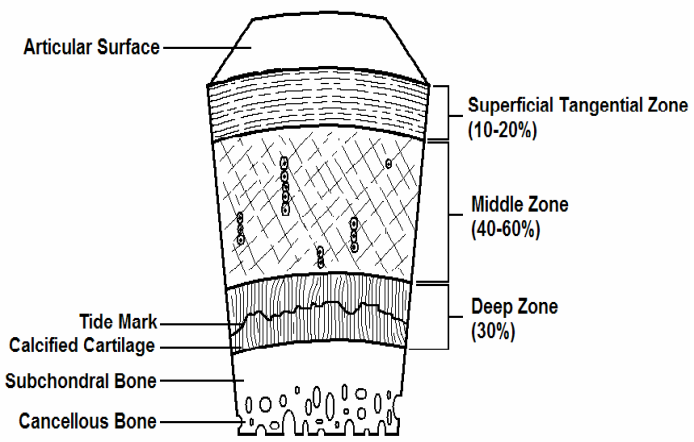

Figure 2: Zonal organization of articular cartilage. Collagen fibrils are arranged parallel to the articular surface in the superficial zone and perpendicular to the articular surface in the deep zone. The fibrils in the middle zone are randomly oriented. Calcified cartilage separates the deep zone from the subchondral bone. Adapted from http://www.geistlich.com/biomaterials/images/products/chondrogide/scheme.jpg

2.1.3 Articular Cartilage degeneration

Cartilage degeneration is the gradual loss of normal function of cartilage as a result of the breakdown in the structure and composition of the cartilage matrix. Osteoarthritis (OA) is a cartilage degenerative disease and one of the leading causes of joint pain and disability worldwide. OA symptoms include joint pain and dysfunction, abnormal muscle tightening and shortening, muscle atrophy and eventually, deformity(1). In current therapies, lesions are debrided to facilitate contact with cells and bioactive molecules of the bone marrow. However, these therapies fail to repair articular cartilage *in vivo* and may lead to further matrix degeneration (26). OA is characterized by increase in tissue water content, appearance of fissures at the cartilage surface, thickening of the subchondral bone, breakdown of the collagen fiber network, decreased proteoglycan content and osteophyte (bone spurs) formation (27),(28). These events are thought to

trigger the changes in cartilage biochemical and metabolic function seen in osteoarthritic cartilage: increased synthesis and degradation of both proteoglycan and collagen molecules as well as modifications in the structure of both compounds.

Although the structural and biochemical changes characteristic of the OA joint are known, the causes of the disease are still undetermined. However, age-dependent modifications in matrix composition and or continuous mechanical assault on the joints are thought to predispose the joints to OA(29, 30). Attrition of the cartilage matrix can be brought about prematurely by certain daily sport activities. Single or repetitive impact loads could injure the articular surface eventually resulting in joint degeneration(31). At first, fissures may develop due to the recurring stresses of regular daily activity leading to a reduced capacity of the cartilage matrix to bear load. These fissures multiply in size and number and eventually, the rate of matrix degradation exceeds the rate at which chondrocytes repair or maintain the tissue, culminating in bulk tissue failure(16).

It is known that cartilage degeneration as well as the specific incidence of osteoarthritis in joints increases with age(16) (32). Reportedly, among the general population below 20 years of age, 0.2% of males and 0.4 % of females suffer from OA; this contrasts sharply with 17% of males and 29.6% of females with the same disability among the population over 60 years of age(16). In some populations, more than 75% of the people over age 65 have OA that involves one or more joints(1); therefore understanding the normal functioning of articular cartilage with age will elucidate the pathological processes of cartilage degeneration and of OA in particular.

2.1.4 Age Related Changes in Cartilage Matrix Composition and Organization

Adult articular cartilage is avascular and as such, has limited capacity for repair and regeneration *in vivo*. Aging cartilage is more susceptible to degeneration because of the modifications in the composition and structure of its matrix. These changes include decreased cellularity, decrease in the size and aggregation of proteoglycans, and increased collagen cross-linking(33),(34, 35). These modifications are thought to be the result of age-related changes in the functions of the chondrocytes(36). Aging chondrocytes synthesize fewer and smaller aggrecan molecules, leading to the formation of smaller and more irregular proteoglycan aggregates. In addition, the collagen network has been reported to be less stable with age allowing for increased hydration and swelling of the PG molecules. This increase in matrix water content lessens the osmotic and electrostatic pressures in the cartilage matrix resulting in a decreased capacity to redistribute loads (31). It is noteworthy that there are differing reports in the literature about the effect of age on the water content of the matrix and these changes in matrix hydration appear to be species-dependent(35, 37, 38). As the proliferative and synthetic capacities of chondrocytes decrease with age, they become less sensitive to biochemical and mechanical stimuli(1, 39). Hence, the impact of autocrine signaling, which is critical to maintaining the structural integrity of the tissue, may be attenuated.

Since the intrinsic material and biomechanical properties of cartilage have been shown to be correlated to its biochemical composition, it is not surprising that cartilage degeneration is characterized by decreased tensile, compressive and shear moduli, as well as increased permeability to fluid flow (33),(34). It is important to note that it is difficult to distinguish changes that are solely pathological from those due to age. Furthermore,

the mechanisms by which age causes the degeneration of the cartilage matrix are still under debate. Nevertheless, pathological changes in the cartilage extracellular matrix, either through aging or disease, will affect not only the mechanical properties of the matrix but also solute transport(40) within the matrix. Conceivably, modifications of solute partition and diffusion coefficients as well as cartilage permeability can disrupt chondrocyte metabolism and result in loss of tissue integrity.

2.2 THE ROLE OF SOLUTE TRANSPORT IN ARTICULAR CARTILAGE

Assuming one-dimensional mass transport, the rate of solute transport within cartilage can be represented by the mass transfer equation:

$$\frac{\partial C}{\partial t} = -D\frac{\partial^2 C}{\partial x^2} + V\frac{\partial C}{\partial x} + R \qquad (1)$$

where D is the diffusivity, C is the local concentration of the solute at any point in the matrix, V is the fluid velocity and R is the rate of consumption or production of a given solute. This equation assumes that the solute is neutral so there is no electrical migration term. On the right side of the equation, the first term is the diffusive flux while the second term is the convective flux. If the solute is not being produced by the cells, R could represent cellular uptake/consumption, the solute binding to the matrix or any other event or process that removes the solute from the available pool of diffusants. In general, interstitial fluid velocity ranges from 0.2-2$\mu m^2/s$.

As cartilage is avascular, nutrient transport from the joint cavity and subchondral bone is primarily through diffusion although convection also plays a role in augmenting the transport of these nutrients(41). Fluid flow or convection is usually compression-

induced, occurring during day-to-day loading of the joints. For most small solutes such as glucose (180Da), diffusive flux is so much higher than convective flux that fluid convection typically has a negligible effect on overall solute transport. The contribution of convection to total flux increases as the molecular weight of the solute increases(42). The diffusivities of large molecules such as serum albumin (67kDa) are so small that fluid convection is necessary to enhance transport. Also at high solute concentrations, the relative contribution of convection also increases. In the experiments conducted during this research work, very dilute concentrations of the solutes were used (less than 0.0001mM) so the convective flux was assumed to be negligible.

Regardless of the mode of solute transport, growth factors and cytokines need to be transported to the cells and metabolic waste products need to be transported out of the matrix to sustain the chondrocytes' metabolic activities including its role in the maintenance of tissue integrity(43). However, the spatial variation in the composition, structure and spatial orientation of the ECM components of articular cartilage confers heterogeneous and anisotropic properties on the tissue and is thought to ultimately shape the transport pathways within the matrix(40). Therefore, modifications in matrix composition and structure may result in changes in diffusion and transport parameters, and these in turn, may influence chondrocyte metabolism by altering the transport rates of nutrients and signaling molecules to the cells(44). Consequently, measuring differences in the transport parameters between normal and structurally modified cartilage may aid the future development of new diagnostic and treatment protocols and in elucidating the pathology of OA.

Furthermore, cartilage, as a result of its location deep within the joint is not readily accessible to systemic treatment making it a prime candidate for localized drug delivery(45). Localized drug delivery while ensuring that the sites of disease and injury are exposed to the appropriate concentrations of the given drug, obviates the need for systemic treatment, which may negatively affect other organ systems. Indeed, there is a push in medical research for localized drug delivery to injured or diseased by regulating cell inflammatory processes, and restoring the balance between cartilage synthetic and degradative activities. However, strategies need to be developed to ensure the safe and regulated delivery of these therapeutic agents to the joint space as well as the matrix(26). One of the challenges of intra-articular drug delivery is the short residence times of the drugs within the joint space(4). However, in order to overcome this problem, the transport mechanisms of these therapeutic agents in articular cartilage including the limits of their penetration distance within the matrix need to be studied and characterized.

2.2.1 Solute Transport Experiments

In articular cartilage, solutes such as nutrients, growth factors, metalloproteinases and proteinase inhibitors must diffuse through the cartilage matrix to influence the chondrocyte function and metabolism. Experiments have shown that solute transport (both diffusive and convective) in cartilage is dependent on solute size, solute charge and matrix composition. Furthermore, solute transport has also been shown to be influenced by mechanical loading (static or dynamic) as well as the application of an electric field. Diffusivities were shown to decrease with increasing molecular weight (21, 46); diffusivities of larger molecules have been reported to have an inverse relationship with

PG content while those of small molecules were unaffected (40, 46). Electric fields, imposed on the matrix, enhanced the diffusion of charged molecules (47) by causing fluid flow within the matrix. Furthermore, static (48)and high amplitude dynamic compression were found to inhibit solute transport while low amplitude dynamic compression enhanced solute transport (49).

Several researchers have simulated matrix degradation in order to study its effects on solute diffusion. The diffusivities of gadolinium (Gd)-labeled proteins in healthy and degraded calf cartilage were compared using one-dimensional (1-D) NMR(46). Cartilage degradation in these samples was simulated by incubating the cartilage samples in trypsin, resulting in PG loss. In similar experiments, the effect of proteoglycan removal on solute mobility in articular cartilage was explored using radioactively labeled solutes(50). Significant increases in solute diffusivities were observed throughout the cartilage matrix after PG loss. However, though these studies looked at PG content/loss, the overarching aim was to simulate degradation hence no care was taken to determine the contribution of each matrix component to solute diffusivity. Also it has been suggested that the PG molecules protect the collagen fibers from disruption; therefore, matrix degradation could have altered both ECM composition and native structure. Consequently, to fully elucidate the transport mechanism of solutes in cartilage, it is necessary to distinguish the contribution of each matrix component (PG and collagen) to diffusion through the cartilage ECM without modifying the existing matrix architecture. Attempts have been made to study the zonal dependence of solute diffusivities(21, 44) within articular cartilage. Although the measured diffusivities were correlated with fixed

charge density, the relationships between these diffusivities and the collagen and water contents as well as collagen fiber orientation were not studied.

Prior to the studies in this thesis work, the diffusion coefficients determined from transport experiments have been mostly radial diffusivities (the direction of diffusion is normal to the articular surface) and very little has been done to investigate diffusional anisotropy in cartilage. Given the dearth of information on cartilage transport in the existing literature, it is necessary to extensively characterize the depth-dependent, direction-dependent and composition dependent diffusion properties of cartilage.

2.2.2 Techniques for Measuring Solute Transport in Tissue

As noted above, several techniques have been employed to measure diffusivities in cartilage. These include magnetic resonance imaging (MRI) (51, 52), nuclear magnetic resonance(46), radiolabeled solute absorption(40, 50, 53), tracking of fluorescent solutes using a diffusion cell(21, 47), fluorescence desorption(48) and fluorescence recovery after photobleaching (FRAP)(44). To the best of our knowledge, the FRAP and MRI methods have higher spatial resolutions than the other measurement techniques. As such, these methods enable the measurement of diffusivities at microscopic length scales and can produce diffusivity maps of the tissue of interest. However, for most academic research labs, the cost of maintaining MRI equipment is prohibitive. Furthermore, as MRI diffusion experiments can take up to 12hrs, there is an increased risk of tissue degradation during measurements.

Thus, FRAP was the technique of choice in this research study because of its advantages over the aforementioned methods as is described in the next paragraph.

FRAP: Theory and Background

In the seventies, Fluorescence Recovery After Photobleaching (FRAP) was developed to observe and quantitatively assess different processes in cells and membranes including solute mobility. In addition, this technique has been used to study the mobility of molecules in natural and engineered tissues as well as polymer hydrogels. As mentioned in the first chapter, FRAP has several advantages over other techniques including localized diffusion measurements and much shorter experimental times. Furthermore, in direct permeation experiments, unlike in FRAP, samples swell when placed next to osmotically active solutions, modifying the matrix structure and distorting measurements(54).

In a FRAP experiment, a brief but intense laser beam is used to irreversibly photobleach a specified region in a fluorescently-labeled sample. An attenuated laser beam (about 2% of the bleaching beam) monitors the recovery of fluorescence in the bleached region due to the diffusive exchange of bleached and fluorescent molecules between the bleached region and the surrounding, unbleached region.

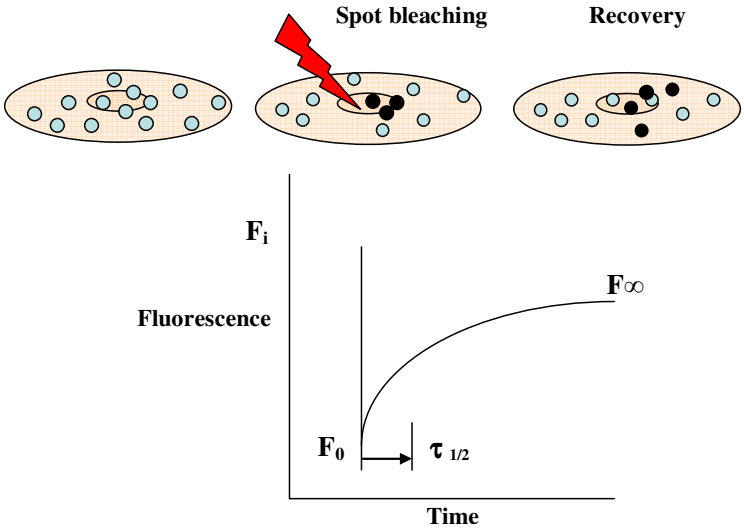

Figure 3: Schematic representation of FRAP. Fi is initial fluorescence intensity (before bleaching), Fo is the fluorescence intensity just after bleaching and F∞ is fluorescence after a long recovery time. $\tau_{1/2}$ is the half time of fluorescence recovery. Adapted from http://www.cellmigration.org/resource/imaging/imaging_approaches_photomanipulation.shtml

Figure 3 above illustrates the sequence of a FRAP experiment. The initial condition represents the unbleached sample; the molecules are still fluorescent within the region of interest (ROI). In the 'photobleach' stage, the sample is illuminated by the laser beam which bleaches the fluorescent molecules within the ROI. The bleached molecules lose their fluorescence as depicted by the black molecules now observed within the ROI. The 'recovery' stage occurs a long time after the sample has been bleached. As depicted in the diagram, the fluorescence after recovery may not equal the fluorescence at the initial condition.

Most FRAP experiments are performed using the confocal laser scanning microscope (CLSM). The configuration of this equipment has inherent limitations that inevitably impact experimentation and analytical models. In order to acquire an image, a laser beam must be scanned across the specimen of interest. With most CLSMs, scanning is usually done with a single beam within a two-dimensional plane. Thus it is impossible

to scan the entire specimen all at once; and scanning time and as a result, bleaching time is finite not instantaneous. It is worthy of note that several improvements have been made on confocal instruments to increase the speed of image acquisition. However with some of these microscopes the gain in temporal resolution has been offset by the loss in signal-to-noise ratio. Nevertheless, to the best of our knowledge most tissue-level FRAP experiments are still performed on the CLSM.

Typically, for FRAP data interpretation, an analytical model is used to determine the diffusivity from the integrated fluorescence recovery (represented by a time-series of images) within the bleached region. Many current models assume that bleaching occurs instantaneously (*i.e.,* no diffusion occurs during bleaching). Therefore, these models assume a uniform concentration profile within the bleached spot. However unless the solute under investigation diffuses extremely slowly, it is highly probable that there would be diffusion during the bleaching period ruling out a uniform post-bleach concentration profile. Furthermore, a uniform concentration profile presumes that the sample is homogeneous, limiting the applicability of the models. A few models have taken into consideration the spatial variation of the initial post-bleach concentration profile but these models were very complex and often involved laborious calculations restricting the usefulness of these models(55). Recently Weiss (56) suggested that FRAP data analysis should be done in conjunction with numerical simulations to considerably improve the accuracy of the parameters estimated. Consequently, there was a need to develop a technique to be used for accurate quantitative interpretation of FRAP data. The model developed in this research work would be used as a tool to analyze the solute transport data in cartilage obtained via FRAP.

CHAPTER 3

IMPROVED ESTIMATION OF SOLUTE DIFFUSIVITY THROUGH NUMERICAL ANALYSIS OF FRAP EXPERIMENTS

3.1 INTRODUCTION

Diffusion of nutrients and solutes is important for the viability and function of biological tissues and is the primary means of solute transport in avascular tissues such as articular cartilage. Furthermore, solute transport is critical in the development of engineered tissue constructs for successful tissue repair and replacement. The expansion in the manufacture of drug carriers and therapeutics has drawn attention to the need to elucidate the transport routes and mechanisms of these substances within biological tissues and polymers(57).

Several techniques including Fluorescence Recovery After Photobleaching (FRAP) have been used to measure the diffusion coefficients of solutes in tissue and within articular cartilage in particular. FRAP offers many advantages over other techniques including ease of use, localized diffusion measurements and fast (short duration) experiments. Furthermore, FRAP obviates the need for samples to be exposed to osmotic solutions for long periods of time, thus reducing such complications as swelling during measurements.

In a FRAP experiment, a target area containing fluorescent molecules is illuminated with an intense laser beam, irreversibly bleaching the fluorophores. An attenuated light beam is used to monitor the recovery of fluorescence in the bleached region due to the diffusive exchange of bleached and fluorescent molecules between the

bleached region and the surrounding unbleached region. However, accurate determination of solute diffusivities from FRAP experiments is often hindered by limitations of existing analytical models.

Thus, this chapter describes the development and validation of a finite-element-based model, the Direct Diffusion Simulation Parameter Estimation (DDSPE) method, for determining solute diffusivities from FRAP data.

3.1.1 FRAP Theory

During the FRAP experiment, a sample containing a fluorescent solute is briefly exposed to intense laser illumination to bleach an initial region of a specified geometry. For a circular bleach region and assuming local homogeneity and negligible out-of-plane concentration gradients, recovery of unbleached particle concentration as a function of radius r and time t is described by the axisymmetric diffusion-reaction equation:

$$\frac{\partial C(r,t)}{\partial t} = \frac{1}{r}\frac{\partial}{\partial r}\left(rD\frac{\partial C(r,t)}{\partial r} \right) + \mathrm{R_e} \qquad (2)$$

where C is the concentration of the labeled solute, D is the solute diffusivity and R_e is a reaction term. R_e is often viewed as negligible under assumptions that the fluorescent molecules do not bind to the matrix or receptors and that photobleaching of these molecules during recovery is negligible. Consequently, if R_e is neglected, Eq. (2) becomes the Fickian diffusion equation. In contrast, under continual photobleaching during image acquisition, this reaction term could be described as a first order reaction:

$$\mathrm{R_e} = -k_s C \qquad (3)$$

where k_s is a rate constant describing bleaching during scanning.

Analytical models

Axelrod *et al* (58) developed the method on which most FRAP data analysis is based and this model is widely used to estimate molecular mobility and binding kinetics from FRAP image data. Most of the current FRAP analysis techniques are still based on the Axelrod equations. In this model, a disk (square well) initial profile (Fig. 4) is assumed, indicative of the assumption that no diffusion occurs during instantaneous bleaching. Under this condition, the fluorescence recovery in a circular bleached area can be represented by a growth curve with the asymptote being the fluorescence intensity of the bleached spot at infinite time after bleaching, $F(\infty)$. Fluorescence recovery data may be represented by fractional fluorescence $f(t)$ defined as:

$$f(t) = \frac{F(t) - F(0)}{F(\infty) - F(0)} \qquad (4)$$

where $F(t)$ is the fluorescence intensity at time, t and $F(0)$ is the fluorescence intensity of the bleach spot just after bleaching. As this model assumes complete recovery unless there is an immobile fraction of the fluorescent particles, $F(\infty)$ is typically set equal to the fluorescence just before photobleaching, $F(i)$. This condition also satisfies the assumption of an infinite reservoir of fluorescent particles in the surrounding medium that readily replenishes the bleached region.

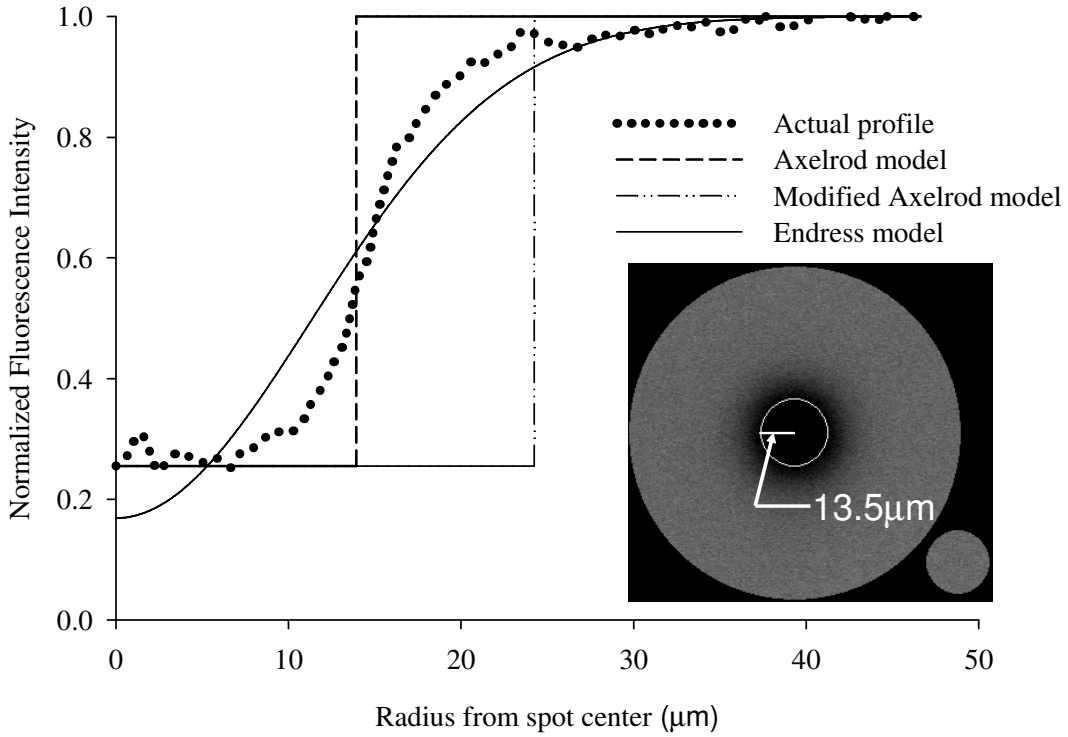

Figure 4: Comparison of initial conditions for different approaches to FRAP analysis. Diffusion during a finite photobleaching period produces a partially bleached halo (inset) surrounding the target spot. The Axelrod analytical model assumes a uniform "square well" pattern of photobleaching the size of the original bleach target, the modified Axelrod model derives an effective radius from the actual post-bleach profile and the Endress model fits a two-dimensional Gaussian curve to the initial concentration distribution. The DDSPE method directly represents the non-uniform profile measured after photobleaching.

The diffusion coefficient is calculated using:

$$D = \frac{r^2}{4\tau_D} \qquad (5)$$

where r is the radius of the bleached spot and τ_D is the characteristic diffusion time that can be calculated by minimizing the difference between the experimental recovery curve and a theoretical recovery curve described by the equation derived by Axelrod but modified by Soumpasis(59):

$$f(t) = e^{-2\tau_D/t}[I_0(\frac{2\tau_D}{t}) + I_1(\frac{2\tau_D}{t})] \qquad (6)$$

where I_0 and I_1 are modified Bessel functions.

Other analytical models (59-61) for FRAP analysis have limited applicability as they are not valid for all time domains, are based on the assumption that the initial post-bleach concentration profile is a square well or are only useful for specific bleach patterns. With finite bleaching times, however, bleached and unbleached molecules diffuse in and out of the bleached spot during bleaching, resulting in a halo of bleached molecules surrounding the target spot and deviation from a uniform square well (Fig. 4). The size of this extended region varies with the solute diffusivity, the size of the target region and the duration of bleaching (or number of bleaching iterations). Weiss (56) observed the fluorescence recovery of a pool of GFP-labeled enzyme in the endoplasmic reticulum of a cell bleached with 2, 5 and 10 scanning iterations and reported that the estimated diffusivity decreased as the number of bleaching iterations increased. To account for the effects of diffusion during photobleaching, Leddy and Guilak (44) implemented an analytical model based on an effective bleached spot radius defined as the radius at which the bleaching depth falls to e^{-2} times the maximum bleaching depth at the spot center(Fig. 4). Like the Axelrod model, this model assumes that the initial post-bleach concentration profile is a square-well (uniform concentration within the bleached spot). Recently, Endress et al. (62) reported improved diffusivity estimates with an analytical solution based on a two-dimensional Gaussian fit to the initial post-bleach concentration profile. This model accounted for the oft-neglected photobleaching during scanning term (-ksC) by adding it as a reaction term to the diffusion equation. The

diffusivity, D, was determined by iteratively adjusting its value to minimize the difference between the experimental and theoretical integrated fractional fluorescence curves described by the equation:

$$f_\sigma = \frac{e^{-bt}}{2}\left[2 + (1 - e^{-KK})\left(e^{-\frac{2\sigma^2}{\sigma^2 + 8Dt}} - 1\right)\right] \qquad (7)$$

where f_σ is the ratio of the integrated fluorescence intensity at any time, $F_\sigma(t)$, to the integrated pre-bleach intensity, $F_\sigma(t<0)$. These intensities are integrated over the area with radius, σ. The parameters for the Endress fractional fluorescence equation are defined as follows: σ, determined from the Gaussian fit of the initial concentration profile, is the radius at height e^{-2} of the gaussian curve, b is the bleaching constant obtained by analyzing the time dependence of the intensity far outside the bleached ROI and is conceptually equivalent to k_s while KK is related to the depth/extent of bleaching and is calculated using the equation:

$$KK = -\ln\left(1 - \frac{2}{1 - e^{-2}} \frac{F_\sigma(t<0) - F_\sigma(0)}{F_\sigma(t<0)}\right) \qquad (8)$$

Numerical models have been developed to surmount the difficulties posed by the aforementioned analytical methods(63, 64). Kubitscheck (64) developed 2D and 3D numerical models for analyzing data obtained from scanning microphotolysis, a combination of fluorescence microphotolysis and confocal laser scanning microscopy enabling random patterns to be bleached within the resolution of one pixel. The numerical analysis for this method is computationally intensive, its application is restricted to $D \leq 1.0\mu m^2/s$ and it entails the purchase of supplementary parts for most commercially available confocal scanning laser microscopes. Sniekers and Donkelaar (65) developed a finite element based model to analyze two-dimensional diffusivity in

inhomogeneous tissues with known (or presumed) patterns of inhomogeneity. This model accounted for diffusion during spot photobleaching by employing the measured initial post-bleach profile as an initial condition. Here we describe a similar approach that also accounts for realistic initial conditions but additionally considers effects of time-varying boundary conditions and photobleaching due to scanning for image acquisition, both of which can decrease the accuracy of the derived diffusivity. We validate the model both through theoretical analyses of simulated FRAP experiments and by measurement of the diffusivities of fluorescently-labeled dextrans in agarose gels.

3.2 MODEL DEVELOPMENT

As an alternative to analytical approximations, we developed a Direct Diffusion Simulation Parameter Estimation (DDSPE) method using COMSOL Multiphysics (version 3.2, COMSOL, Inc., Burlington, MA) finite element simulations in conjunction with MATLAB (version 6.5 Mathworks, Inc., Natick, MA) minimization functions (Fig. 5). This approach determines the value of the diffusivity producing the best fit to the entire spatially and temporally varying concentration field measured during a FRAP experiment. While the following procedure involves specific choices of numerical tools, it should be noted that the same general approach could be implemented using other approaches to the numerical solution of Equation (2) (e.g. finite differencing) and different approaches to minimize the overall difference between predicted and experimentally observed changes in fluorescence intensity values.

Each image collected during a FRAP experiment defines the concentration profile of the scan region at a specific point in time. In the axisymmetric implementation utilized here, the raw pixel values from each FRAP image were read using the '*imread*' function in MATLAB, which reads the pixel intensities from a 2-D image field and produces a 2-D matrix of intensity values. Intensity values at equal radial increments over 36 equally spaced radii emanating from the spot center were averaged for each image and assembled to produce a two-dimensional matrix, $C_{exp}(r,t)$ representing a time-varying, axisymmetric concentration field within a circular region. Rather than using an assumed bleaching pattern, the initial condition $C(r,0)$ for the simulation was defined by the first post-bleach image. Likewise, a time-varying boundary condition $C(r_o,t)$ was defined by fitting a fourth degree polynomial in time to the measured concentration at the outer boundary of the simulation region. A one-dimensional, axisymmetric finite element mesh was generated within COMSOL Multiphysics using two-node, linear elements with equally spaced nodal positions corresponding to the radial positions with known initial concentrations. The default time stepping algorithm (implicit DASPK solver with fifth order backward differentiation formula, automatic step size determination and specified output times corresponding to the experimental time increments) was used to simulate the evolution of the concentration profile, producing a two-dimensional matrix $c_{sim}(r,t)$ representing a simulated concentration field. This finite element model was converted to a MATLAB subroutine.

Within MATLAB, an objective function Φ was defined as the sum of squared differences between the experimentally measured and simulated time-varying concentration profiles:

$$\Phi = \sum_{i=1}^{N}\sum_{j=1}^{M}\left[C_{exp}\left(r_i,t_j\right) - c_{sim}\left(r_i,t_j\right)\right]^2 \qquad (9)$$

where $c_{sim}(r,t)$ was repeatedly generated by calling the finite element subroutine with defined initial and boundary conditions and a given set of fit parameters. This objective function thus produces a single number that represents the difference between the actual and predicted concentration fields for a given set of parameters. An initial single parameter fit was performed using the MATLAB bounded minimization function *fminbnd,* which finds the minimum of a function of a single variable within a fixed interval, to determine the diffusivity D that minimized the objective function with the scan photobleaching rate constant k_s set to zero. This function was found to be insensitive to the initial guess and lower and upper bounds were consistently set at 0.0001 and 1000. This estimate of D and a k_s of zero were then used as initial guesses for a second, two parameter fit using the constrained minimization function *fmincon* to identify the values of D and k_s (both constrained to be non-negative) that minimized the objective function, producing the best overall fit to the entire spatially and temporally varying concentration field.

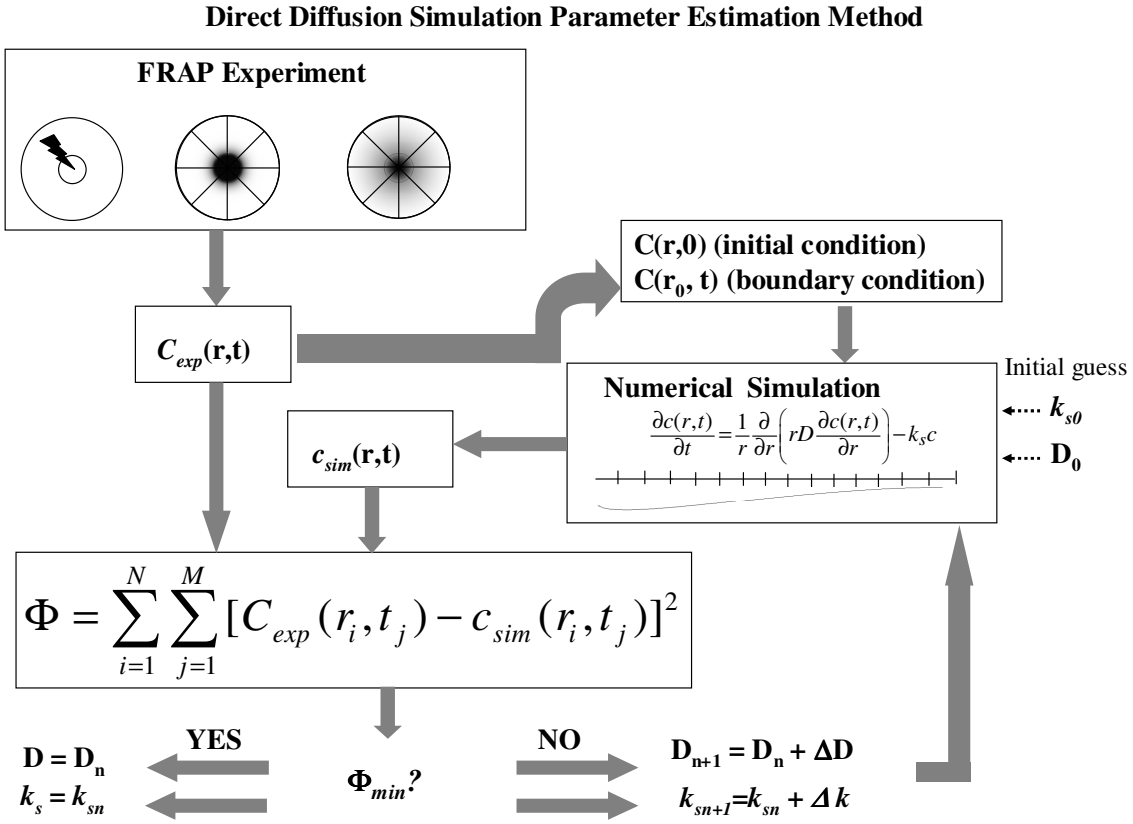

Figure 5: Flowchart describing the DDSPE method for numerical analysis of FRAP experiments. Estimates for the solute diffusivity D and scan photobleaching rate constant k_s are produced by minimizing the objective function Φ.

3.3 MODEL VALIDATION

3.3.1 Theoretical Validation of DDSPE Model

The DDSPE model was first evaluated and compared to existing analytical methods, by attempting to determine known (prescribed) diffusivities from simulated *FRAP 'pseudodata'* generated by finite element models. An axisymmetric finite element model of the diffusion reaction equation was implemented in COMSOL Multiphysics as

a MATLAB subroutine. The reaction term R_e in Eq. 2 represented the photobleaching term:

$$R_e = \begin{Bmatrix} -k_b c(r,t);\ r \le r_i \text{ and } t \le t_b \\ -k_s c(r,t);\ t > t_b \end{Bmatrix} \tag{10}$$

where $c(r,t)$ is the concentration at radius r and time, t, k_b is the bleaching rate constant during the specified bleach interval t_b and k_s is the rate constant that defines photobleaching during scanning. The radius of the outer scan region (r_o) was 76.3μm for r_i = 7 & 14μm and 114.45μm for r_i = 21μm. These bleach spot sizes were chosen to represent values typically seen in FRAP literature (In FRAP experiments, most spot radii were much less than 10μm in cells and >10 μm in tissues). The outer scan regions (76.3μm and 114.45μm) were chosen to be 5 times the bleach radius to minimize boundary effects on diffusive recovery and to be consistent with existing literature.

For this initial comparison, FRAP pseudodata were generated using a highly refined finite element mesh with 872 elements (corresponding to mesh sizes of 0.0875μm and 0.13125μm for the two outer radii). These simulations were run with $k_b = 2s^{-1}$, t_b = 0.8s and $k_s = 0$. The initial concentration was assumed to be uniform and arbitrarily set equal to 200 units, and simulated concentration profiles were reported at 0.5s intervals for 50s (for the 7 and 14μm bleach spot radii) after the initial photobleaching (100s to allow for sufficient recovery in the 21μm radius simulations and 200s for all 10 $\mu m^2/s$ simulations). Three analytical approaches and the DDSPE method were compared for simulations with specified diffusivities of 10, 50, 100, 150, or 200$\mu m^2/s$ and bleach radii (r_i) of 7, 14 or 21μm. Simulated concentration profiles were sampled at 0.7μm intervals corresponding to the nodal locations in the coarser finite element model used for analysis

with the DDSPE method. The Axelrod, modified Axelrod and Endress analytical models were used to analyze the pseudodata without down-sampling to give a best case estimate of their accuracy.

Effect of a time-varying boundary concentration

Even though the imaging area was much smaller than the tissue sample, we observed that the fluorescence intensity at the scan boundary changed with time. This variation could be due to a number of factors including diffusive exchange of bleached and unbleached particles across the outer boundary or fluorescence decay during image acquisition. To determine the effect of a time-varying boundary concentration on the accuracy of the estimated diffusivities, FRAP photobleaching and diffusive recovery was simulated using a range of diffusivities (10-500$\mu m^2/s$), a bleach radius of 14μm, an outer radius of 76.3μm, and an outer boundary concentration held at the initial value of 200 units. The pseudodata obtained from these simulations were truncated at a simulated scan radius r_o = 48.3μm, resulting in a time varying concentration at the simulated scan radius. The DDSPE method was used to estimate the diffusivity using either a constant boundary condition with the initial post-bleaching concentration or a time-varying boundary concentration at the simulated scan radius. To isolate the effect of the time-varying boundary concentration, identical 0.7μm mesh densities were used to generate and analyze the pseudodata.

Determination of the effect of acquisition photobleaching

Following spot photobleaching, image acquisition requires scanning at reduced laser intensity (typically 1-2% of the bleaching intensity). Increasing the laser intensity during scanning decreases the level of noise but can induce some photobleaching during image acquisition. Therefore, a tradeoff is required between these two issues. During initial experiments, we noted that fluorescence recovery curves reached asymptotic values and then began to decrease with time, implying that some fluorescence decay was actually occurring. To distinguish between fluorescence decay resulting from diffusion of bleached particles and from image acquisition scanning, control spots were imaged (and not bleached) at 0.75% excitation. The results showed a 12% decrease in fluorescence intensity during the first 20s. To investigate the implications of this background fluorescence decay on the accuracy of diffusivity estimates (a factor that is typically neglected), we simulated photobleaching during scanning using r_i of 7μm, r_o of 76.3μm, D =100μm^2/s and k_s values ranging from 0-0.02 (note that the rate constants do not directly correspond to the experimental laser power settings as the scan rate also has an influence). Diffusivities determined with the modified Axelrod model, the Endress model and DDSPE method with or without accounting for the effects of photobleaching were compared to the prescribed value. To isolate the effect of scan photobleaching, identical 0.7μm mesh densities were used to generate and analyze the pseudodata, and the time-varying boundary concentration was accounted for in the simulation.

3.3.2 Experimental Validation and Methods

Preparation of fluorescent solutes

As an initial experimental application, the DDSPE method was used to analyze FRAP experiments using fluorescently labeled dextrans in agarose gels. Neutral fluorescein isothiocyanate (FITC) labeled dextrans with average molecular weights of 10, 10.5, 70 and 250kda (Sigma, St. Louis, MO) were dissolved at 0.1mg/ml in phosphate-buffered saline (1X). Pilot experiments verified that this concentration fell within the linear range of the fluorescence-concentration curve for each solute.

Preparation of agarose gels

Agarose gels (2%, 4% and 6%) were prepared by autoclaving low melting point (LMP) agarose (Sigma, St. Louis, MO) in distilled water and allowing it to gel for 1 hour at room temperature between two parallel glass plates with 1mm separation. Agarose disks (6mm diameter by 1mm thick) were punched from the gel sheets using disposable biopsy punches. Each disk was immersed in a fluorescent dextran solution at 4^{o}C for at least 1 day prior to FRAP measurements.

FRAP experiments

FRAP measurements were performed on a LSM 510 laser scanning confocal microscope (Zeiss, Germany) using a Plan-Neofluor 40X /1.3 N.A oil objective with a 25mW Argon laser. Samples were sandwiched between glass coverslips and were kept

moist in the labeling solution during the FRAP experiments. Spot photobleaching was performed for 20 iterations at 488nm excitation and 75% laser power, and images were acquired at 488nm excitation and 0.75% laser power, with emission recorded above 505nm. Note that the time required to perform an individual iteration increases with the size of the target region. All images were taken at 40X magnification with a resulting pixel size of 0.45x0.45μm. For each experiment, approximately 60 images were acquired at 205ms intervals, including three pre-bleach images. The DDSPE method was implemented with 0.63μm and 0.9μm elements for experiments with 47.25μm and 63.9μm scan radii, respectively. All experimental results are presented as the mean ± standard deviation.

To evaluate the repeatability of DDSPE/FRAP diffusivity estimates, six repeat measurements (bleach spot radius of 13.5μm) were taken at the same location in a 2% agarose gel sample containing the 70kda fitc-dextran. After each repeat measurement, the spot was allowed to recover and equilibrate completely for 5 minutes without laser illumination.

To evaluate the sensitivity of diffusivity measurements to the photobleached spot size, FRAP experiments were performed to determine the diffusivity of 10.5kDa fitc-dextran in 2% agarose disks using three different spot radii (6.75, 13.5 and 20.25 μm, with outer scan radii of 47.25, 47.25 and 63.9 μm, respectively). For each of 12 different disks, measurements were taken at 3-5 random locations for 1-3 of the radii, resulting in a total of 32 measurements at independent locations for each radius. Results from each FRAP experiment were analyzed using the DDSPE method and the Axelrod and modified Axelrod analytical models. The effects of spot radius and photobleaching rate

constant on the estimated diffusivity for each method were analyzed using one-factor general linear models with significance at $p<0.05$ and Tukey's test for pairwise comparisons.

To examine the variation in solute diffusivity with solute size and agarose gel density, FRAP experiments were performed to determine the diffusivities of 10kDa, 70kDa and 250kDa fitc-dextrans in 2%, 4% and 6% agarose gels using a 13.5μm radius photobleached spot and a scan radius of 63.9μm. For each combination of dextran size and gel density, measurements were taken on 4 disks at 3-5 random locations, resulting in 12-18 independent measurements per combination. The DDSPE method was used to determine the estimated diffusivity for each FRAP experiment. Estimated diffusivities were analyzed using a three-factor (dextran, gel density, disk) general linear model with disk as a nested factor (to account for the fact that different subsets of parameters were measured for each disk) and a term to account for the interaction between dextran and gel density with significance at $p<0.05$ and Tukey's test for pairwise comparisons.

For comparison to DDSPE experimental results, theoretical diffusivity values were determined using an empirical model described by Gu *et al*. (66) for the diffusivity of solutes in agarose or soft tissues:

$$D = D_o \exp\left[-1.25\left(r_s / \kappa^{1/2}\right)^{0.68}\right] \tag{11}$$

where D_o is the diffusivity in free solution, r_s is the effective Stokes radius of the solute and κ is the Darcy permeability of the porous medium. The free solution diffusivities were calculated using the Stokes-Einstein equation:

$$D_o = kT / 6\pi\eta r_s \tag{12}$$

where k is the Boltzmann constant (1.381×10^{-23} J/K), T is the absolute temperature (298.15K) and η is the viscosity of water at room temperature (0.89×10^{-3} Pa-s). Effective Stokes radii were determined using a power law function of molecular weight M fit via nonlinear regression to compiled experimental values reported by Bert *et al.*(67) and by Armstrong *et al.* (68):

$$r_s = 0.8094 * M^{0.4798} \qquad (13)$$

yielding values of 2.71nm, 6.34nm and 11.0nm for the 10kDa, 70kDa and 250kDa dextrans, respectively. The Darcy permeabilities of 2%, 4% and 6% agarose gels were determined by multiplying the hydraulic permeabilities reported by Gu *et al.* (69) by the viscosity of water at 298.15K, giving values of 588 nm^2, 58.9 nm^2 and 26.8 nm^2, respectively. Gu *et al.* (69) determined the hydraulic permeabilities by fitting creep data obtained from confined compression tests of agarose gels made with DMEM (Dulbecco's modified Eagles' medium) to the biphasic theory. DMEM is assumed to have the same specific density and viscosity as water. The combined model thus has no free parameters and was used to determine a theoretical diffusivity value for each combination of dextran and gel density.

Implementing the Axelrod, modified Axelrod and Endress analytical models

As described earlier in the Analytical models subsection, both Axelrod and modified Axelrod (MA) assumed that the initial concentration profile was a square-well. However, while the Axelrod model defined the spot radius as the radius of the region of interest that was prescribed to be bleached, the effective radius for the modified Axelrod

model was estimated by calculating the radius at which the bleaching depth falls to e^{-2} times the maximum bleaching depth at the spot center. For all three models, the experimental recovery curve was obtained from the image data by using Equation (4). These recovery curves were obtained by integrating the intensity profile within the radius specific to each model. For both the Axelrod and modified Axelrod models, the characteristic diffusion time τ_D was estimated by iteratively adjusting its value to minimize the difference between the experimental and theoretical recovery curves. For both models, the theoretical recovery curves were calculated using Equation (6). The diffusivities were subsequently calculated (for Axelrod and modified Axelrod models) using Equation (5).

For the Endress model, the width of the Gaussian distribution at e^{-2} of the Gaussian height was determined by fitting the intensity profile immediately following bleaching to a 2-D Gaussian curve, and the decay rate constant, b, was determined by fitting a first order kinetic equation to the fluorescence decay at ~90% of the scan radius after spot bleaching. The fluorescence decay curve was fit for the initial 3s for simulations and the initial 5s for experimental data due to noise. The Endress model was then used to estimate the diffusivity providing the best fit (least squares minimization) to the fractional fluorescence intensity profile within the Gaussian radius.

3.4 RESULTS

3.4.1 Theoretical Validation Studies

Comparison of models

In initial analyses of simulated FRAP pseudodata, the DDSPE method provided exact estimates of the known (prescribed) diffusivity across a range of simulated conditions (Fig. 6). As anticipated, the DDSPE method precisely identified the prescribed diffusivity for all diffusivities and spot radii. The diffusivities estimated by the Axelrod model were strongly dependent on spot size, with decreased accuracy for smaller spot radii and higher diffusivities (both of which exacerbate the halo effect). The modified Axelrod model performed much better than the Axelrod, but the estimated diffusivities were also somewhat dependent on spot size and were less accurate for small spots. The Endress model, like the modified Axelrod (MA) model, performed much better than the Axelrod model (and also outperformed the MA model) although it consistently underestimated the diffusivities by about 10%. It should be noted that this set of simulations did not include any photobleaching during scanning and covered a region large enough that bleached particles did not reach the model boundary during the simulated experiment.

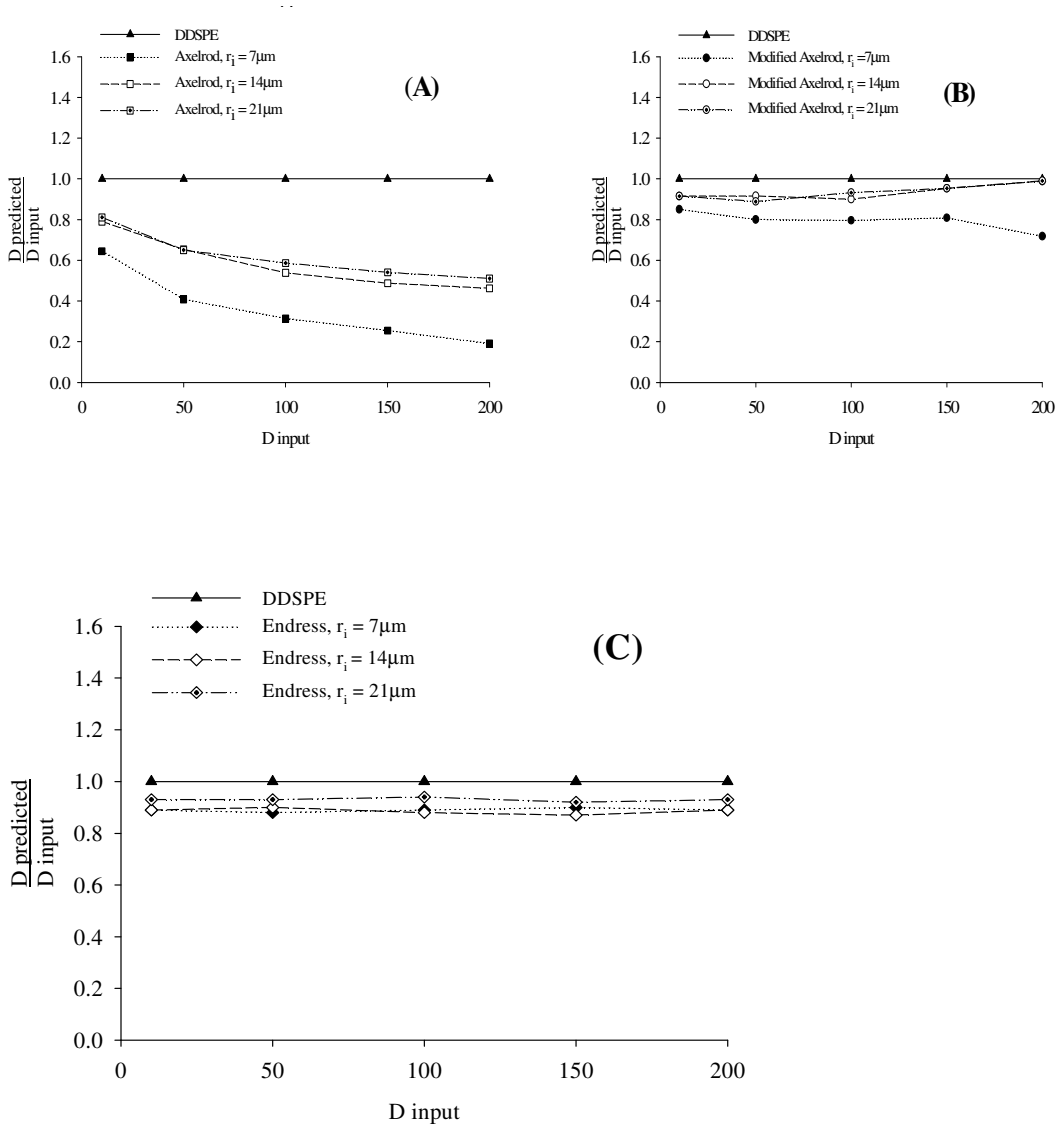

Figure 6: Comparison of the three methods for analysis of simulated FRAP experiments over a range of conditions. The estimated diffusivity is presented as a fraction of the diffusivity prescribed for each simulation. The sensitivity of the estimated diffusivities to spot radius is determined and compared to the DDSPE method for (A) Axelrod model, (B) modified Axelrod model and (C) Endress model. For all spot sizes and diffusivities, the DDSPE method exactly identified the prescribed diffusivity.

Constant versus Varying Boundary concentration

When simulated fluorescence data were truncated at a smaller simulated scan radius, the concentration at the model boundary varied with time even without any photobleaching during scanning, with different patterns depending on the prescribed diffusivity (Fig. 7*A*). Application of the DDSPE method without accounting for the time-varying boundary concentration produced errors in the estimated diffusivity of up to 20% (Fig. 7*B*), with an error proportional to the average deviation from a constant boundary concentration. When a time-varying boundary concentration was accounted for, however, the accuracy of the DDSPE method improved dramatically. Note that the residual errors in the DDSPE estimates are due to the approximate representation of the boundary variation by a fourth order polynomial, consistent with the approach used to analyze experimental data.

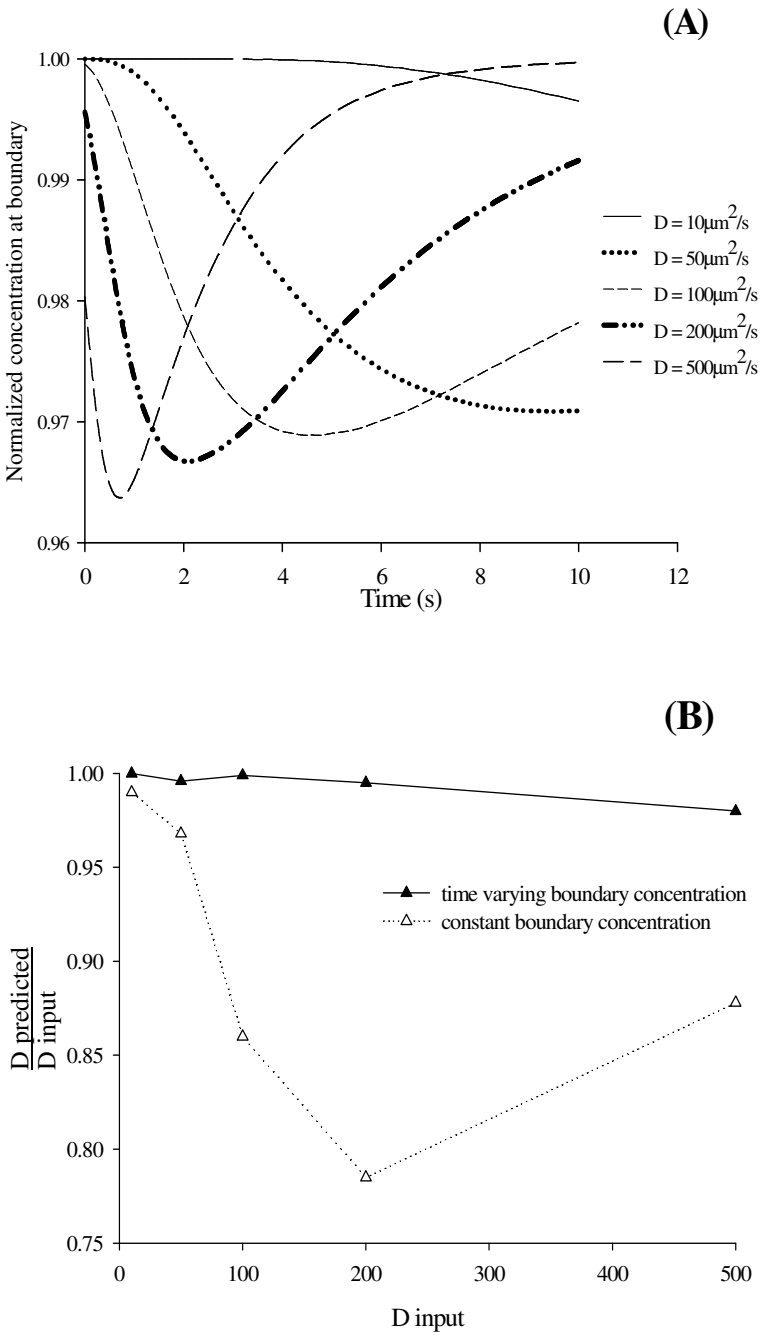

Figure 7: Effects of time-varying boundary concentrations on the accuracy of DDSPE diffusivity estimates for simulated FRAP experiments. (A) Concentration variation at the truncated boundary for a range of prescribed diffusivities. (B) Failing to account for the time-varying boundary concentration produces substantial errors in the estimated diffusivity.

Effect of Acquisition Photobleaching

The addition of a reaction term representing a reduced level of photobleaching during simulated scanning substantially slowed the rate of apparent fluorescence recovery, resulting in underestimations of the diffusivity when the DDSPE method did not account for this effect (Fig. 8). Note that the range of scan photobleaching intensity extended well beyond the level typically induced in FRAP experiments, but substantial errors occurred even for low levels of photobleaching. The addition of a second fit parameter representing a scan photobleaching rate constant restored the ability of the DDSPE method to determine the prescribed diffusivity. The accuracy of the modified Axelrod model was similarly degraded by photobleaching during scanning. As the reaction term is already included in the Endress model, it was able to account for the photobleaching effect, outperforming both the Axelrod and modified Axelrod models. However, the accuracy of the Endress model did decrease with increased photobleaching.

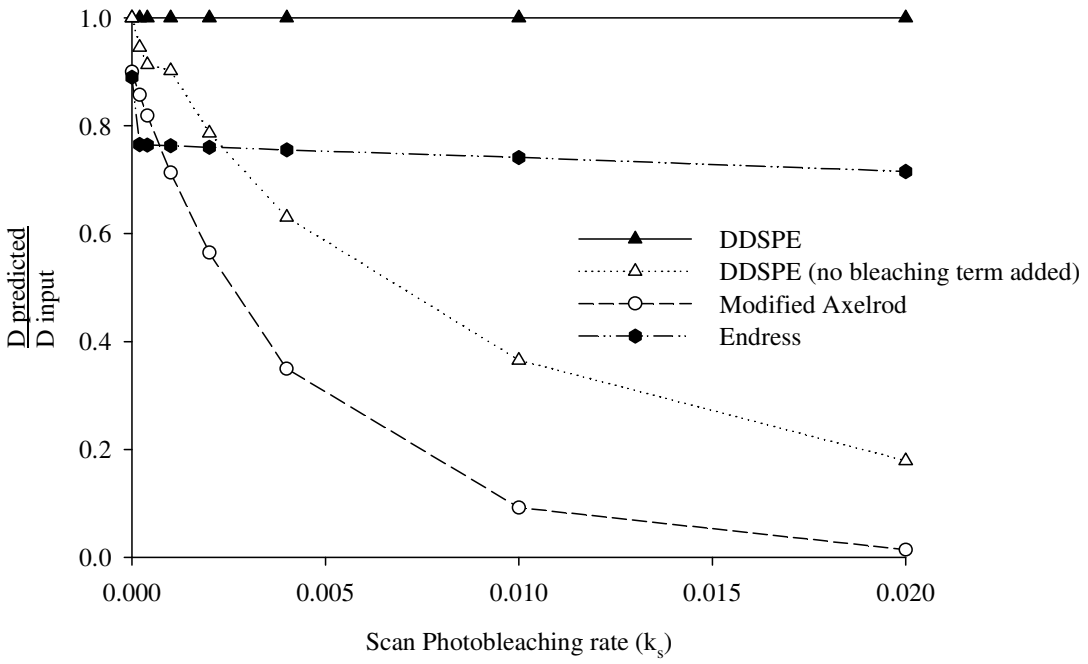

Figure 8: Effects of photobleaching during image acquisition scanning on the accuracy of DDSPE, modified Axelrod, and Endress diffusivity estimates for simulated FRAP experiments. Failing to account for photobleaching during scanning can produce substantial errors

3.4.2 Experimental Studies

As an application of the DDSPE method and a further comparison to analytical models, FRAP experiments were performed on fitc-dextrans in agarose gels. Repeatability was evaluated through five sequential measurements on 70kDa fitc-dextran at the same spot on a 2% agarose gel. The diffusivity determined using the DDSPE method was found to be 24.6±0.4μm^2/s, indicating excellent repeatability of the experimental and analytical procedures (not shown).

Effect of spot radius on estimated diffusivity: Comparison of models

The effects of spot radius on the estimated diffusivity of the 10.5 kDa fitc-dextran in 2% agarose determined with the four methods were consistent with the results of the theoretical validation studies. The diffusivity determined with the DDSPE method varied slightly with the radius of the photobleached target (Fig. 9*A*). The DDSPE diffusivity determined with the 6.75μm spot radius was significantly lower than that determined with the 13.5μm ($p=0.016$) and 20.25μm ($p=0.023$) spot radii, although the difference in the means was small (~5%). The diffusivities for the two larger spot sizes were not significantly different. As in the analyses of simulated experiments, the diffusivities determined with the Axelrod model (Fig. 9*B*) varied significantly and substantially with radius ($p<0.0001$ for all comparisons), with a mean value determined for the 6.75μm spot radius 36% of the value determined for the 20.25μm spot radius. The mean diffusivities determined with the Axelrod model were 11-30% of the corresponding values determined with the DDSPE method. The diffusivities determined with the modified Axelrod (Fig. 9*C*) and Endress models (Fig 9D) also varied significantly with radius. The mean diffusivities determined by the modified Axelrod model were 24-34% of the corresponding DDSPE values with the modified Axelrod model having a significantly lower value for the 6.75μm spot radius than for the 13.5μm or 20.25μm spot radii ($p<0.0001$ for both) but no significant difference between the larger radii. In contrast to the other analytical models, the Endress model predicted mean diffusivities that were 80%-160% of the DDSPE values with a strong dependence on radius ($p<0.0001$ for all radii). The scan photobleaching rate constant k_s estimated with the DDSPE method had values of $0.0162\pm0.0046s^{-1}$, $0.0148\pm0.0046s^{-1}$ and $0.0108\pm0.0028s^{-1}$ for the 6.75μm,

13.5μm and 20.25μm spot radii, respectively. The value of k_s determined for the 20.25μm spot radius was significantly ($p<0.001$) lower than the values for the two smaller radii, consistent with the lower scan frequency associated with the larger scan region used for the 20.25μm spot radius. However the Endress model estimated rate constant values of $0.0083\pm0.0021 s^{-1}$, $0.010\pm0.0016\ s^{-1}$ and $0.015\pm0.0018\ s^{-1}$ for the 6.75μm, 13.5μm and 20.25μm spot radii, respectively. The value of k_s determined for the 6.75μm spot radius was significantly different ($p<0.0001$) from the other two radii and although the difference between the values determined for the 13.5μm and 20.25μm radii were significant ($p<0.047$), the mean values were quite similar.

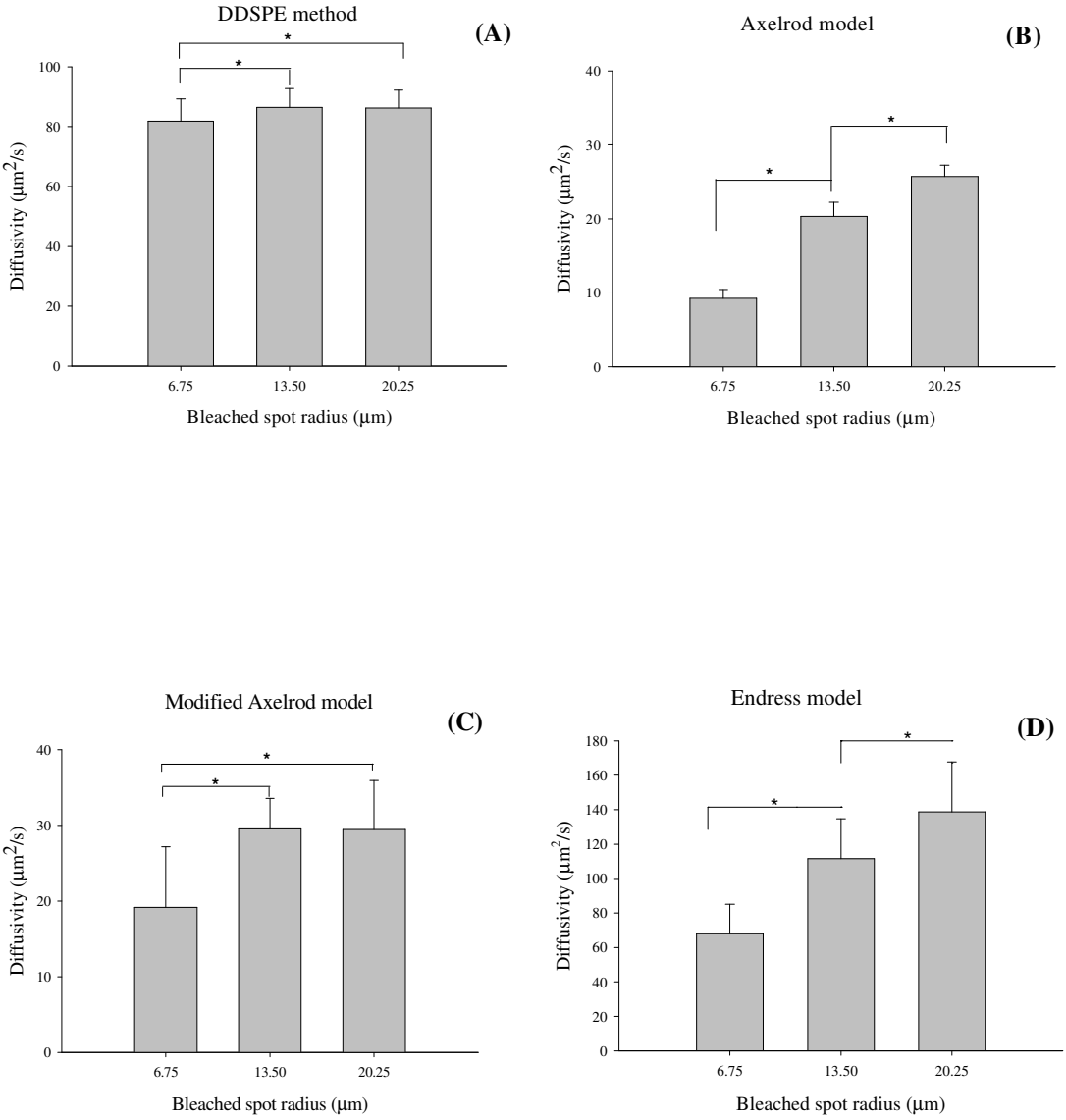

Figure 9: Effect of varying the photobleached spot radius on the estimated diffusivity of 10.5kda fitc in 2% agarose determined with (A) the DDSPE method, (B) the Axelrod analytical model, (C) the modified Axelrod analytical model and (D) the Endress analytical model. * indicates $p<0.05$.

Effect of dextran size and gel density on diffusivity

The variations in solute diffusivity with dextran size and with gel density (Fig. 10*A*) were consistent with classical theories of diffusion (Stokes-Einstein relationship) and effects of tortuosity on molecular transport through porous media. For each gel density, the diffusivity determined via DDSPE analysis decreased significantly with increasing solute size ($p<0.0001$ for all pairwise comparisons). The diffusivities of the 70kDa and 250kDa fitc-dextrans decreased significantly with increasing gel density ($p<0.0001$ for all pairwise comparisons), while the diffusivity of the 10kDa dextran was significantly lower in 4% and 6% agarose than in 2% agarose (both $p<0.0001$) but did not differ between 4% and 6% agarose. Accuracy of the DDSPE estimated diffusivities was supported by the excellent agreement for all combinations of dextran size and gel density between the experimental values and the theoretical diffusivities determined using Eqs. 7-9, as indicated by a highly significant linear regression with a slope close to 1 (Fig. 10*B*).

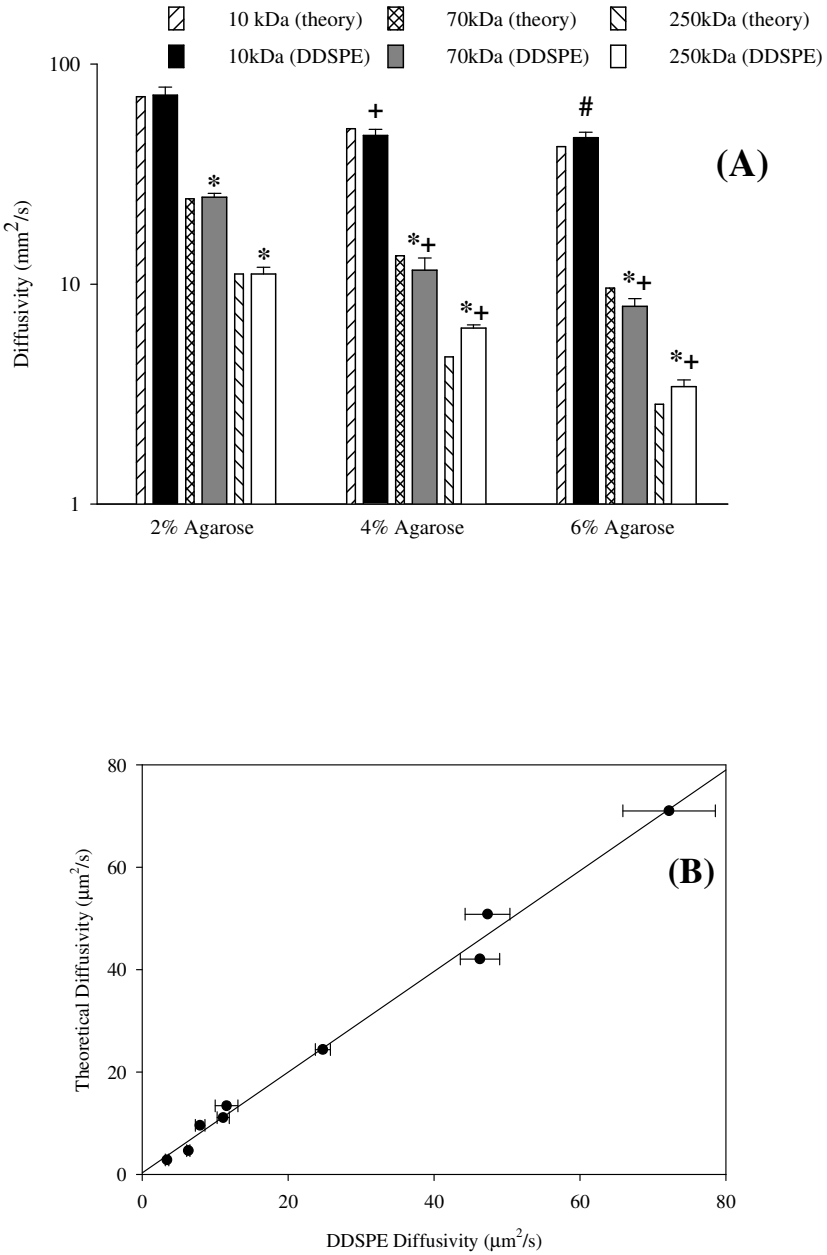

Figure 10: Comparison of the diffusivities of dextrans in agarose gels estimated using the DDSPE method with those calculated with an empirical model from the literature. (A) Variations in DDSPE and theoretically estimated diffusivity with gel density and solute size. * indicates different from all smaller solutes ($p<0.0001$), + indicates different from all lower gel densities ($p\leq0.0001$) and # indicates different from 2% gel only ($p<0.0001$). **(B)** Relationship between the DDSPE and theoretical diffusivities across experimental conditions.

3.5 DISCUSSION

FRAP and other imaging-based techniques offer several advantages over other experimental techniques for examining solute diffusivity in gels and hydrated tissues, including short experimental times, localized measurements and fewer complications such as swelling during measurements. While analytical models based on idealized conditions are commonly used to derive diffusivities, experimental data that deviate from these conditions can lead to inaccurate results. We developed the finite element based DDSPE method to incorporate more realistic experimental conditions, resulting in more accurate determination of diffusion coefficients of solutes in agarose gels and tissue samples.

As a target region is photobleached, diffusive exchange between the target region and the surrounding, unbleached region produces a partially bleached halo surrounding the target, increasing the time needed for recovery. Unlike common analytical models, the DDSPE method accurately accounts for the actual, measured fluorescence intensity distribution following bleaching and thus explicitly accounts for this halo effect. As anticipated, the DDSPE method accurately determined the specified diffusivity from simulated FRAP data. Even under the highly idealized theoretical conditions in which linear, Fickian diffusion is strictly accurate, the Axelrod (Fig. 6A), modified Axelrod (Fig. 6B) and Endress (Fig. 6C) models could be inaccurate, although the Endress model was generally more accurate than the others. In analyses both of theoretical and experimental FRAP data (Fig. 9), the DDSPE method was fairly insensitive to the bleach spot size while the diffusivities estimated with the Axelrod and Endress models varied with the spot radius. The modified Axelrod model was not as strongly influenced by spot

radius, but still underpredicted the diffusivity for some conditions (albeit not as severely as the Axelrod model). Although the Endress model predictions were slightly dependent on radius, it performed very well under idealized theoretical conditions with estimated diffusivities that were 90% of the prescribed/actual diffusion coefficients. For the Axelrod model, the assumption that the bleached region is the size of the original target region leads to an artificially low ratio of r^2/τ_D in Eq. 5 and hence an underestimation of the actual diffusion coefficient. The modified Axelrod model employs an effective bleached radius larger than the specified spot radius, resulting in a better estimate of the diffusion parameter than the Axelrod model. These analytical models rely on the ability to accurately determine the characteristic bleaching time constant, and deviations between experimental and theoretical conditions or in the method for estimating the time constant from experimental recovery curves will influence the estimated diffusion constant. Because these approaches do not fully account for the true radial variation in bleaching intensity, they are inherently less accurate for conditions such as smaller spot sizes and higher diffusivities that exacerbate the halo effect (55). In contrast, the Endress model attempts to account for the radial variation in concentration by fitting the initial concentration profile to a two dimensional Gaussian. However some of the initial profiles and subsequent profiles at later time points are not best described by Gaussian curves so this introduces substantial errors to the analyses of those conditions leading to inaccurate estimations of the diffusion coefficients. In essence, while any analytical model will perform well under a restricted set of conditions, the DDSPE method works across a much broader range of conditions because it does not require a priori assumptions about bleaching profiles, boundary conditions, etc.

Most analytical FRAP models often require determination of $F(\infty)$, the asymptotic fluorescence intensity at infinite time (often assumed to be equivalent to the initial intensity before bleaching). Direct determination of $F(\infty)$ can be difficult, as the fluorescence intensity may take substantial time to reach a steady state value and experimental noise or photobleaching can adversely affect the estimation of $F(\infty)$. As the half time calculated is sensitive to value of the fluorescence recovery at infinity, this can affect the accuracy of the estimated diffusivity. In contrast, the DDSPE method does not require knowledge of the unbleached or asymptotic fluorescence intensity or distribution and does not require that experiments continue until full recovery is achieved, as it determines the diffusivity that produces the best fit to the available experimental data. As with other methods, however, greater degrees of recovery will produce better estimates of solute diffusivity.

Depending on the size of the bleach spot and the duration of the recovery, it may not be practical for the size of the experimental scan region to be large enough that photobleached solutes do not reach the boundary of the scan region. Because the DDSPE method explicitly accounts for the time varying boundary concentration produced as initially bleached particles reach the boundary of the scan region (or resulting from continued photobleaching during scanning), this method does not actually require that an infinite bath exists. In cases where the boundary concentration does vary substantially, the accuracy of the estimated diffusivity decreases if the time dependence of the boundary concentration is not taken into consideration It should be noted that accurately fitting the boundary concentration is also important. In our simulations, the fourth order polynomial was able to fit the boundary variation well for solutes with low diffusivities,

resulting in excellent agreement with the prescribed value. At higher diffusivities, however, more bleached particles reached the boundary during the simulation period and the fit equation was less accurate, resulting in some reductions in solution accuracy (Fig. 7).

Aside from accounting for realistic initial concentration profiles, the DDSPE method independently accounts for the effects of photobleaching during the recovery period due to laser illumination for image acquisition. Although this effect is typically neglected, scanning of non-bleached control spots at 0.75% excitation revealed that substantial fluorescence decay could occur on a time scale relevant to our experimental measurements. Simulations revealed that failing to account for further photobleaching during scanning could decrease the accuracy of diffusivity estimates, indicating that including a second fit parameter describing photobleaching was necessary. Although the Endress model adds a reaction term to the Fickian diffusion equation to account for photobleaching during scanning, it still is unable to fully compensate for the bleaching during image acquisition (Fig.8) especially as the bleach rate constant increases. The accuracy with which diffusivities are predicted is strongly dependent on the correct estimation of the rate constant by the Endress model. An accurate determination of the rate constant relies on choosing a spot that is neither influenced by the diffusion of bleached molecules from the bleach spot nor the boundary flux, and as a result correctly reflects the background fluorescence decay or photobleaching during scanning. This may prove difficult to achieve as it would require either extremely large outer scan regions or very slowly diffusing molecules to obtain accurate estimates of k_s. Also the k_s values determined by the Endress model from the experimental data deviated significantly from

those determined by the DDSPE method. Both simulations and experimental data revealed that underestimation or overestimation of the rate constant leads to underestimation and overestimation of the diffusivity. As noted previously, the scan photobleach rate constant depends on the scanning frequency and therefore on the size of the scan region. If the same scan region is used across experimental conditions, the rate constant is unlikely to vary. To further underscore the importance of accounting for photobleaching during image acquisition, some of the experimental data were analyzed with and without accounting for the scan photobleaching term. All scan regions were the same size (r_o = 47.25μm) with an average k_s value of 0.013±0.004s^{-1}. Analysis of the results showed that the accuracy of the diffusivity estimates decreases with decreasing diffusivity if scan photobleaching is neglected. The dimensionless parameter D/ $r_o^{\wedge 2}*k_s$ measures the relative contributions of diffusion and reaction (or photobleaching terms). Values >>1 indicate that photobleaching is insignificant while values <1 indicate that photobleaching is significant For D/ $r_o^{\wedge 2}*k_s$ values of 2.89, 0.21 and 0.11 corresponding to actual diffusivities of 84±6.8$\mu m^2/s$, 6.2±0.32 $\mu m^2/s$, and 3.3±0.19 $\mu m^2/s$, the predicted diffusivities (when scan photobleaching was neglected) were 94%, 73% and 64% of the actual diffusivities respectively.

As an experimental application of the DDSPE method, we studied the effects of gel concentration and solute size on diffusivity in agarose gels (Fig. 10). As expected, the diffusivities of the solutes decreased with increasing gel concentration, consistent with an increased tortuosity, and for a given gel density the diffusivities decreased with increasing molecular weight (size). The diffusivity values determined with the DDSPE

method were consistent with experimental results in the literature and were in excellent agreement with theoretical values based on empirical fits. Although the validity of this method for more complex media must be confirmed, these results indicate that the DDSPE method implemented here is highly accurate for analysis of FRAP experiments on isotropic hydrogels.

Although the specific implementation of the DDSPE method presented here assumes one-dimensional, axisymmetric diffusion, it can easily be modified to account for two- or three-dimensional, anisotropic diffusion. Sneikers (65) used a similar approach involving a two-dimensional finite element simulation to account for inhomogeneous diffusivities in agarose gels and the cartilaginous growth plate, although that model did not account for the potentially substantial effects of photobleaching during image acquisition and time-varying boundary concentrations. It should also be noted that while most models assume that the diffusive recovery for FRAP experiments is purely two-dimensional (i.e. lateral diffusion within the focal plane), the actual concentration profile does vary out of plane due to out of plane bleaching and beam focusing (which produces a non-cylindrical profile). The relative insensitivity of the DDSPE method to the photobleached spot size and the close agreement with literature values for dextran diffusivity in agarose suggests that out-of-plane effects (which would be expected to differentially affect recovery for the different spot sizes) did not substantially influence these measurements. Should out-of plane diffusion prove to be important in other situations, the DDSPE model could be adapted to measure three-dimensional diffusive recovery by sequentially scanning in different focal planes and fitting model predictions

to a four-dimensional matrix $C(x,y,z,t)$ although the temporal resolution would be substantially degraded.

Although the numerical model developed in this work enables the accurate determination of diffusivities, the accuracy of any FRAP measurement still depends on the spatio-temporal resolution of the equipment being used. To accurately measure high diffusion rates, the rate of image acquisition should be fast enough to capture the diffusive recovery process and provide sufficient temporal information for the parameter estimation process. Also, if recovery rate (or solute diffusivity) is much slower than the rate at which the solute is bleached during image acquisition (i.e. the product of the scan photobleach rate and the area of the scan region), the accuracy of the estimated diffusivities might be impacted.

In addition, it should be noted that the typical FRAP image obtained from a CLSM is a juxtaposition of pixels scanned at different time points. That is to say that if it takes half a second to scan a region of interest, the first last pixel of the image is scanned 0.5s later than the first pixel. But in the most of the analytical models, including the DDSPE, the different time points of the pixels are not taken account as all the pixel intensity values are assumed to be state of the image at the end of the scan time (scanning time is assumed to be negligible). This may further affect accuracy of the models.

However, given the excellent agreement of the DDSPE diffusivities with the theoretical diffusivities, it is likely that errors introduced with this assumption are minimal. Furthermore, most of the aforementioned limitations can be overcome by using equipments with much shorter scan times (or faster scanning devices) validating the

assumption that scanning time is negligible and considerably improving temporal resolution.

In summary, we have developed a combined experimental-numerical technique for determining solute diffusivity via FRAP that takes into account diffusion during bleaching and is insensitive to the bleached spot radius or bleaching profile. This model incorporates realistic initial conditions, time varying boundary conditions, and accounts for potential photobleaching during image acquisition, resulting in highly accurate and repeatable estimates of solute diffusivities in porous media. The development of this FRAP analysis model will support investigations into the transport mechanisms of polymers and tissues which may ultimately aid in efficient and localized drug delivery to diseased sites, early detection of degeneration by measuring changes in transport parameters and the development of successful tissue engineered constructs.

CHAPTER 4

DIFFUSIVE PROPERTIES OF IMMATURE ARTICULAR CARTILAGE: THE ROLE OF MATRIX COMPONENTS

4.1 INTRODUCTION

Articular cartilage is an avascular, aneural, alymphatic connective tissue that covers the articulating surfaces of bones in joints. The shape and density of chondrocytes vary through the articular cartilage depth; in addition, these cells remodel the extracellular matrix, maintaining the functional integrity of the tissue(5). Cellularity, extracellular matrix composition and organization have all been shown to vary with cartilage depth (and within the different zones). Chondrocyte density is highest in the superficial zone and decreases with depth; proteoglycan content increases from the superficial layer through the deep layers(5). Furthermore, in human articular cartilage, collagen content has been reported to be highest in the superficial zone and lowest in the middle zone(10, 70, 71). As with the other extracellular matrix components, the distribution of water is depth-dependent. In addition, the spatial orientation of the collagen fibers differs from zone to zone: the fibers are oriented parallel to the articular surface in the superficial zone, randomly oriented in the middle zone and in the deep zone, the fibers are perpendicular to the articular surface(10). This spatial variation in ECM composition and structure confers inhomogeneous and anisotropic properties on the cartilage ECM.

Given its major role in load bearing and support within the joints, the goal of many studies of cartilage mechanics over the years has been to determine the relationships between composition, structure (micro and macro), and mechanical properties of healthy articular cartilage. As a result, numerous testing configurations and devices have been developed to accurately measure these material properties (shear, tensile, compressive moduli) and relationships between ECM components (PG and collagen) and the aforementioned mechanical coefficients have been established.

However, little attention has been given to an equally important feature that plays a pivotal role in cartilage function: its transport properties.

As stated in the earlier chapter, diffusion is the principal means of transport of nutrients, growth factors and metabolites in articular cartilage. Deficiency in the supply of nutrients and growth factors may lead to the pathological degeneration of extracellular matrix. Therefore, knowledge of the diffusion properties of the cartilage extracellular matrix environment is essential to understanding many mechanisms of cartilage function.

Studies have shown that the heterogeneous composition and micro-structural organization of cartilage result in inhomogeneous and anisotropic mechanical properties. Indeed, depth-dependent compressive and tensile modulus distributions have been determined for articular cartilage(5, 72). It follows then that spatial variation in ECM composition and structure may also influence cartilage diffusion properties, resulting in diffusion coefficients that are depth (zone)-dependent and direction-dependent.

As mentioned in the background to this thesis project, a few attempts have been made to determine the depth-dependent diffusion properties of articular cartilage. Diffusion experiments have been performed on human articular cartilage explants from

different depths(21) but spatial resolution was limited as the sample volumes were large and diffusivities were reported as a function of fixed charge density and not of depth (or cartilage zone). In another study that examined the zonal dependence of diffusion using FRAP, the diffusion coefficients were determined from a FRAP analytical model that did not incorporate the experimental conditions of this present investigation. Recently, diffusion studies using MR diffusion tensor imaging (DTI) reported on water diffusivity through the cartilage thickness in human patellar and femoral condyles. As DTI is limited to the measurement of the diffusion of water molecules, these studies reported very low values of diffusional anisotropy in the cartilage samples owing to the negligible hindrance to water mobility(73, 74).

Furthermore, to the best of our knowledge, there are no detailed and conclusive studies on diffusion of solutes of physiologically relevant sizes within articular cartilage. Therefore, we used a 4kDa solute as it is in the same size range as compounds (such as insulin (5kDa)) used for intra-articular drug delivery and growth factors such as insulin-like growth factor 1 (IGF-1, 7kDa) necessary for the maintenance of matrix integrity in cartilage. Furthermore, this size is optimal for probing the articular matrix structure as matrix anisotropy or inhomogeneity may not be detectable with smaller solutes and larger solutes may be excluded from the matrix.

The objectives of this study, therefore, were to determine the depth-dependent distribution of solute diffusivity within the cartilage matrix with finer spatial resolution than has been published, to correlate the measured diffusivities with matrix collagen, proteoglycan and water contents and to investigate diffusional anisotropy by comparing the transverse and radial diffusivities across the different cartilage zones.

4.2 MATERIALS AND METHODS

4.2.1 Experimental Methods

Tissue Harvest and Sample Preparation

Using a #22 scalpel and 6mm-diameter biopsy punches, twenty-four (24) full-thickness cartilage explants were excised non-sterilely from the medial femoral condyles of 6 right stifle joints of immature (6-8 week old) calves within 24 hours of slaughter. The height of each explant was measured using a digital caliper. The average height of the explants was 6.53±1.05mm. Each cartilage explant was subsequently cut axially in the anterior-posterior plane into two hemi-cylinders producing, a flat vertical plane perpendicular to the articular surface (Fig. 11). A blade mark was made on the explants before excision to ensure that they were cut in the same orientation. The excised hemi-cylindrical cartilage explants were subsequently placed in vials filled with a PBS + protease inhibitor cocktail solution and frozen at -20^{o}C until ready for use. Afterwards, explants were thawed at room temperature prior to use. The explants were then embedded in OCT (Optimal Cutting Temperature) compound and sectioned using a freezing stage microtome (HM 450, Microm, Germany).

Each hemi-cylindrical explant was cut into 100µm-thick slices parallel to the articular surface (transverse slices) and the other corresponding half was sectioned into 100µm-thick slices perpendicular to the articular surface (radial slices). Prior to sectioning, a wedge of tissue was cut off from an edge of each hemi-cylindrical explant to serve as a registration mark. On the transverse slices, this registration mark identified the tissue face closer to the articular surface; while for the radial slices, it was used to

distinguish the superficial from the deep zone. During sectioning, all radial and transverse slices obtained from the OCT-embedded explants were placed in phosphate buffered saline (PBS) to prevent tissue dehydration.

For the first three animals, diffusion measurements were taken on every other transverse slice for the first 1.2mm of the cartilage explant and on every fourth slice for the remainder of the explant. Thus, a depth-dependent diffusivity profile was obtained for all the disks. Each transverse slice adjacent to that used for FRAP was analyzed for biochemical content. A total of 5 radial slices were obtained from each cartilage explant. Because the tissue samples were too small to ensure accurate measurement of water content, additional biochemical quantification was done on cartilage explants excised from sites adjacent to those used for the FRAP experiments in the other three animals.

Six explants were obtained from each animal – three were used for diffusion measurements and the other three for biochemical measurements. Five to seven transverse slices from each cartilage zone were used for diffusion experiments. Tissue samples for the superficial zone were taken from the first 15% of the cartilage explant. The middle zone was assumed to be the next 40-60% and the deep zone was taken as the last 25% of the explant. Care was taken to not include the calcified zone with the tissue samples for any of the experiments. Any tissue slice (at the deep zone) with a grainy texture was discarded.

Tissue samples to be used for FRAP experiments were labeled by immersing the slices in 0.2mg/ml of 4kda FITC-dextran dissolved in PBS solution for 2 days at 4^{o}C to allow for maximum permeation and equilibration of the solute in the matrix. Protease inhibitor cocktail set 1 (used in 1X concentration) was added to the labeling solution to

prevent tissue degradation. Pilot experiments demonstrated that tissue immersed from 30hrs to 48hrs had the same dye distribution and intensity. When samples immersed for less than 24hours were examined under the CLSM, images were observed to be noisy (with lower fluorescent intensity values) and it was evident that the dye was still excluded from much of the tissue.

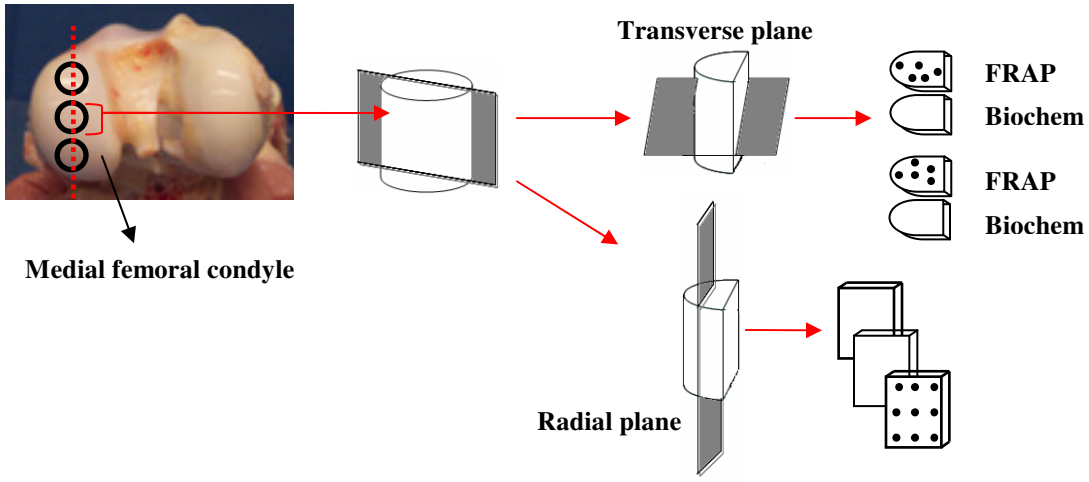

Figure 11: Tissue harvest and Sample preparation. Cartilage explants are harvested from the medial femoral condyle of a bovine stifle joint. The red dotted line shows the anterior–posterior plane. The cartilage explants were cut into two hemi-cylinders along the anterior-posterior plane. One hemi-cylinder was sectioned into 100µm thick slices parallel to the transverse plane while the other was sectioned into 100µm thick slices parallel to the radial plane. The black circles on the tissue slices represent sites for FRAP experiments. Five (5) FRAP measurements were taken on each transverse slice while 3 FRAP measurements were taken in each zone for each radial slice (resulting in a total of 9 measurements per radial slice).

4.2.2 FRAP Experiments and Analyses

FRAP experiments were performed on a LSM 510 laser scanning confocal microscope (Zeiss, Germany) using a 63X /1.2 N.A water objective with a 25mW Argon laser. All photobleaching was performed at 488nm emission at 100% laser power. All imaging was done with a (75%) 25mW Argon laser at 1% power with excitation at 488nm and emission recorded above 505nm.

Five FRAP experiments were performed on each transverse slice while for the radial slices, three spots on each cartilage zone were bleached resulting in a total of 9 FRAP experiments per radial slice. Statistical analyses of preliminary data revealed that most of the variation was between animals and not within each animal. Thus, 3 FRAP measurements for each zone or slice were sufficient to obtain statistical significance. The radius of the bleached spot on all tissue samples was 20.3μm (with an outer square scan region, 148.48μm width). For the radial slices, gridded cover slips (Electron Microscopy Sciences, Hatfield, PA) were used to precisely determine the location of the spot to be bleached within the tissue. The gridded cover slips were 25mm in diameter with a square grid pattern, 10mm x 10mm etched on it. The grid contained 10,000 alphanumeric coded squares, each square 0.1mm width. Each 0.1mm square had 4 equidistant tick marks on each side of the square. Thus, the spot location was accurate to within ~12μm. For each radial slice, diffusion measurements for the superficial zone were taken 75-90μm from the articular surface. However, the sites of FRAP measurements for the middle and deep zones were dependent on the height of the specific cartilage explant. In general the diffusion measurements were taken at distances from the articular surface that corresponded to 40% and 80% of the total cartilage explant height respectively.

Furthermore, care was taken to avoid bleaching atop a cell, thus the bleach sites were not completely random locations.

To evaluate the repeatability of FRAP diffusivity estimates, five repeat measurements were taken at the same location in a cartilage tissue sample containing the 4kDa FITC-dextran. After each repeat measurement, the spot was allowed to recover and equilibrate completely for 10 minutes without laser illumination.

To determine the effect of freezing on the diffusion measurements, FRAP experiments were done on fresh tissue samples taken from the cartilage middle zone. The samples were then frozen, thawed after 3 days in the freezer and diffusion measurements were repeated.

All FRAP image data was analyzed using the 1D axisymmetric model (DDSPE) described in the previous chapter. The radialization (conversion of 2D image to 1D profile) algorithm was modified slightly by averaging the pixel intensity values within concentric rings centered about the nominal center of the bleached spots.

Briefly, the raw pixel values from each FRAP image were read using the '*imread*' function in MATLAB, which reads the pixel intensities from a 2-D image field and produces a 2-D matrix of intensity values. This matrix was subsequently partitioned into 73 concentric rings of equal width i.e. the differences between the outer and inner radii were equal for all the rings. Intensity values within each concentric ring were averaged representing the average intensity value for a known radial position. Thus, the intensity profiles for all the images were calculated and assembled to produce a two-dimensional matrix, $C_{exp}(r,t)$ representing a time-varying, axisymmetric concentration field within a circular region. Again, the initial condition $C(r,0)$ for the simulation was defined by the

first post-bleach image. However, the time-varying boundary condition $C(r_o,t)$ was not fit to a polynomial but rather was represented by a vector of intensity values - the measured concentration at the outer boundary of the simulation region.

A one-dimensional, axisymmetric finite element mesh was generated within COMSOL Multiphysics using two-node, linear elements with equally spaced nodal positions corresponding to the radial positions with known initial concentrations. An objective function ϕ was defined in MATLAB as the difference between the theoretical and experimentally-measured concentration profiles. A two parameter fit using the constrained minimization function *fmincon* was used to identify the values of D (diffusivity) and k_s (photobleaching rate constant) that minimized the objective function, producing the best overall fit to the entire spatially and temporally varying concentration field.

Due to non-ideal experimental conditions, criteria were developed to exclude aberrant data. Histogram plots of diffusivities and normalized least square error values (ϕ/numel) were made to illustrate the spread of the values (Appendix B, Figure 41). To be able to compare the objective functions from matrices of different sizes, the least square error (which is the objective function (ϕ), was divided by the total number of elements within the matrix. Diffusivities that were outside the range $1\mu m^2/s<D<65\ \mu m^2/s$ were discarded. Diffusivities estimated from simulations that yielded values of ϕ/numel >20.42 were excluded from the analysis. Images that had cells in the center of the bleached spot were not analyzed. It should be noted that the 1-D axisymmetric model

failed to converge to a solution if the bleaching depth was insufficient and if the bleach spot was on a cell.

4.2.3 Biochemical quantification

Tissue samples were weighed wet, lyophilized, weighed dry, and digested in 1mg of Proteinase K (in 100mM of ammonium acetate) per 80 mg of tissue. To ensure consistency in the weighing protocol, all samples were blotted with tissue paper to remove excess fluid. Samples were subsequently placed on weighing paper and weight measurements were recorded when digits on mass balance were relatively steady. Ten to fifteen tissue slices from each cartilage explant was used for the biochemical quantification. Samples were placed in an oven at 60^{o}C overnight for digestion. Sulfated glycosaminoglycan (sGAG) content was quantified from the tissue digests using the colorimetric 1,9-Dimethylmethylene blue (DMMB) dye binding assay (75) using a chondroitin sulfate (shark cartilage) standard. For the sGAG assay, the digest samples were diluted (1:10 or 1:20 depending on tissue weight) and 200µl of DMMB dye was added to 10µl of digest solution and subsequently read on the plate reader.

Total collagen content was also quantified using the colorimetric chloramine-T/p-Dimethylaminobenzaldehyde (pDAB) collagen(76) assay using a hydroxyproline standard. Briefly, 50-100µl of digest solution was hydrolysed in 1ml of 6N hydrochloric acid solution at 120^{o}C overnight. Each sample was reconstituted using 1ml of sodium phosphate buffer. Chloramine-T and pDAB solutions were made up 24 hours before use. Both solutions are light sensitive so they were made in amber-colored bottles (wrapped in

aluminum foil) and kept in the dark. Fifty micro-liters (50µl) of standards and digest solution were pipetted into a clear flat-bottomed 96-well plate. Subsequently, 50µl of chloramine-T was added to each well and left to incubate in the dark for 15mins. After sufficient incubation of the samples, 50µl of p-DAB was added to the solution in each well and subsequently incubated at 60^{o}C for 30mins. Samples were left to cool before being read in the plate reader. Both colorimetric reactions were read on Power Wave 340X-I plate reader at wavelengths of 525 and 557 nm for the sGAG and collagen assays, respectively. Measurements of both sGAG and hydroxyproline contents were made in triplicate.

4.2.4 Histochemical staining of immature articular cartilage

Tissue samples from an immature cartilage explant were fixed in 10% neutral buffered formalin for 24 hours per mm of thickness of tissue at room temperature. After fixation, the tissue samples were rinsed several times in PBS and subsequently dehydrated in 70% ethanol until ready for paraffin embedding. Using a rotary microtome, 5□m slices were sectioned from the tissue paraffin blocks. Haematoxylin & Eosin (H&E) staining was done to visualize overall matrix morphology (Haematoxylin stains the cell nuclei while eosin stains the matrix).

4.2.5 Statistical Analyses

All statistical analyses were done using the Minitab Release 12.23 software (Minitab Inc). Diffusivities were analyzed using Multifactor ANOVA with a general linear model with a partially nested design. For the independent variables, animal and cartilage explants were designated as random factors, zone and orientation were fixed factors while both radial and transverse diffusivities were dependent (response) variables. Tukey's test for pair-wise comparisons was used for the zone term.

To determine the relationship between zone and the extracellular matrix components (sGAG, collagen and water), one-factor ANOVA as a general linear model was used with each ECM component as a response variable and zone as a fixed factor (independent variable). When the differences were found to be significant, Tukey's test for pair-wise comparisons was used for the zone term. In addition, one-factor ANOVA was also used to examine the zonal dependence of other explant parameters such as diffusional anisotropy (ratio of radial to transverse diffusivities)

Diffusivities were averaged for each cartilage explant and normality tests were performed on radial and transverse diffusivities and on each biochemical component (sGAG, collagen and water) using the Anderson-Darling normality test. Non-normal data (both diffusivities and ECM components) were ranked and the nonparametric Spearman rank correlation was used to test the strength of the relationship between the ranked variables. Correlation tests were performed on both dependent and independent variables. For the difference between any two normal populations, the Student t-test was used.

Multiple regression analyses were performed with radial and transverse diffusivities as dependent variables and sGAG, collagen and water contents as

independent variables. The tests for the regression coefficients were performed at the significant level $\alpha = 0.05$.

All results except diffusivity values were presented as mean ± SD. Diffusivities were reported as mean ± SEM.

4.3 RESULTS

4.3.1 Histological images: Cartilage zones

Representative low magnification (10X) images of H&E stained 8-week old articular cartilage sections are shown in Figure 12. The superficial, middle and deep zones are images A, B, and C respectively. Nuclei are stained dark blue while the matrix is stained purple. The intensity of the matrix staining increases from the superficial to the deep layers.. Cell size/diameter increases with increasing distance from the articular surface. The pericellular matrix is also more visible and more deeply stained in the deep zone than in the superficial or middle zones. Furthermore, cells appear as pairs or doubles in the deep zone but less so in the middle zone. Almost all the cells in the superficial zone are unpaired. These observations are consistent with the literature.

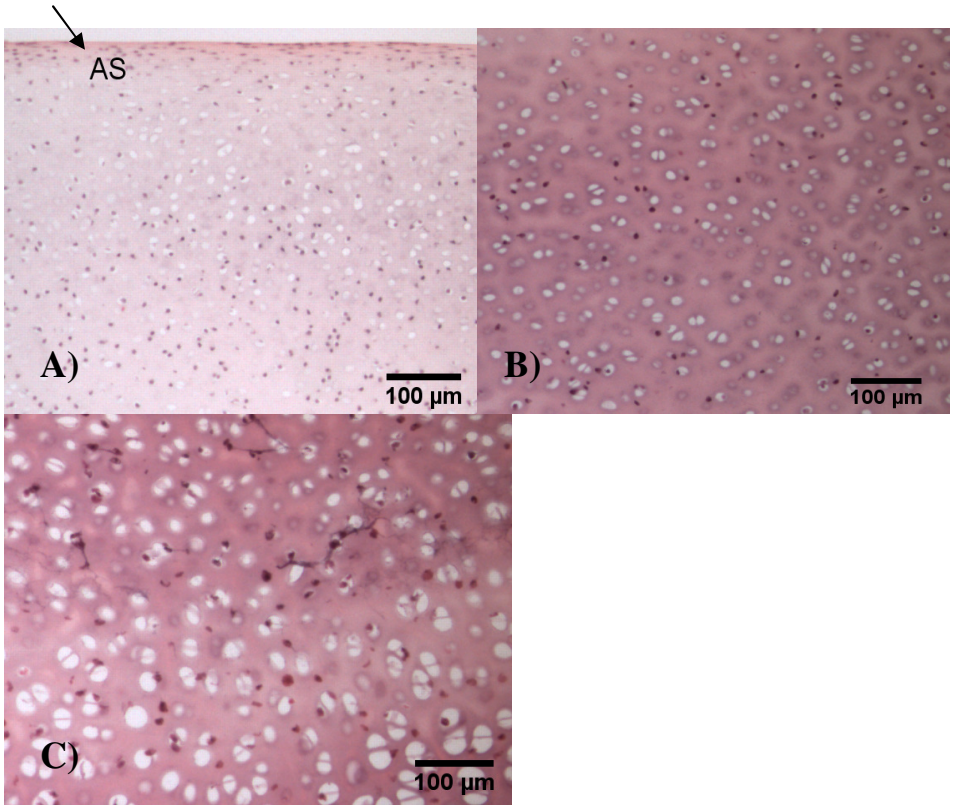

Figure 12: Light micrographs of H&E stained 8 week-old cartilage sample (10X) depicting the various cartilage zones: A) Superficial, B) middle and C) deep zones. Nuclei are stained dark blue, matrix is stained purple. Arrow points to the articular surface in the superficial zone.

4.3.2 Immature cartilage tissue composition

Measured biochemical composition is presented in figures 13-18. Tissue from the different zones (superficial (SZ), middle (MZ) and deep (DZ)) were compared to each other. Sulfate and hydroxyproline contents, measures of sulfated glycosaminoglycan and collagen contents, respectively, were normalized by the tissue wet weight. These results are presented as mean ± standard deviation. sGAG content increased with increasing

distance from the cartilage surface (Fig. 13). Figure 13A illustrates the variation in sGAG content with depth in 3 sample cartilage explants from the same animal (Leg VI). For ease of comprehension and analyses, measured sGAG contents in all animals were subsequently pooled together according to zones (the first 15% for the superficial zone, the next 30-70% for the middle zone and the last 30% for the deep zone) as shown in figure 13(B). sGAG content was highest in the deep zone and was significantly different from the superficial zone ($p<0.0001$). The zonal distribution of sGAG in each animal is shown in Figure 14. All of the trends are the same, with the highest sGAG concentration in the superficial zone. In addition, the deep and middle zones were not significantly different from each other except in one animal (Leg 1, ($p=0.03$)) (Fig. 14i).

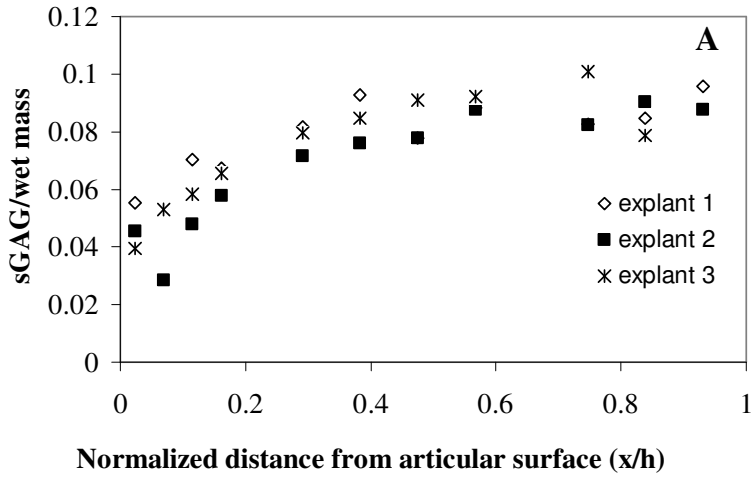

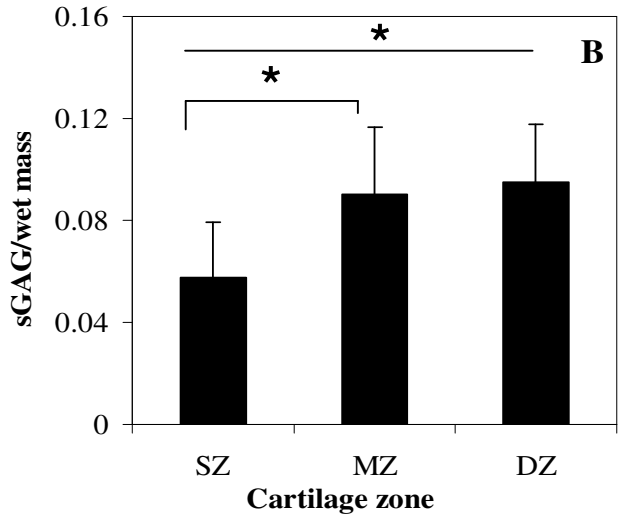

Figure 13: Distribution of sGAG contents, expressed per wet mass (mg/mg) in immature bovine cartilage. Cartilage samples were from 6-8 week old calves. A) sGAG/wet mass measurements from 3 sample explants as a function of distance from the articular surface. Distance is normalized to explant height. B) sGAG/wet mass averaged over all animals, n=24 cartilage explants (15-20 slices per explant). * ($p<0.05$) denotes significantly different from superficial zone; Values presented as mean ± SD

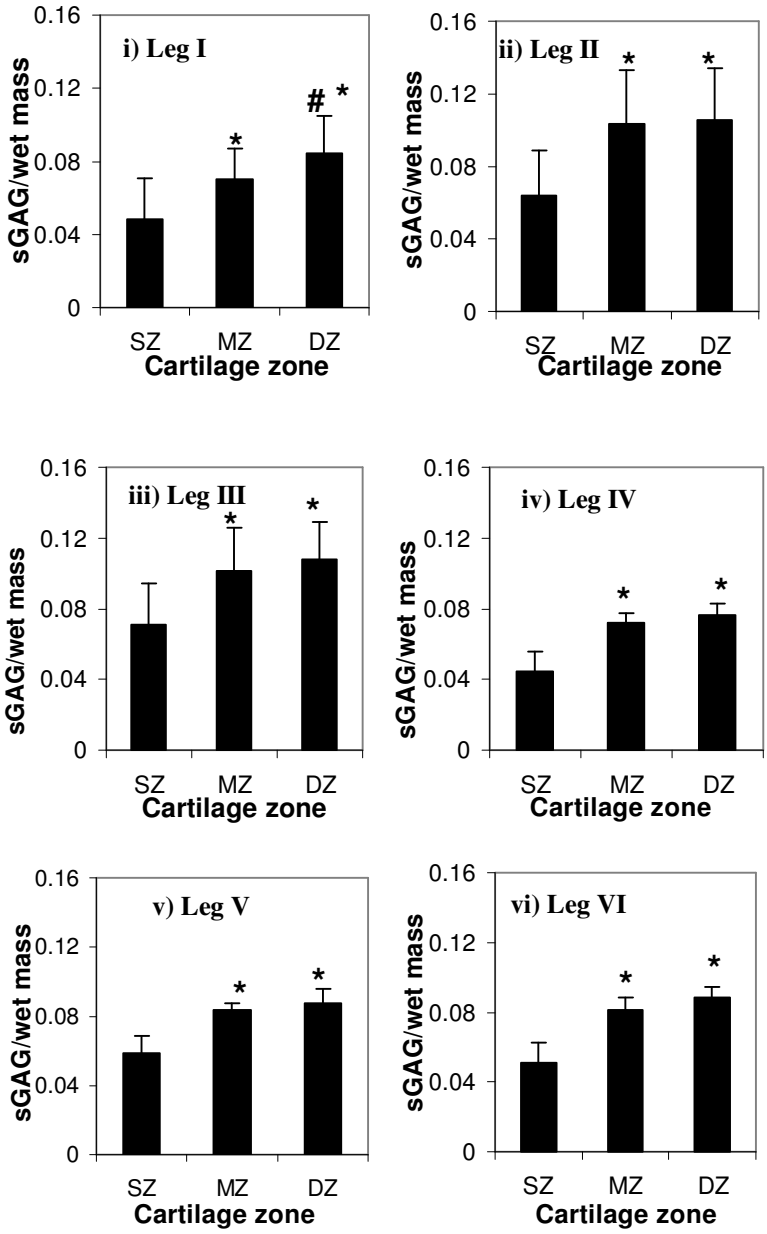

Figure 14: Zonal dependence of sGAG/wet mass contents in the six immature bovines (Leg 1-VI). n=3-5 cartilage explants per animal (15-20 slices per explant). (i)-(v) mean sGAG/wet mass for each animal * ($p<0.05$) denotes significantly different from superficial zone, #($p<0.05$) denotes significantly different from middle zone Values presented as mean ± SD

Mean collagen content (averaged across all animals) in the middle zone was higher than in the superficial zone ($p=0.0001$) and the deep zone ($p<0.0001$), although

the superficial and deep zones were not significantly different from each other (p=0.41) (Figure 15B). The depth-dependent distribution of collagen (Fig 15A) shows a similar trend: an increase in collagen concentration from surface to middle layers followed by a subsequent decrease in concentration in the deep zone regions. Figures 16(i-vi) shows the mean collagen contents in each animal: the middle zone had the highest collagen content across all the animals. Collagen content in mature human articular cartilage has been reported to be highest in the superficial zone and lowest in the middle zone which is contrary to the results presented here. It may be collagen distribution may be specie-dependent. Indeed, in an investigation of the relationship between bovine cartilage biomechanical properties and matrix composition, collagen content was measured in the first 1mm of the explants (only superficial and middle zones)(5). Those results showed an increase in collagen content from the superficial to the middle zone, thus supporting the results of this study.

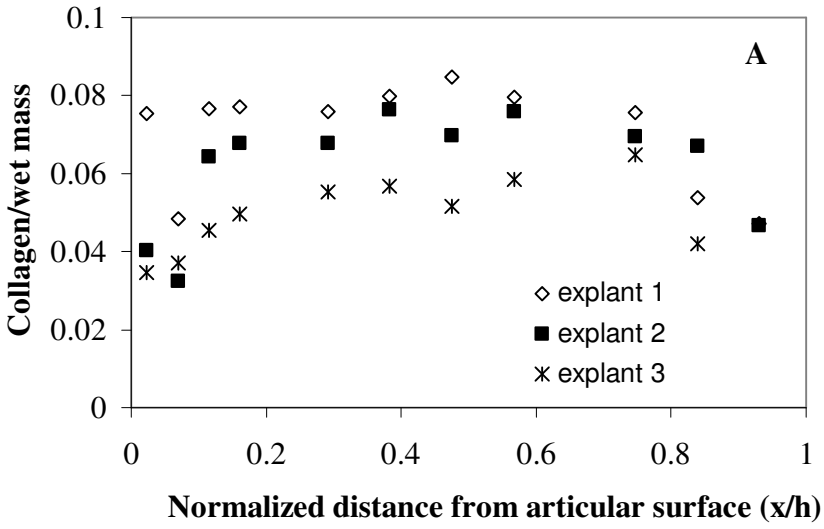

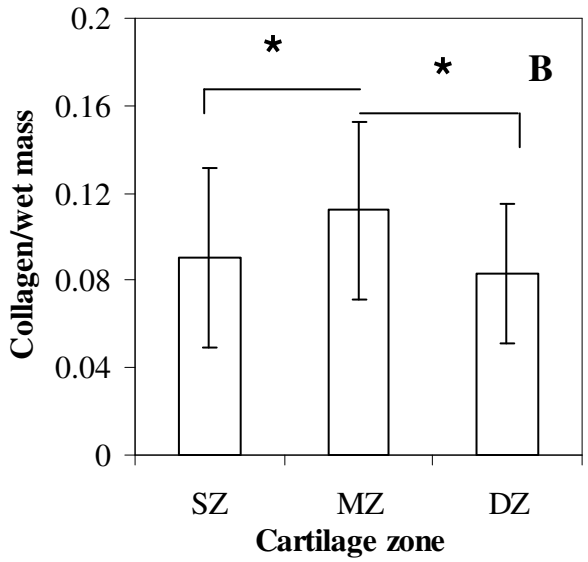

Figure 15: Distribution of collagen contents, expressed per wet mass (mg/mg) in immature bovine cartilage. Cartilage samples were from stifle joints of 6-8 week old calves. A) collagen/wet mass measurements from 3 sample explants as a function of distance from the articular surface. Distance is normalized to explant height. B) Collagen/wet mass of the different cartilage zones averaged over all animals, n=24 cartilage explants (15-20 slices per explant). * ($p<0.05$) denotes significantly different from superficial zone; Values presented as mean ± SD

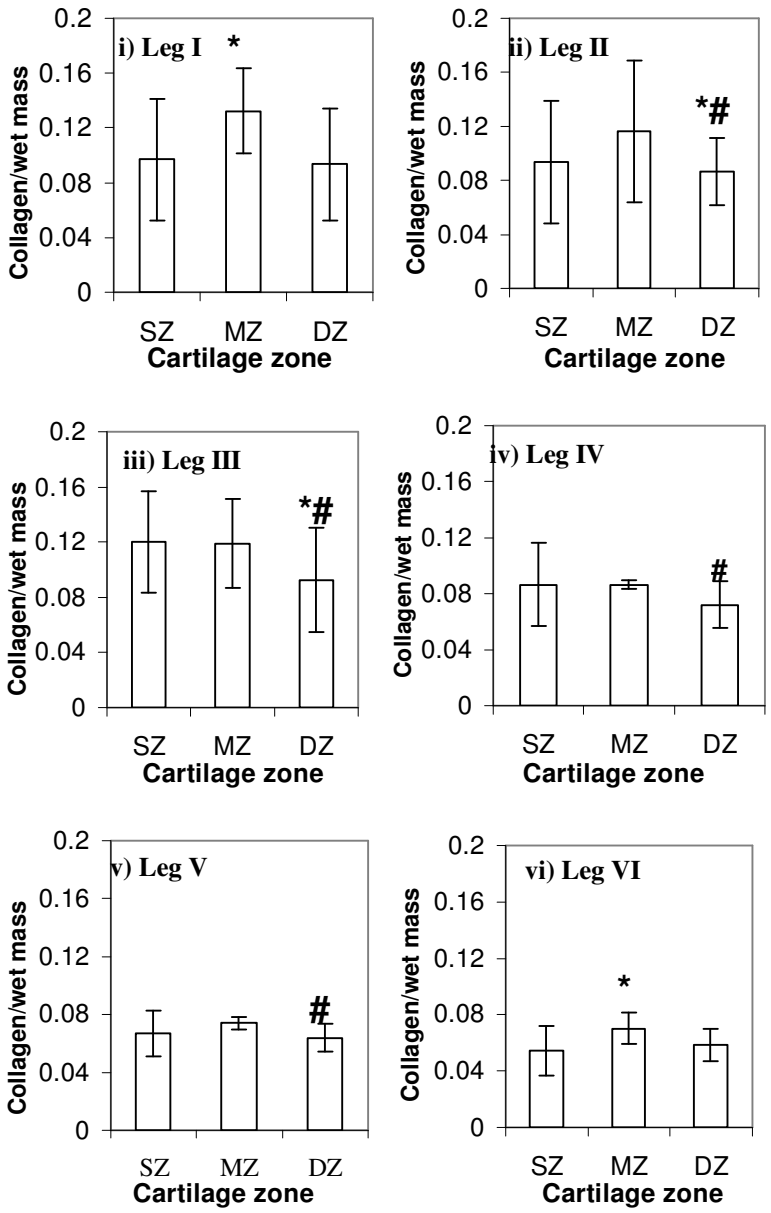

Figure 16: Collagen contents of the different cartilage zones expressed per wet mass. n=3-5 cartilage explants/animal (10-20 slices per explant); (i)-(vi) are mean values in each animal. * indicates significantly different from superficial zone, # indicates significantly different from middle zone. Significance is at $p<0.05$.Values presented as mean ± SD

Water fraction was calculated as the difference in wet and dry weight per tissue wet weight and ranged between 74-84% for entire tissue (Figure 17). Both graphs

illustrated the decrease in water content from the superficial to the deeper layers. The water content in the superficial zone was higher than in the middle ($p<0.0001$) and deep ($p<0.0001$) zones but the middle and deep zones were not significantly different from each other ($p=0.36$). This trend was seen in each animal (Figure 18). However in Leg IV, the middle and deep zones were found to significantly different from each other ($p<0.05$). There were no water fraction data for Leg I-III as the samples were too small and could not be weighed accurately after being lyophilized.

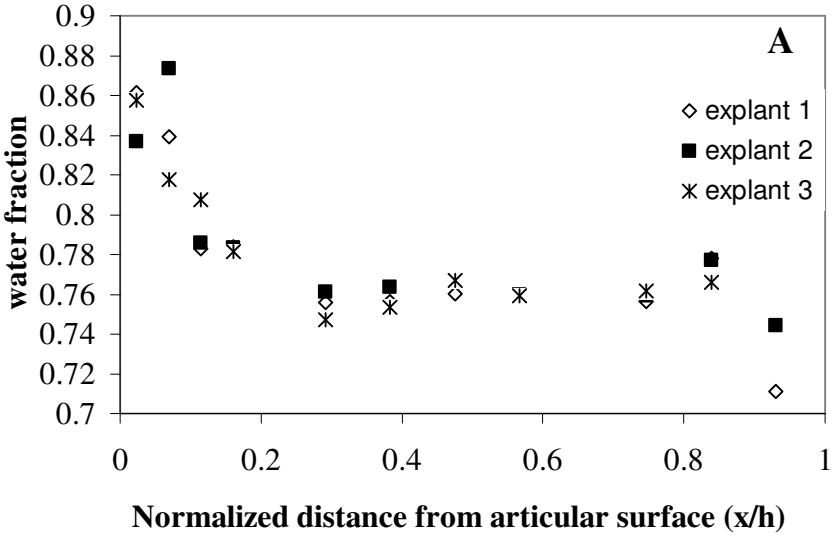

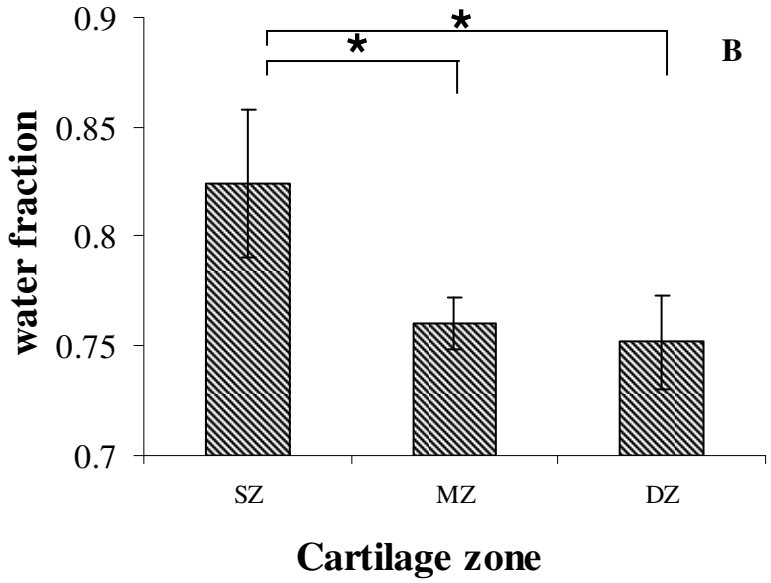

Figure 17: Distribution of water, expressed per wet mass (mg/mg), as in cartilage. Cartilage samples are from 6-8 week old calves. A) Water fraction measurements from 3 sample explants as a function of distance from the articular surface. Distance is normalized to explant height. B) Water contents of the different cartilage zones averaged over 3 animals, n=9 cartilage explants (10 slices per explant). * ($p<0.05$) denotes significantly different from superficial zone; Values presented as mean ± SD

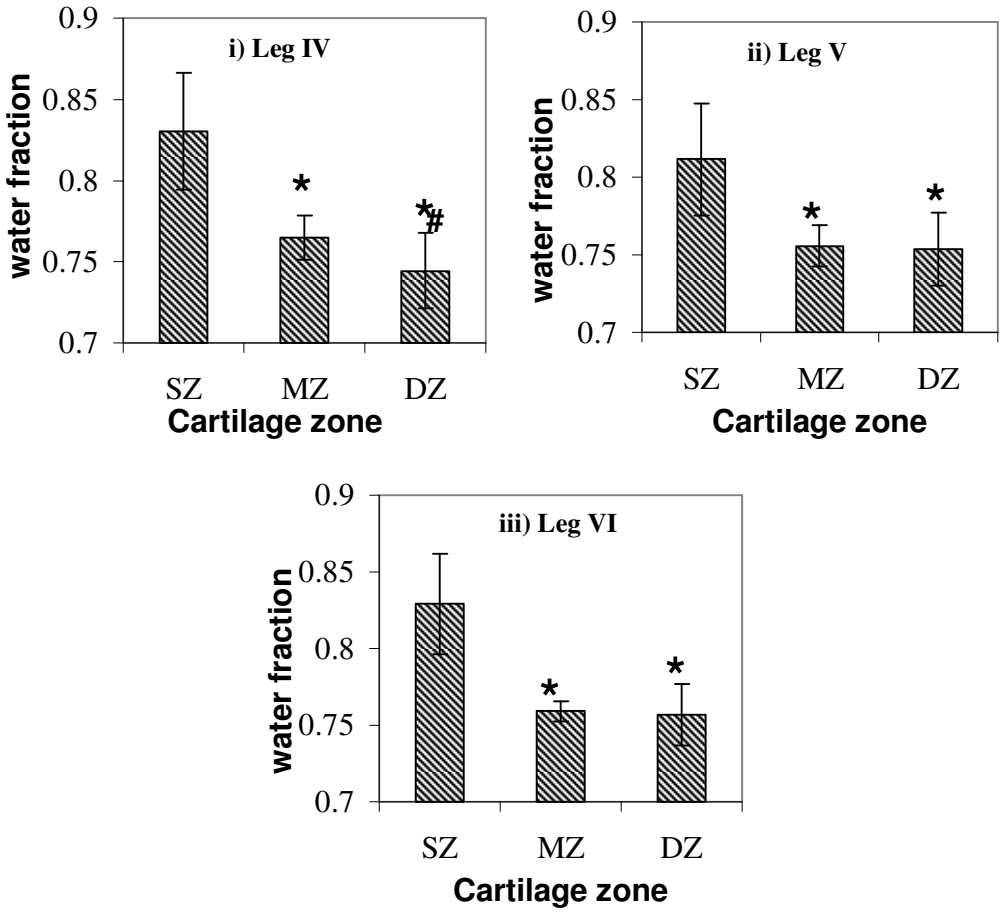

Figure 18: Fractional water content of the different cartilage zones. n=3 explants for each animal/ 10 slices per explant (i)-(iii) Mean water fractions of each animal. * denotes significant difference from superficial zone ($p<0.05$); # denotes significant difference from middle zone ($p<0.05$). Values presented as mean ± SD

4.3.2 Cartilage diffusion measurements:

FRAP experiments were performed on 4kda FITC-dextran-labeled cartilage with measurements taken at various depths within the different cartilage zones and at different orientations. Diffusivities were subsequently estimated from the FRAP image data using the 1-D DDSPE model. Below are typical images from the FRAP experiments before

bleaching (t-), immediately after bleaching (t0) and some time during the recovery period (t+) (figure 19).

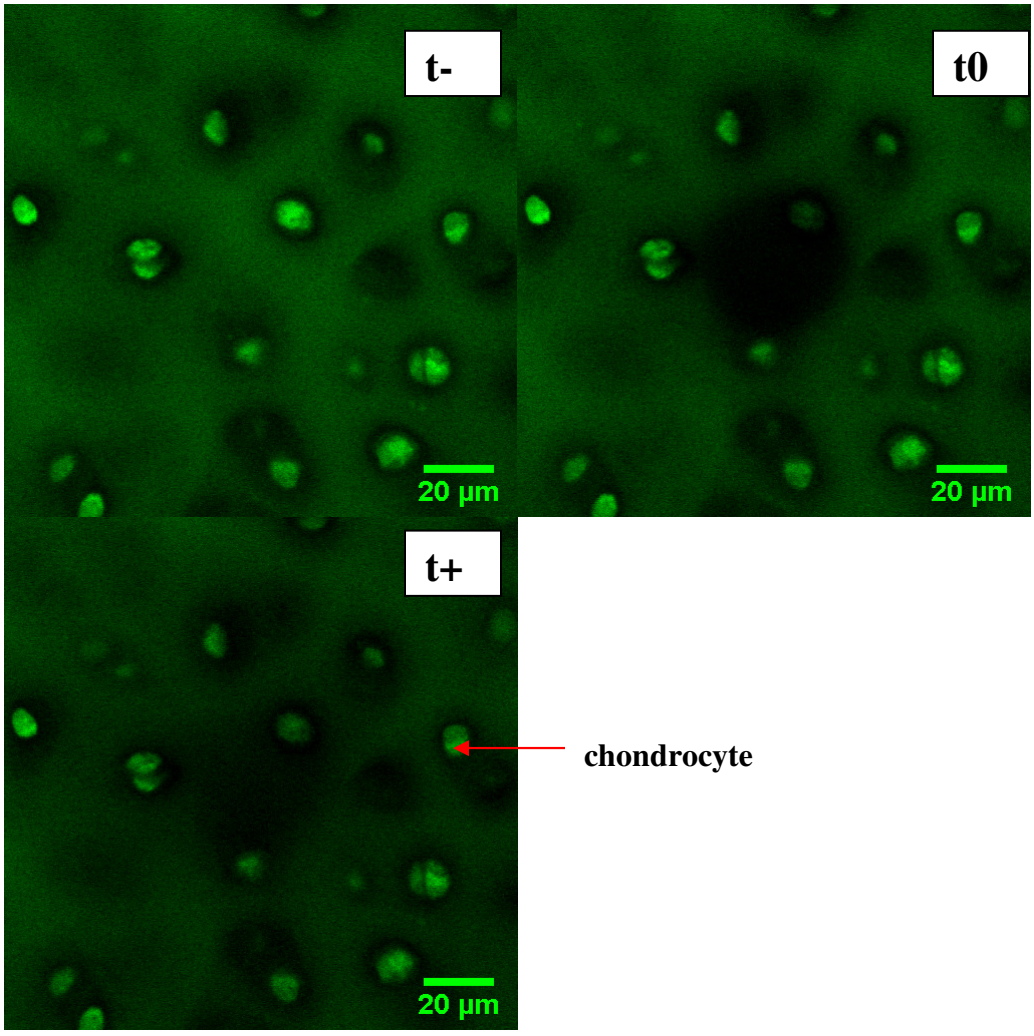

Figure 19: Confocal micrograph of fluorescently-labeled cartilage sample at different time points during a FRAP experiment (100X). t- is before bleaching, t0 is just after bleaching and t+ is sometime during recovery. Bright colored structures are chondrocytes surrounded by a dark pericellular matrix.

The bleach spot is seen in the center of the t0 & t+ images shown above (Figure 19). The chondrocytes can be observed to be at a much brighter intensity. It appears that the pericellular matrix (i.e. the dark-colored bands around the cells) was excluding the

fluorescent dye. This observation helped to elucidate the complexities of modeling matrix diffusion. The pericellular matrix, as mentioned earlier, has made up of network of collagen fibers and proteoglycans and is reported to have a much lower permeability than the surrounding ECM. Thus, it serves as a "boundary" around the cells, effectively reducing solute flux into or out of the cells. This resistance to solute movement creates a concentration gradient between the cells and the extracellular matrix. It is also noteworthy that there are other dark structures dispersed within the matrix.

Effect of freezing on diffusivity measurements

Figure 20 shows the transverse diffusivity measurements taken in the cartilage middle zone of the same samples labeled right after harvest and 3 days after a freeze-thaw cycle. The measured diffusion coefficients were 5.35 $\pm$0.73$\mu m^2/s$ and 4.17$\pm$0.53$\mu m^2/s$ for the fresh and thawed samples, respectively (mean $\pm$ SD). There was not a significant difference between the diffusivities measured in the fresh and thawed samples ($p=0.21$). To determine the effect of freezing on a sample by sample basis, Student t-test was used to compare the measurement obtained before and after freezing each sample. Only one sample showed a significant difference between the fresh and thawed conditions ($p<0.05$) (not shown).

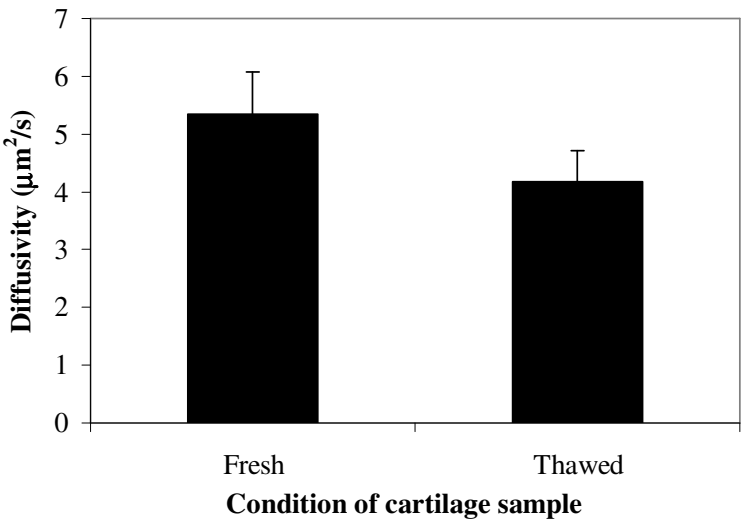

Figure 20: Effect of freezing on estimated diffusivities. n=3 cartilage samples (5 measurements per sample); p=0.21

Zonal- and depth-dependence of diffusivity measurements

Transverse diffusivity as a function of depth in two sample cartilage explants (Leg I) is shown in Figure 21(A). For comparison between explants, the distance of each cartilage slice from the articular surface (x) was normalized to the total height of the specific cartilage explant (h). Measured transverse diffusivity was highest at the articular surface (~12$\mu m^2/s$ at the surface) and was observed to decrease significantly with depth. Deep layer transverse diffusivities for both explants were less than 6$\mu m^2/s$. There was an abrupt decrease in the measured diffusion coefficients from the surface (first 10-15%) to the middle region. Furthermore, the trend of the diffusivity profiles seems to indicate that there were no substantial changes in the value of the transverse diffusivity as one moved from the mid to the deeper layers.

For easier interpretation and comprehension of results, measured diffusivities were presented as zonal diffusivities. Briefly, diffusivities measured in the first 15% of the explant thickness were averaged and assumed to be representative of superficial zone diffusivities. In the same vein, diffusion coefficients measured in the next 30-70% of the cartilage thickness were regarded as middle zone diffusivities and the last 30% as deep zone diffusivities. Measured radial and transverse diffusivities exhibited zonal dependence as shown in Figure 21(B). Radial diffusivities measured in the superficial, middle and deep zones were 34.0±1.22$\mu m^2/s$, 1.11±0.48 $\mu m^2/s$ and 1.16±0.41 $\mu m^2/s$ respectively (mean ± SEM). For the radial orientation, the diffusion coefficients measured in the superficial zone were significantly higher than those in the middle ($p<0.0001$) and deep ($p<0.0001$) zones although radial diffusivities in the middle zones and deep zones were not significantly different from each other ($p>0.05$).

Transverse diffusivities followed this same trend with diffusivities in the superficial layer significantly higher than those in the middle ($p<0.0001$) and deep ($p<0.0001$) layers and with middle and deep zone diffusivities that were not significantly different from each other ($p=0.83$). Mean transverse diffusivities for the superficial, middle and deep zones were 10.6±0.47$\mu m^2/s$, 5.43±0.20 $\mu m^2/s$ and 5.12±0.25 $\mu m^2/s$, respectively (mean ± SEM). For relative comparison among animals all radial and transverse diffusivities measured for each animal were averaged for each zone and normalized to the transverse diffusivity in the middle zone of the specific animal (Fig 22 (i-vi)). In general for each animal, the trends were consistent with Fig. 22B, with higher radial diffusivities than transverse diffusivities. In addition, the highest diffusivity values were invariably within the superficial layer.

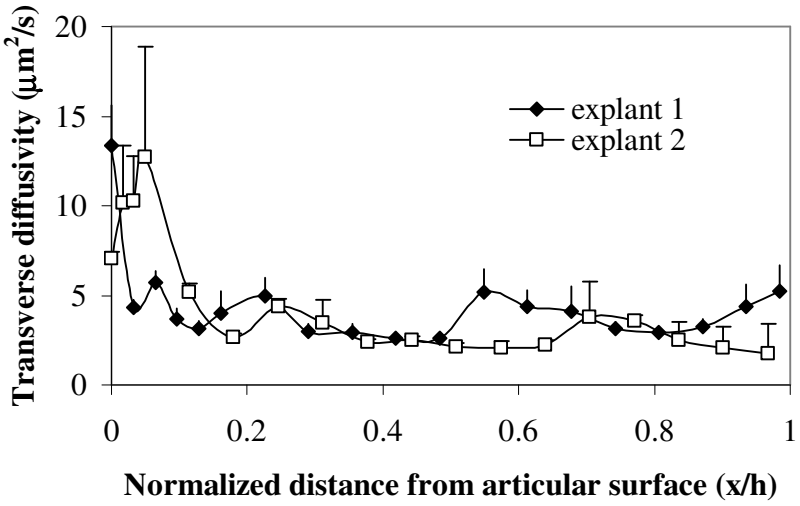

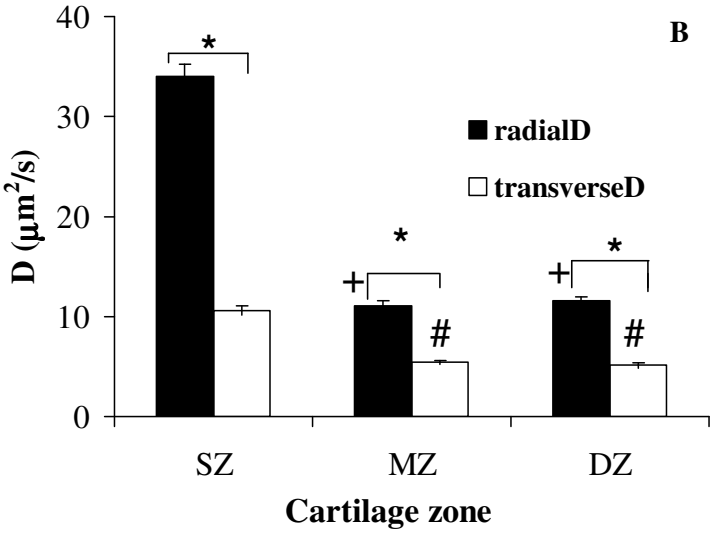

Figure 21: Diffusivity profiles of 4kDa dextran within articular cartilage. A) Transverse diffusivities measured in sample explants as functions of normalized depth from the articular surface. B) Radial and transverse diffusivities in the different cartilage zones (superficial (SZ), middle (MZ) and deep (DZ)) averaged over all six animals. + indicates significant difference from superficial radial D. # indicates significant difference from superficial transverse D. * indicates significant difference ($p<0.05$).n=23 cartilage explants (20-25 slices per explant, 5-9FRAP measurements/slice)

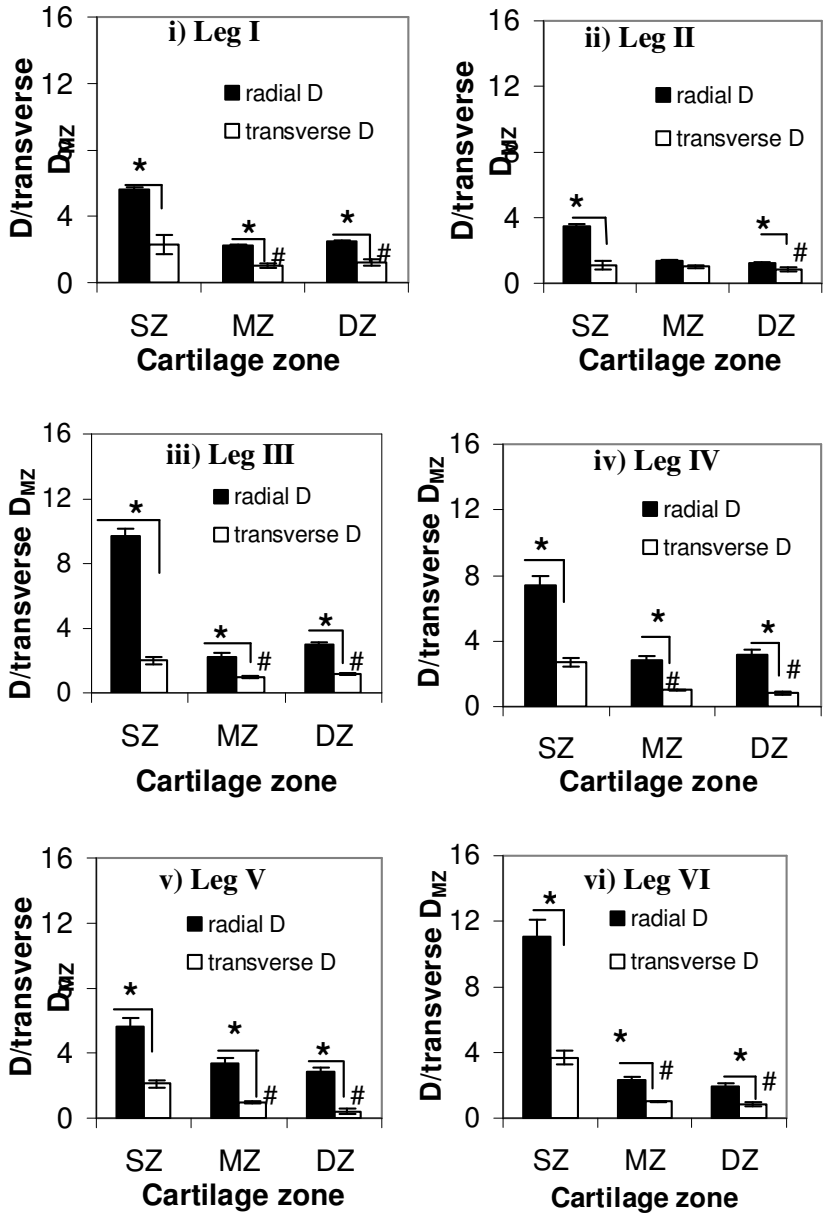

Figure 22: Diffusivity of 4kda FITC-dextran in the different cartilage zones (superficial (SZ), middle (MZ) and deep (DZ)) and in radial and transverse orientations. Radial D and transverse D represent radial and transverse diffusivities respectively. (i)-(vi) Mean diffusivities normalized to transverse diffusivity in the MZ for each animal. n=3-5 cartilage explants/animal, 20-25slices/explant, 5-9 measurements/slice. * indicates significant difference, # indicates significant difference from superficial transverse diffusivity ($p<0.05$). Values are expressed as mean ± SEM.

Effects of tissue orientation

The diffusion coefficients determined from the radial slices were compared to diffusivities measured in the transverse slices. Radial diffusivities were much higher than transverse diffusivities in each zone and for all animals ($p<0.0001$) (Figure 21B). Mean Diffusional anisotropy (DA) values defined as the ratio of the radial to transverse diffusivities in each zone are presented in figure 23. To compute the DA values, transverse and radial diffusivities in each zone were averaged for each cartilage explant. The ratio of the mean radial diffusivity to the mean transverse diffusivity was calculated for each zone. Thus, for the 23 cartilage explants used in this study, there were a total of 23 DA values for each zone resulting in 69 measurements. Mean DA values for the superficial, middle and deep zones were 3.42±1.48, 2.46±0.93 and 2.47±1.15 respectively. The mean value of DA in the superficial zone was significantly higher than in the middle zone ($p<0.02$) and the deep zone ($p=0.037$) (Figure 23). The value of DA was lowest in the middle zone was not significantly different from that in the deep zone ($p>0.1$).

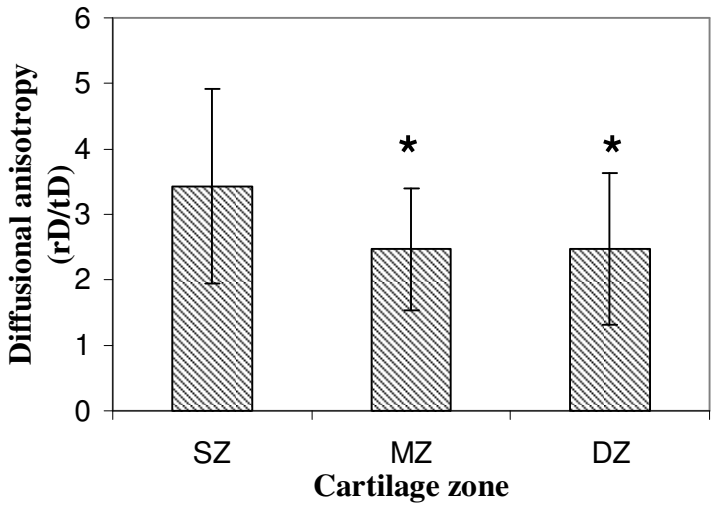

Figure 23: The ratio of radial to transverse diffusivities (diffusional anisotropy) of each cartilage zone expressed as mean ± SD. * indicates significantly different from superficial zone ($p<0.05$). n=23 cartilage explants, 20-25slices/explant, 5-9 measurements/slice.

4.3.3 Relationship between diffusivities and biochemical content: Statistical results

To determine the relationship between the measured diffusivities and biochemical components, mean diffusivities were calculated per zone for each of the 23 cartilage explants used for these experiments, resulting in 69 measurements. Likewise, sGAG, collagen and water contents determined from individual tissue slices were pooled and average values were calculated per cartilage zone for each of the 23 cartilage explants. Subsequently, correlation analysis was performed on the measured diffusivities, sGAG, collagen and water contents. High correlations between independent variables may induce multicollinearity in the model and could weaken the statistical validity and hence the interpretation of the results.

For the 23 cartilage explants, the independent variables used to predict the variation in the diffusivities were sGAG/wet mass and collagen/wet mass. To begin with,

no significant correlation was found between sGAG/wet mass and collagen/wet mass (r = 0.2, p=0.07).There were no significant correlations between collagen/wet mass and radial diffusivity (r = -0.02, p=0.85) (Fig 24A) or transverse diffusivity (r=0.072 and p=0.55) (Fig 24B). sGAG per wet mass was negatively and significantly correlated with radial diffusivity (r =-0.306, p=0.011) (Fig 25A) but was not significantly correlated with transverse diffusivity (r=-0.164, p=0.178) (Fig. 25B).

Of the 23 cartilage explants mentioned above, explant water content could only be measured in nine of them (Legs IV-VI). sGAG and collagen contents measured in these explants were also normalized to dry mass. Therefore, the independent variables were sGAG/dry mass, collagen/dry mass and water fraction. To ensure the significance of the statistical tests, correlations between the independent variables was examined (Fig. 27). Results showed that water fraction and sGAG/dry mass were not significantly correlated with each other, r = -0.34, p=0.082. However, there were significant correlations between water and collagen/dry mass (r = 0.5, p=0.007) and between collagen/dry mass and sGAG/dry mass (r = -0.427, p=0.026). The correlation coefficients between sGAG per dry mass and the radial and transverse diffusivities were -0.48 (p=0.011) and -0.326 (p=0.097) respectively (Fig. 28). There also appeared to be significant correlations between collagen/dry mass and both radial (r = 0.387, p=0.046) and transverse (r = 0.43, p = 0.025) diffusivities (Fig. 29). Furthermore, fractional water content was found to be positively correlated with radial and transverse diffusivities with r values of 0.69 (p<0.0001) and 0.763 (p<0.0001) respectively (Fig. 26).

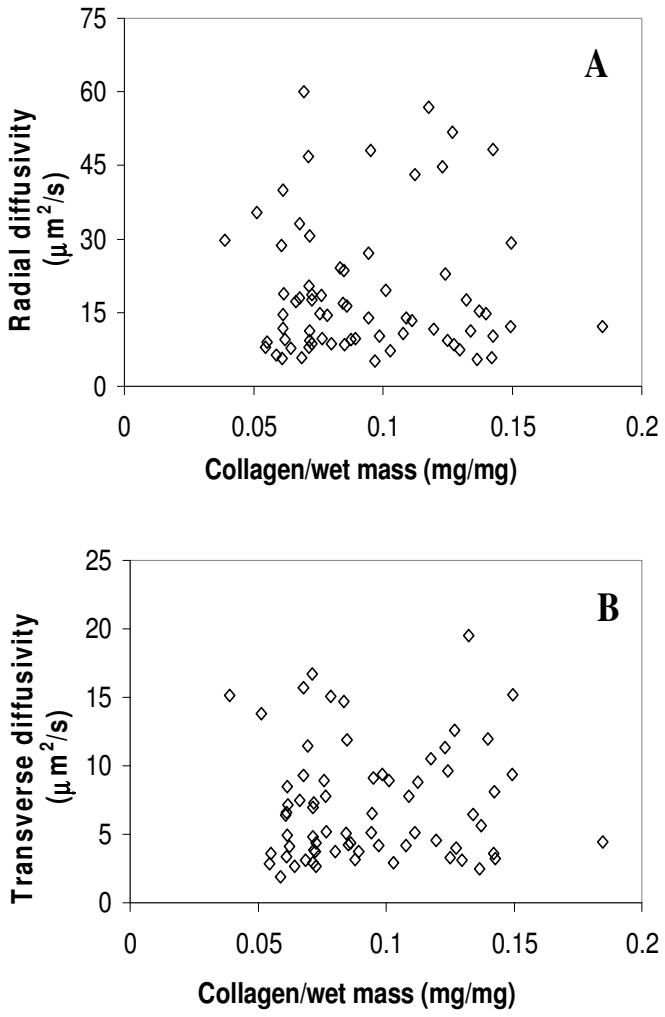

Figure 24: Diffusivity as a function of collagen per wet mass. A) Radial diffusivity values are plotted against corresponding collagen per wet mass values for the same cartilage explants. B) Transverse diffusivities as a function of collagen content. There is no correlation between collagen and either of the two diffusivities ($p>0.05$).n= 23 cartilage explants.

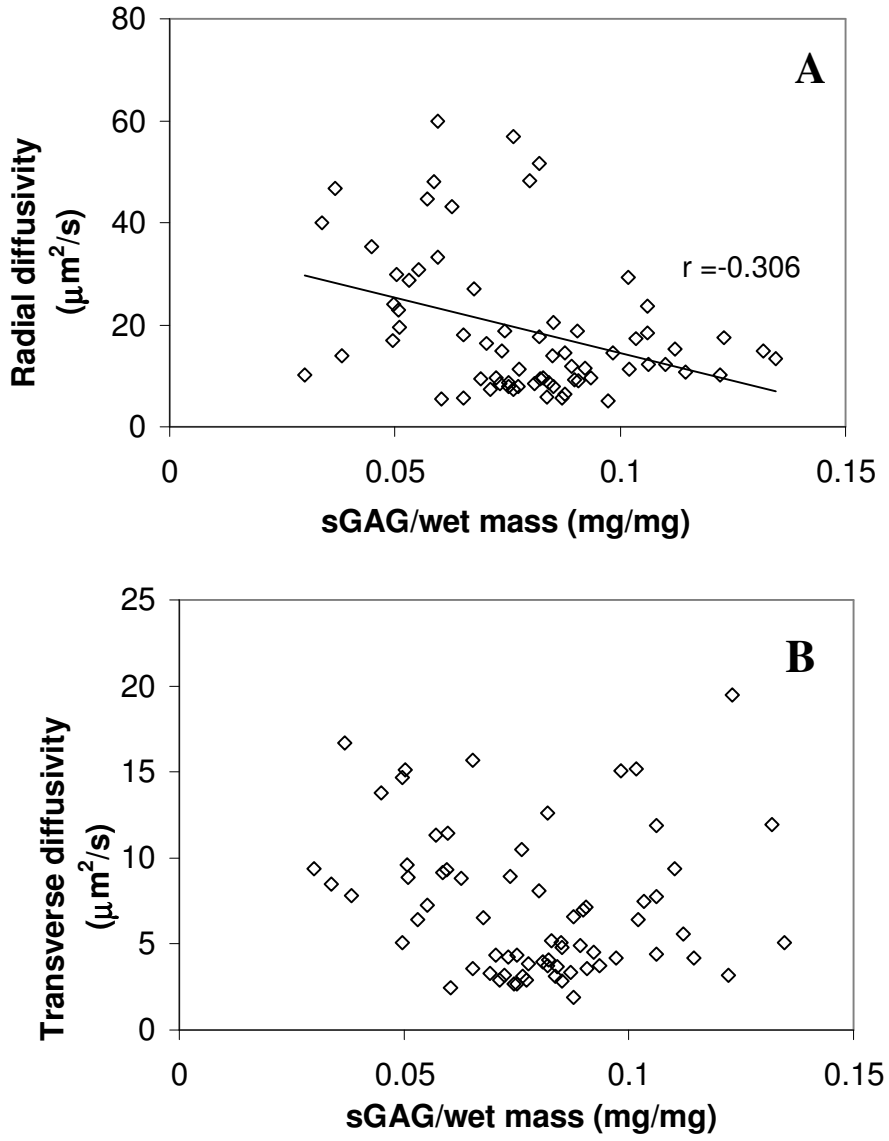

Figure 25: Diffusivity as a function of sGAG content. A) Radial diffusivity values are plotted against corresponding sGAG per wet mass values for the same cartilage explants. B) Transverse diffusivities as a function of sGAG content. Both radial ($p<0.05$) and transverse ($p>0.1$) diffusivities show negative correlation of sGAG content. n= 23 cartilage explants.

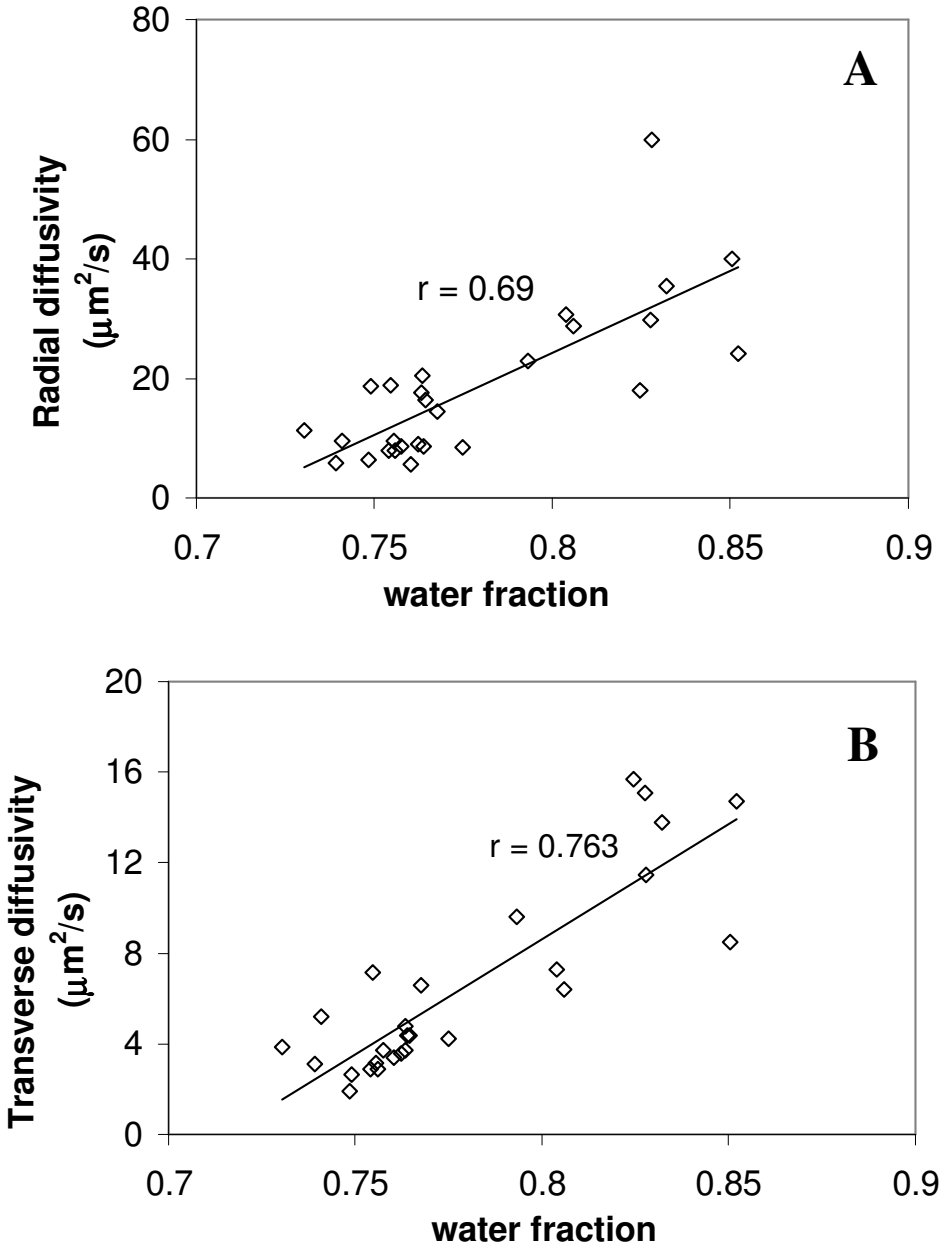

Figure 26: Diffusivity as a function of the water content of cartilage explants. A) Variations in radial diffusivity as a function of cartilage water fraction and B) Transverse diffusivity as a function of water fraction. Both correlations were significant ($p<0.05$). n= 9 cartilage explants (10 slices per explant).

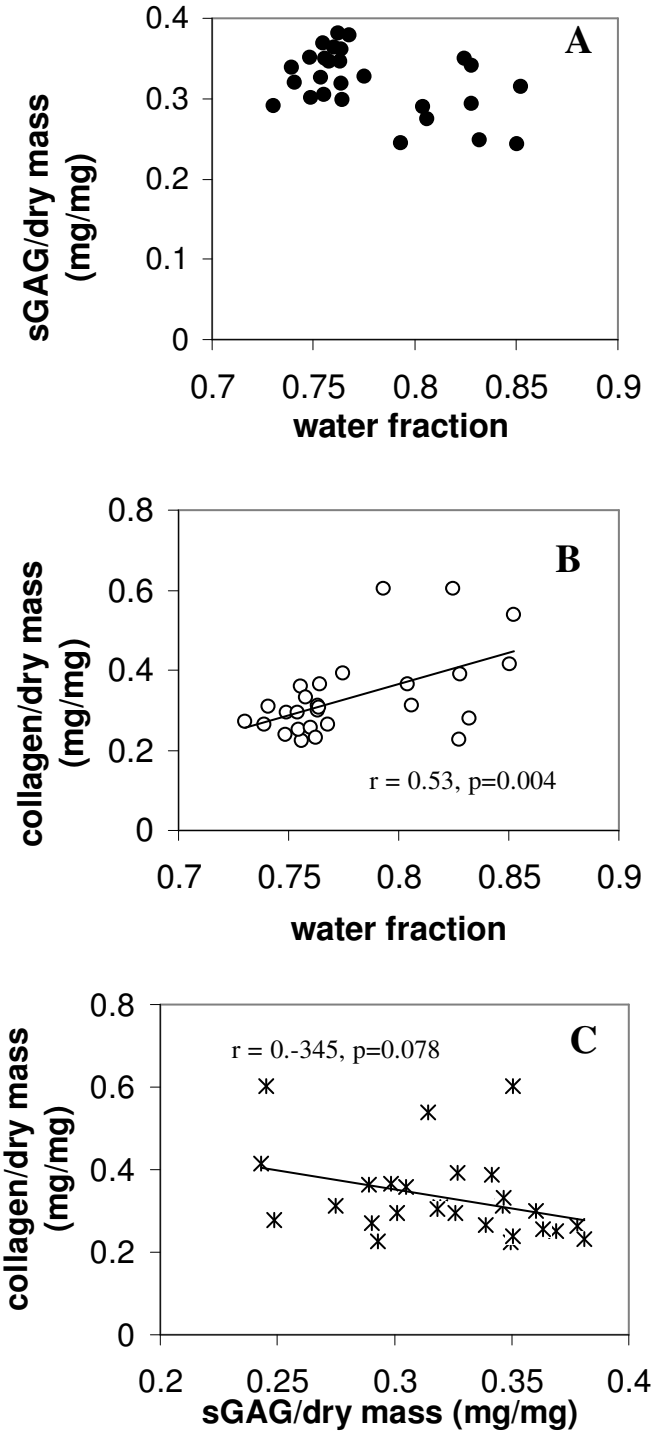

Figure 27: Relationship between the biochemical components. A) Correlation between fractional water content and sGAG/dry mass; B) Correlation between fractional water content and collagen/dry mass; C) Correlation between collagen/dry mass and sGAG/dry mass. Apart from sGAG/water correlation, all the other correlations are significant. n=9 cartilage explants, 10 slices/explant

Consequently, multiple regression models were developed to test the predictive ability of the independent variables. For all 23 cartilage explants, radial and transverse diffusivities were regressed on sGAG/wet mass and collagen/wet mass. For radial diffusivity, the regression coefficients for sGAG and collagen were -0.316±0.119 (p=0.01) and 0.0475±0.119 (p=0.693) respectively. For transverse diffusivity, the regression coefficients for sGAG and collagen were -0.188±0.123 (p=0.13) and 0.113±0.123 (p=0.36) respectively. The adjusted R-square values for radial and transverse regression equations were 6.8% and 1% respectively. In addition, for the subset of 9 cartilage explants, radial and transverse diffusivities were regressed on sGAG/dry mass, collagen/dry mass and water fraction. For radial diffusivity, the regression coefficients for water, sGAG and collagen were 0.614±0.165 (p=0.001), -0.29±0.15 (p=0.07) and -0.046±0.171 (p=0.78) respectively. For transverse diffusivity, the regression coefficients for water, sGAG and collagen were 0.722±0.157 (p <0.0001), -0.064 ±0.149 (p=0.673) and 0.038±0.163 (p=0.81) respectively. The adjusted R-square values for radial and transverse regression equations were 48.6% and 53.4% respectively. Subsequently, radial and transverse diffusivities were regressed on water, sGAG/dry mass and collagen/wet mass. For radial diffusivity, the regression coefficients for water, sGAG and collagen were 0.588±0.145 (p<0.001), -0.33±0.14 (p=0.034) and -0.07±0.14 (p=0.60) respectively with an adjusted R-square of 54.6%. For transverse diffusivity, the regression coefficients for water, sGAG and collagen were 0.786±0.137 (p< 0.0001), -0.046 ±0.141 (p=0.746) and 0.034±0.134 (p=0.79) respectively with an adjusted R-square of 59%. All regression coefficients are reported as mean ± SD. All figures were plotted with raw data (not ranked data).

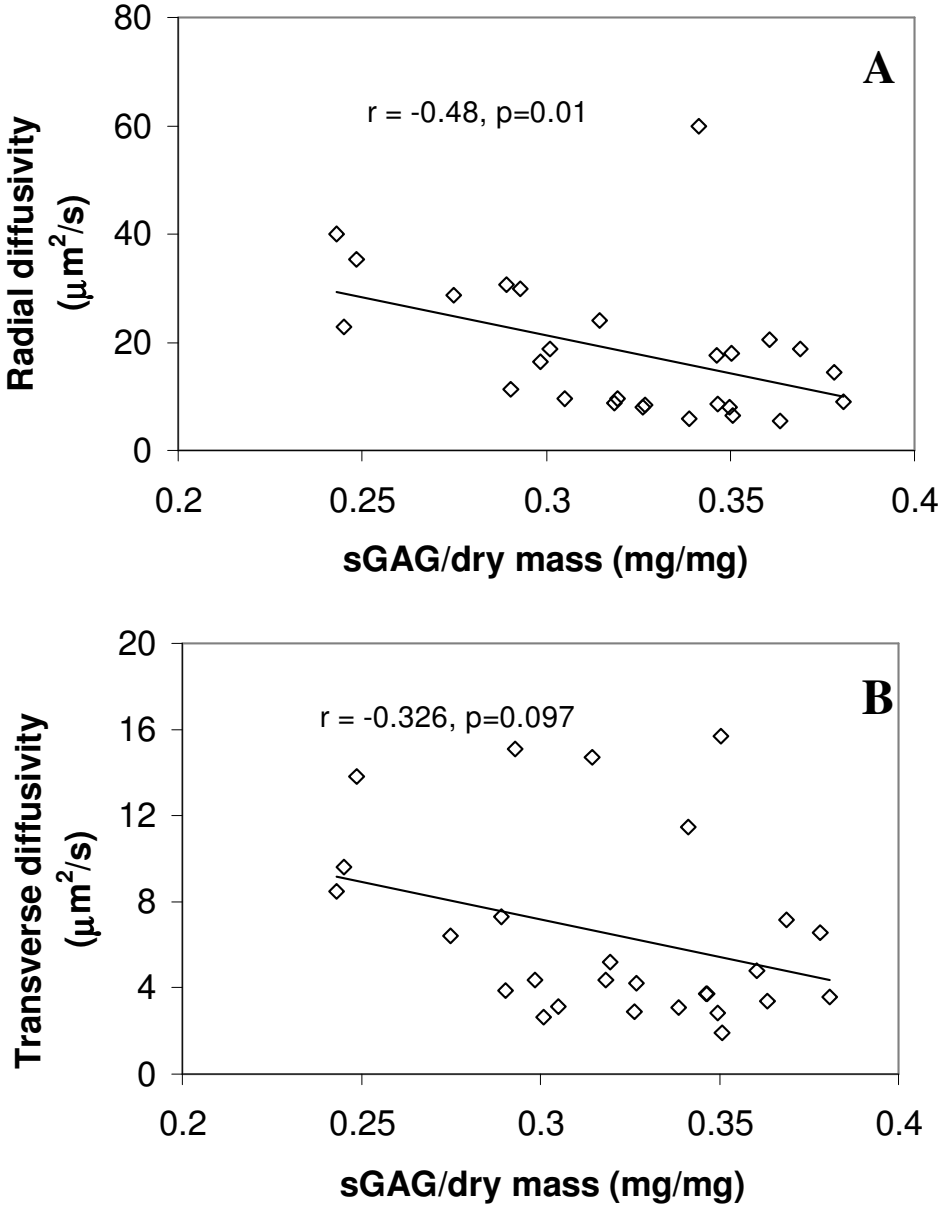

Figure 28: Diffusivities as a function of sGAG per dry mass (mg/mg). A) Variation in radial diffusivity as a function of sGAG per dry mass. B) Dependence of transverse diffusivity on sGAG per dry mass. n=9 cartilage explants, 10-20 slices per explant, 5-9 FRAP measurements per slice. Significant correlation coefficients have $p<0.05$.

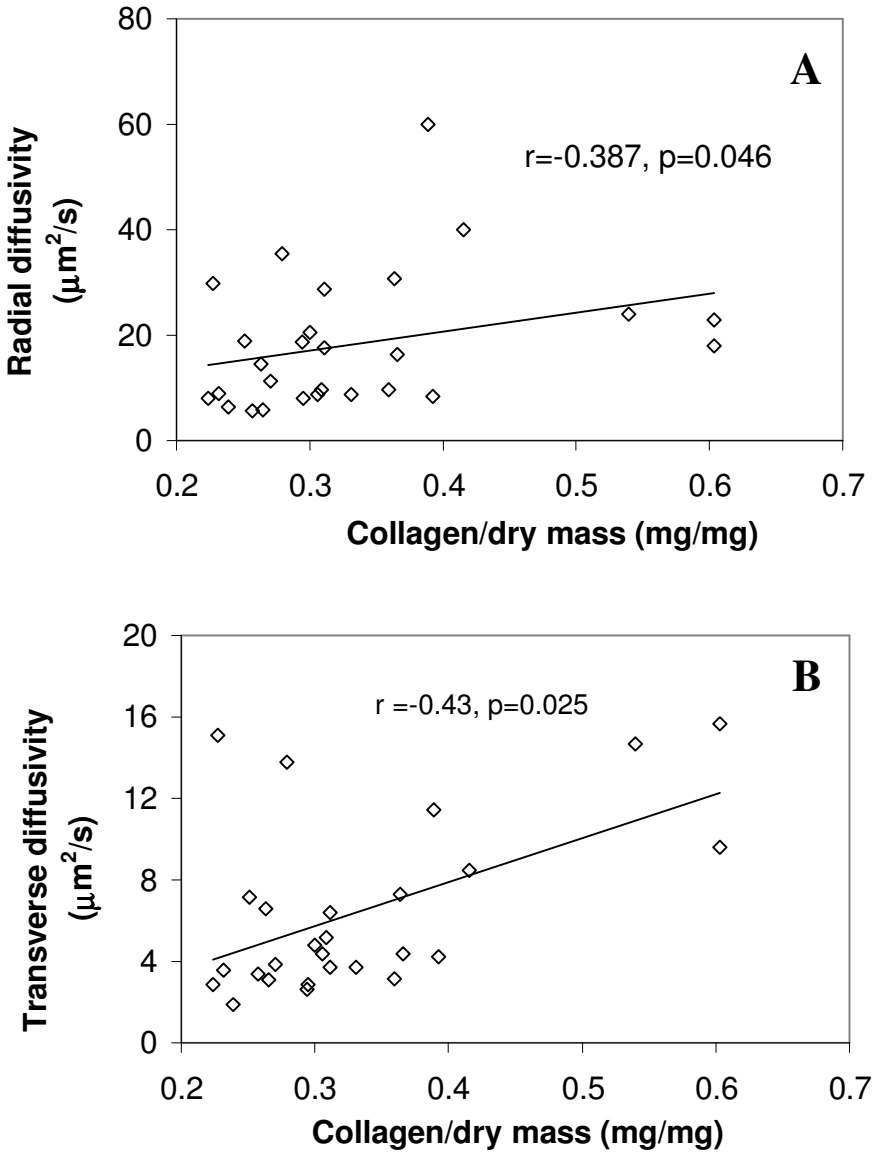

Figure 29: Diffusivities as a function of collagen per dry mass (mg/mg). A) Variation in radial diffusivity as a function of collagen per dry mass. B) Dependence of transverse diffusivity on collagen per dry mass. n=9 cartilage explants, 10-20 slices per explant, 5-9 FRAP measurements per slice. Significant correlation coefficients have $p<0.05$.

4.4 DISCUSSION

In this study we have obtained cartilage diffusivity profiles with high spatial resolution by measuring diffusion coefficients at microscopic length scales. The measured diffusivity profiles are spatially resolved to within 100μm, which is much finer than the current gold standard in diffusion mapping, MRI diffusion tensor imaging. This detailed diffusion distribution map allowed the determination of the roles of water, sGAG and collagen in solute diffusivity within the matrix. In addition, our use of a much larger solute (4kDa) than water was pivotal to the detection of matrix anisotropy and the differentiation between zones.

The characterization of ECM composition in immature bovine articular cartilage, as done in this study, yielded results that were in agreement with the current literature. We measured sulfate content, which should have a one to one ratio to sGAG content which in turn is a measure of proteoglycan content and fixed charge density (FCD). sGAG was found to increase significantly from the surface to the deep layers (Fig 13-14).

Prior to choosing specific bleach parameters - bleach spot radius of 20.3μm and 100 bleaching iterations - for these studies, pilot experiments were performed to optimize the FRAP experimental protocol. It was extremely difficult to bleach cartilage because of its high optical density and light scattering properties. As a result, several scanning iterations were required to obtain a significant bleach depth within the samples. Furthermore, with small bleach spots, there was greater variability in the values of the diffusivities derived from the same slice. Smaller bleach radii will yield highly localized diffusivities resulting in average diffusivities that are not representative of the slices in

question. Moreover, larger bleach spots with radii at least twice the radius of the cells may lessen the effect of the cells on the measured diffusivity.

Furthermore, in the diffusion experiments for all of the cartilage studies, the data sampling rate was approximately 2Hz (one image every 0.5secs). Subsequent analysis on sample images revealed that for diffusivities less than 45$\mu m^2/s$, sampling frequency can be reduced to as low as 0.2Hz without introducing significant errors to the parameter estimation process. Although decreasing the sampling rate may not shorten the experimental times, it will greatly decrease data volume and cut simulation times.

Freezing and repeatability experiments were performed to validate our experimental methods. As shown in figure 20, mean solute diffusivity (averaged over three samples) derived from the fresh tissue (before freezing), 5.35±0.73$\mu m^2/s$, was not significantly different from the mean diffusivity measured after one freeze-thaw cycle, 4.17±0.53 $\mu m^2/s$ ($p = 0.21$). These results suggest that the diffusion measurements were not substantially affected by freezing of the tissue samples. However, multiple freeze-thaw cycles could change the structure of the tissue and subsequently influence diffusivity results so samples were subjected to only one freeze-thaw cycle. Analysis on a sample by sample basis showed that one sample seemed to have been affected by freezing. Larger sample size may be required to test the actual effect of freezing. Nevertheless, all samples were treated equally so it is unlikely that any significant variability was introduced in the measurements.

In addition, repeatability was evaluated through five sequential measurements on 4kDa FITC-dextran at the same spot on a cartilage slice from the middle zone. The diffusivity determined using the DDSPE method was found to be 4.99±0.83$\mu m^2/s$,

indicating good repeatability of the experimental and analytical procedures (figure not shown) even in the heterogeneous tissue samples. This implies that the relative % error for the diffusivity estimates obtained in these experiments is approximately 17%.

In general, diffusivities in the radial direction were found to be higher than those in the transverse direction and diffusivities were found to be higher in the superficial zone than in any other part of the cartilage matrix. The prevailing view is that the synovial fluid is by far the greatest source and contributor to cartilage nutrition. Brower et al(77) studied diffusion pathways in immature and mature rabbit knee joints by injecting dyes into the bloodstream and joint space. When the synovial fluid was isolated from the articular cartilage surface, it was found that, regardless of the age of the animal, there was negligible diffusion between the cartilage matrix and the underlying bone. They also investigated the effect of time on the dye intensity and reported that the deep zone was the last layer to be cleared of the dye. This result is an indication of either one of two things: the rate of diffusion is much slower in the deep zone than in the superficial zone or diffusive exchange is mostly through the superficial zone so the deep layers, being the furthest away, are the last to be cleared. In either case, these findings support the results of our study and suggest that nutrients or solutes most likely diffuse radially from the synovial fluid in the knee joint through the superficial to the deep zones.

It is important to compare the diffusivities measured in these studies to those obtained by other researchers in various cartilage diffusion experiments. The samples used in this investigation were of two orientations: radial and transverse. As mentioned earlier, radial slices were full-depth strips cut normal to the articular surface while

transverse slices were obtained by cutting parallel to the articular surface (Figure 11). Thus, both radial and transverse diffusivities were measured in this study.

However, it is important to explain the physical interpretation of the term "radial diffusivity" as used in these studies. The diffusivities measured in the radial slices is actually an average diffusivity that can be resolved into 2 directions. Thus, radial diffusivities reported here likely have a transverse component. Therefore it is possible that one-dimensional (uni-directional) diffusivity normal to the articular surface could be higher than the values reported here. This also will likely have an effect on the measured diffusional anisotropy (DA). If the estimated "radial" diffusivities are lower than the actual values, then DA values will be underestimated.

In the other cartilage diffusion studies using solutes in the same size range as the 4kDa used in these experiments, all reported diffusivities were in the radial direction. Our results showed that radial diffusivities decreased from 34$\mu m^2/s$ in the superficial zone to 11$\mu m^2/s$ in the deep zone. Using radiolabeled solutes, Torzilli et al.(40, 78) measured the diffusivity of inulin (5kDa) in full-depth adult bovine cartilage as 92$\mu m^2/s$ and the diffusivity of 10kDa dextran in immature bovine cartilage as 509$\mu m^2/s$. Nimer et al.(43) estimated the diffusivity of inulin in adult human cartilage (middle zone) as 18$\mu m^2/s$. All three studies estimated the diffusivities from concentration-distance curves. In addition, using the FRAP technique, Leddy et al(44) measured the diffusivity of 3kDa dextran in mature porcine cartilage and found that it decreased from 100 $\mu m^2/s$ in the superficial zone to 60 $\mu m^2/s$ in the deep zone. Also, Quinn et al(48) measured the diffusivity of 3kDa dextran in middle zone bovine cartilage (at 8% static compression) as 30 $\mu m^2/s$. These widely varying diffusivity values may be as a result of the different

animal species used, dissimilar measurement techniques and the assumptions on which the analytical models were based. Apart from the FRAP study, most of the other diffusion experiments assumed that diffusion was one-dimensional. In addition, it is noteworthy that the diffusivities measured in the aforementioned studies were all macroscopic measurements and so could differ from the microscopic diffusivity measurements obtained in the present investigation.

Both radial and transverse diffusivities were found to decrease significantly with depth. Previous studies using diffusion tensor imaging showed that the mean diffusivity of water in canine and human articular cartilage decreased from the superficial zone to the deep zone by up to 50%(74, 79, 80). It should be noted that in these studies the diffusivities are averaged within a control volume. In our experiments, mean radial diffusivity decreased from the superficial to the deep zone by 67% while mean transverse diffusivity decreased by 50% from the superficial to the deep zone. To fully explain this decrease in diffusivity with increasing distance from the articular surface, the relationship between the diffusivities and ECM composition was examined. It is noteworthy that correlation between variables (both dependent and independent) does not imply a cause-and-effect relationship nor is it a sufficient measure of the variables' predictive abilities.

As collagen was correlated with both sGAG and water, it was important to check for multicollinearity or serious correlation between these independent variables. A major indicator of multicollinearity is that the calculated regression coefficients vary substantially when an independent variable is added or subtracted from the model including changes in the signs of the coefficients. Another measure of multicollinearity is

the variable inflation factor (VIF). VIF values greater than 10 indicate a serious problem with correlation between the independent variables. However, the VIF values of all the independent variables (water, sGAG and collagen) were less than 1.6. The R-square in the predicted model could be improved by taking principal components instead of original variables. We decided against that since the meaning of the principal components would not be clear and they may not have a physical interpretation.

The positive correlation between collagen per dry mass and diffusivity is most likely due to the correlation and relationship between collagen and water content. Indeed, in cartilage, water is reported to be in two different compartments – between the collagen fibrils or outside of the collagen fibrils(43). Hence, the terms intrafribrillar and extrafibrillar water are often used to describe the water contents of the different compartments. Thus, water content is closely associated with collagen content. However, normalizing collagen to water content appeared to drastically reduce the correlation between collagen and water.

Therefore, another regression model was developed by using less-correlated variables to ascertain the significance of the estimated regression coefficients. Water fraction, collagen/wet mass and sGAG/dry mass were used. Correlation tests on these variables yielded p values that were all greater than 0.1. Both water and sGAG were found to have statistically significant coefficients of 0.58 and -0.33 respectively in the regression equation for predicting radial diffusivities. However, the only significant predictor variable for transverse diffusivity was the water fraction (coefficient =0.78).

The true implications of these results are that if sGAG content and all other variables were held constant, a unit increase in water content will result in a 58% increase in radial diffusivity and conversely, if water content were held constant a unit increase in sGAG will result in a 33% decrease in radial diffusivity. Similar interpretation will hold true for the transverse diffusivity. Ensuring constant tissue composition, however, is a difficult thing to achieve. Nevertheless, from these results, we can infer that of the matrix components examined in this study, water is the best predictor of solute diffusivity in both orientations.

The finding that transverse diffusivity is not a function of sGAG content suggests that GAG molecules are not randomly organized but have some preferred orientation. If the glycosaminoglycan chains were randomly organized, it would hinder solute diffusion in both orientations in a similar fashion. Indeed, it has been suggested that the GAG molecules, as a result of their close association with the collagen fibrils, will be oriented along the axis of the fibrils(81). Moreover, hydraulic permeability, which has been shown to be a function of matrix proteoglycan content, was observed to be anisotropic in compressed middle zone articular cartilage but remained isotropic in compressed agarose gels(82, 83). Since the GAG molecules are much smaller than the collagen fibrils, it could be that any anisotropy associated with the GAG chains will be undetectable during macroscopic transport measurements.

Other researchers had postulated based on their data that GAG molecules hindered solute diffusivity via steric exclusion(21, 23, 40, 84). Based on our results, we believe that this indeed might be the case. The solute used in this study (4kDa FITC-

dextran) has an effective hydrodynamic radius of about 2nm. The spacing between the GAG chains is reported to be between 3-4nm(85). Solute mobility and hence diffusivity, will likely be hindered by the presence of the GAG chains. Furthermore, as the water content of the matrix increases, diffusing solute molecules experience less frictional drag (due to the interaction between the fluid molecules and the ECM) resulting in higher diffusion coefficients within the matrix. Water also acts as a solvent modifying the rigid structure of solid solutes into more flexible liquid phases that diffuse more easily through the tissue.

However, tissue water content is a measure of the volume or spacing available for molecular transport within the tissue and therefore is indirectly related to matrix structure. Volpi and Katz(20) reported that collagen fibril packing density decreased from the articular surface to the deep zone of bovine femoral head cartilage with the steepest decline seen in older animals. This gradient in packing density may account for the differences in water content amongst the zones. Nevertheless, given that collagen fibrils also increase in diameter from the superficial (20nm) to the deep (70-120nm)(10), a solute will likely experience greater restriction to its motion in the deep zone when compared to the superficial zone. Larger fiber diameters are a greater physical obstruction to the transport pathway and result in increased frictional drag force on the solute because of the increase in surface area. However, we did not see any significant correlation with diffusivity and collagen content because differences in fibrillar arrangement and thickness do not necessarily correlate to differences in content.

Moreover, the coefficients of determination for the regression models indicate that the ECM components under investigation (sGAG and water) contribute to only 54% and 59% of the radial and transverse diffusive resistance (or conductance) in the cartilage matrix respectively. Other variables that could account for the remaining 40% of the variation in diffusion include the cartilage matrix structure and tissue cell volume.

It is worthy of mention that previous studies have assumed that cells have a negligible effect on diffusion. Most of these experiments were done on non-viable tissue so cellular uptake was considered negligible. Also, considering the low cell volume fraction of adult cartilage (<3%)(16), cells were thought to have no influence on the macroscopic diffusion measurements. However, during the analysis of the results of this study, we found that cells (even non-viable) do impact microscopic diffusion measurements and consequently could affect the estimated diffusivities. As was shown in figure 19, chondrocytes are surrounded by a pericellular matrix (PCM) that is about 2-6μm in width. Immature cartilage has about twice the cellularity of mature cartilage(86). The PCM has been reported to be significantly less permeable than the ECM substantially reducing solute flux through the matrix by as much as a factor of 30(13). At microscopic length scales, cells and the PCM will have a significant effect on solute transport. Thus it is probable that a steep increase in cell volume might increase the effective diffusion time of a solute within the matrix (Chapter 6 has a detailed description of the effect of the cells on the parameter estimation process).

If the matrix structure and fiber architecture strongly modulates transport, it is expected that the collagen fibers will affect diffusion uniquely in the different zones as a

result of the dissimilarity in fiber orientation amongst the zones. Furthermore, fiber alignment should result in diffusional anisotropy as diffusivities parallel and perpendicular to the run of the fibers are likely to differ. Indeed, we found that diffusional anisotropy (DA), i.e. the ratios of the radial to the transverse diffusivities, was zone-dependent: it was higher in the superficial zone than in the middle or deep zones but the middle and deep zones were not significantly different (Figure 23). Diffusional anisotropy values for the superficial, middle and deep zones were 3.4±1.4, 2.46±0.93 and 2.47±1.1 respectively. Isotropic diffusion should have a DA value of 1 and the more anisotropic the diffusion, the greater the deviation of DA from unity.

These results show that in skeletally immature cartilage, the zones are not as clearly demarcated as in the mature cartilage so the middle and deep zones are very structurally similar but differ significantly from the surface zone. The findings may also indicate that the collagen fibers in the deep zone are not as highly ordered as those in the surface zone. It may be that the blood vessels which pervade the deep zone of immature cartilage disrupt fiber orientation and consequently modifies the tissue structure. Indeed, immature cartilage is reported to lack the structural features of deep zone cartilage(86) and to have tangentially oriented fibers in all its zones. The large DA value of the middle zone indicates that the fibers or molecules of the middle zone have a preferred spatial orientation. Indeed, it has been reported that both the collagen fibers in middle zone and the GAG chains in the cartilage matrix are not randomly organized but have preferred orientations (18) (83). These findings further support the claims that matrix structure modulates transport and the structural anisotropy of the matrix influences solute diffusion.

It is clear from the results of this study, that a single factor or variable cannot predict diffusion patterns in the matrix. Furthermore in some cases, these factors (composition and structure) have counteracting influences on solute transport. For example, the greatest hindrance to radial diffusion should have been in the superficial zone but this is mitigated by the decreased fibrillar diameter, increased fibrillar spacing, decreased sGAG content and increased water content of the superficial zone.

Implications of findings and Conclusions

In summary, we measured fine-scale diffusivities with a spatial resolution that was <<100μm creating a detailed profile of the distribution of diffusivity within articular cartilage. Hitherto, to the best of our knowledge, the immature articular cartilage ultrastructure has not been probed using a solute within the size range of several other physiological solutes. Solute diffusion in cartilage was found to be accurately modeled using Fick's Law as has been reported previously. The experimental results showed that diffusivities decreased from the articular surface to the deep zone correlating with the decrease of water content and increase in sGAG content through the depth of the cartilage matrix. However, we have shown that the gradients in solute mobility cannot be ascribed to matrix composition alone. Matrix ultrastructure is a highly significant contributor to solute diffusion within cartilage and has a greater influence on transport than does sGAG content. Furthermore, diffusion in cartilage was shown to be highly anisotropic in all the zones proving that the collagen fibrillar network (and possibly GAG network geometry) contributes to transport within this avascular tissue.

These results suggest that diffusion in cartilage is primarily regulated by the water volume fraction and the collagen fiber network. Diffusion models based solely on steric exclusion by the GAG chains are unable to accurately predict solute diffusivities. Thus, in the fabrication of tissue constructs to mimic native tissue, water content and the fibrillar architecture of the matrices should be foremost in the considerations to avoid impedance to nutrient transport. The balance has to be struck between engineering a construct with material properties that withstand high impact loads but enable the efficient transport of nutrients and growth factors.

Furthermore, the finding that the middle zone of articular cartilage is not isotropic should be taken into account during modeling of both mechanical and transport properties of the matrix. This also has implications when interpreting results from experiments using middle zone cartilage. In addition, the relationship between structure and diffusion as seen in the observation of diffusional anisotropy in structurally anisotropic matrices suggest that diffusion parameters can be used as indices to detect changes in structure due to disease or injury. This persistence of anisotropy in the tissue material properties could imply that it plays a role in maintaining the cartilage matrix physiological function of load support and joint lubrication.

Moreover, the 4kDa solute used in these experiments is similar in size to other solutes (e.g. insulin (5kDa), insulin-like growth factor-1 (7kDa)) that are candidates for intra-articular drug delivery to halt or reverse the progression of OA. In some cases, frequent intra-articular injections have been reported to cause inflammation of the joint space. Thus, knowledge of the diffusion coefficients and the concentration profiles of

these drugs within the matrix will aid in planning more controlled dose-response experiments. It may also aid in developing drug delivery strategies that will ensure that drugs get to the site of injury or disease before they are cleared from the synovial space.

Finally, knowledge of the diffusion rates and pathways of solutes in the ECM will provide more insight into cartilage matrix ultrastructure and consequently help in elucidating mechanisms of cartilage degeneration.

4.6 LIMITATIONS

One of the challenges faced during this study was with the determination of tissue water contents and the accurate correlation of biochemical composition with diffusivities. Samples obtained from half of the animals used in this study were too small for accurate measurement of dry weights. Therefore, ECM components had to be normalized to wet mass and the diffusivities were correlated to these normalized values. Biochemical quantification for these plugs was done on neighboring slices on the same explant. However for the other three animals, samples for biochemical quantification were site matched from adjacent explants. The latter explants had stronger correlations with ECM components when compared to those obtained from all six animals. Exact relationship between ECM components and diffusion coefficients will be best be obtained by using the same samples for both FRAP analysis and diffusion measurements.

In addition, only one solute (a 4kDa neutral dextran) was used in this study. It is possible that a few of the results obtained from these experimental studies might differ

for a charged solute or for a much larger solute. Burstein et al, using NMR, observed no differences in cation, anion and water diffusivities within calf articular cartilage. In contrast, Fischer et al used MRI to visualize the mass transport of small paramagnetic organic molecules and metal ions (CuEDTA, Cu^{2+}) through chicken knee femoral condyles and found that the binding interactions of the cations to the matrix significantly impeded transport through the matrix. However, the charges solutes used in the aforementioned studies were all had molecular weights less than 400Da. It may be that the effect of solute charge might become more apparent with larger solutes. Furthermore, solute-matrix binding interaction may spatially vary within the tissue and thus may have different effects on the diffusivities within each zone.

As there was no external loading, the contribution of convection was neglected in the overall transport of the 4kDa solute in immature cartilage. However, it is possible that the diffusing solutes could carry solvent water molecules along which could in turn draw in more solutes.

CHAPTER 5

SOLUTE DIFFUSION IN CARTILAGE SUPERFICIAL ZONE: DIFFERENCES BETWEEN IMMATURE AND MATURE TISSUE

5.1 INTRODUCTION

Articular cartilage superficial zone is known to be essential to the normal function of the tissue. Removal of the SZ was shown to reduce the underlying cartilage's load-bearing and fluid retention capacity(87). Scanning electron micrographs have shown distinct layers within the articular cartilage superficial zone: "a nonfibrous acellular layer, a fibrous layer and a tangential layer"(88) with collagen fibrils oriented parallel to the articular surface.

When intact, the superficial zone plays a vital role in joint lubrication because of its low coefficient of friction. As such, injury to this layer would lead to cartilage degeneration(88). Indeed, it is thought that disorganization of the collagen fiber architecture in the superficial zone triggers osteoarthritis in articular cartilage.

Furthermore, the superficial zone serves as an external barrier for the rest of the articular cartilage tissue and as a result may selectively determine the nature of solutes entering the matrix and the rate at which these solutes are transported from the synovial fluid or joint space to the remaining cartilage underneath.

Much has been written about the differences between the structural and mechanical properties of immature and mature cartilage but not much attention has been given to the effect of maturation on the matrix transport properties. Furthermore, there have been contradictory reports about the effects of age on matrix permeability and diffusivity(19, 78, 89, 90). It should be noted that the term "aging" is used in this work to denote progressive change from birth to senescence. Maturation is regarded as an aging process but represents the period between birth and adulthood (skeletal maturity). Thus, with respect to the work done in this study, maturation is aging but aging extends beyond the maturation period.

Previous studies have shown that solute transport and solute concentrations within cartilage decrease with the removal of the superficial layer(41, 50). Moreover, nutrients need to diffuse from the synovial fluid through the superficial layer to the rest of the cartilage matrix, particularly in adult cartilage where subchondral nutrition is thought to be non-existent. In addition, reduced nutrition is thought to be one of the primary causes of matrix degeneration. Therefore, in this study, we investigated the role of maturation in cartilage solute transport by comparing the diffusivities of 4kda fitc-dextran in the superficial zone of immature and mature bovine articular cartilage. The experiments in this chapter were done on only mature bovine articular cartilage and the results were compared to the data already obtained from the immature cartilage.

5.2 MATERIALS AND METHODS

5.2.1 Tissue Harvest and Sample Preparation

Using a drill press and a bone saw, eighteen (18) full-thickness cartilage explants (attached to the subchondral bone) were excised non-sterilely from the medial femoral condyles of 6 right stifle joints of mature (2year-old) bovines within 24 hours of slaughter. The cartilage explants were subsequently peeled off from the bone using a #22 scalpel. A brief description of the sample preparation methods will be made here as a detailed description of the methods is in the previous chapter. The height of each explant was measured using digital calipers and subsequently, each cartilage explant was cut axially in the anterior-posterior plane into two hemi-cylinders producing a flat vertical plane perpendicular to the articular surface. The anterior-posterior plane divides the condyle into medial and lateral halves. The average thickness of the explants is 1.1 ± 0.15mm. Prior to sectioning, each hemi-cylindrical cartilage explant was embedded in OCT compound. Subsequently, using a freezing-stage microtome (HM 450, Microm, Germany), each explant was sectioned to produce three 50µm-thick slices parallel to the articular surface (transverse slices) corresponding to the superficial zone and the other half was sectioned into 100µm-thick slices perpendicular to the articular surface (radial slices). A total of 5 radial slices were obtained from each cartilage explant. All samples were placed in phosphate buffered saline (PBS) to prevent tissue dehydration.

Tissue samples to be used for FRAP experiments were labeled by immersing the slices in 0.2mg/ml of 4kda FITC-dextran dissolved in PBS solution for 2 days at 4^{o}C to allow for maximum permeation and equilibration of the solute in the matrix. Protease inhibitor cocktail set 1 (used in 1X concentration) was added to the labeling solution to

prevent tissue degradation. Cartilage explants were excised from adjacent sites for biochemical quantification.

5.2.2 FRAP Experiments

FRAP experiments were performed on a LSM 510 laser scanning confocal microscope (Zeiss, Germany) using a 63X /1.2 N.A water objective with a 25mW Argon laser. All photobleaching was performed at 488nm emission at 100% laser power. All imaging was done with a (75%) 25mW Argon laser at 1% power with excitation at 488nm and emission recorded above 505nm. Three to five FRAP experiments were performed on each transverse slice, while for the radial slices, three spots on the cartilage superficial zone were bleached. The radius of the bleached spot on all tissue samples was 20.3μm. For each radial slice, diffusion measurements for the superficial zone were taken 75-90μm from the articular surface.

5.2.3 Biochemical quantification

Tissue samples were weighed wet, lyophilized, weighed dry, and digested in 1mg of Proteinase K (in 100mM of ammonium acetate) per 80 mg of tissue. Samples were placed in an oven at 60^{o}C overnight. Sulfated glycosaminoglycan and collagen contents of the tissue samples were measured using the DMMB dye and the chloramine-T/pDAB assays as detailed in the preceding chapter.

5.2.4 Histochemical staining of mature articular cartilage

Tissue samples from were fixed in 10% neutral buffered formalin for 24hours per mm of thickness of tissue at room temperature. After fixation, the tissue samples were rinsed several times in PBS and subsequently dehydrated in 70% ethanol until ready for paraffin embedding. 5µm slices were sectioned from the tissue paraffin blocks using a rotary microtome. Overall matrix morphology was visualized using the Haematoxylin & Eosin (H&E) stains.

5.2.5 Statistical Analyses

All statistical analyses were done using Minitab Release 12.23 (Minitab Inc). Radial and transverse diffusivities from both age groups were analyzed using the General Linear ANOVA model where age and orientation were the two fixed factors and diffusivity was the response variable. Tukey's test for pair-wise comparisons was used for both age and orientation terms with a 95% confidence interval. Student's t-test was used to test the difference between the diffusional anisotropy data obtained from the immature and mature cartilage explants. Statistical significance for all tests was set at α=0.05

5.3 RESULTS

The immature cartilage samples were much thicker than the mature samples with a mean thickness of about 6.53 ± 1.05mm compared to a thickness of 1.1 ± 0.15mm. Younger cartilage samples had a vascularized appearance especially at the cartilage-bone interface while there was no evidence of vasculature in the older animals. The immature cartilage explants were crisp and easy to cut while the older explants appeared to be fibrous.

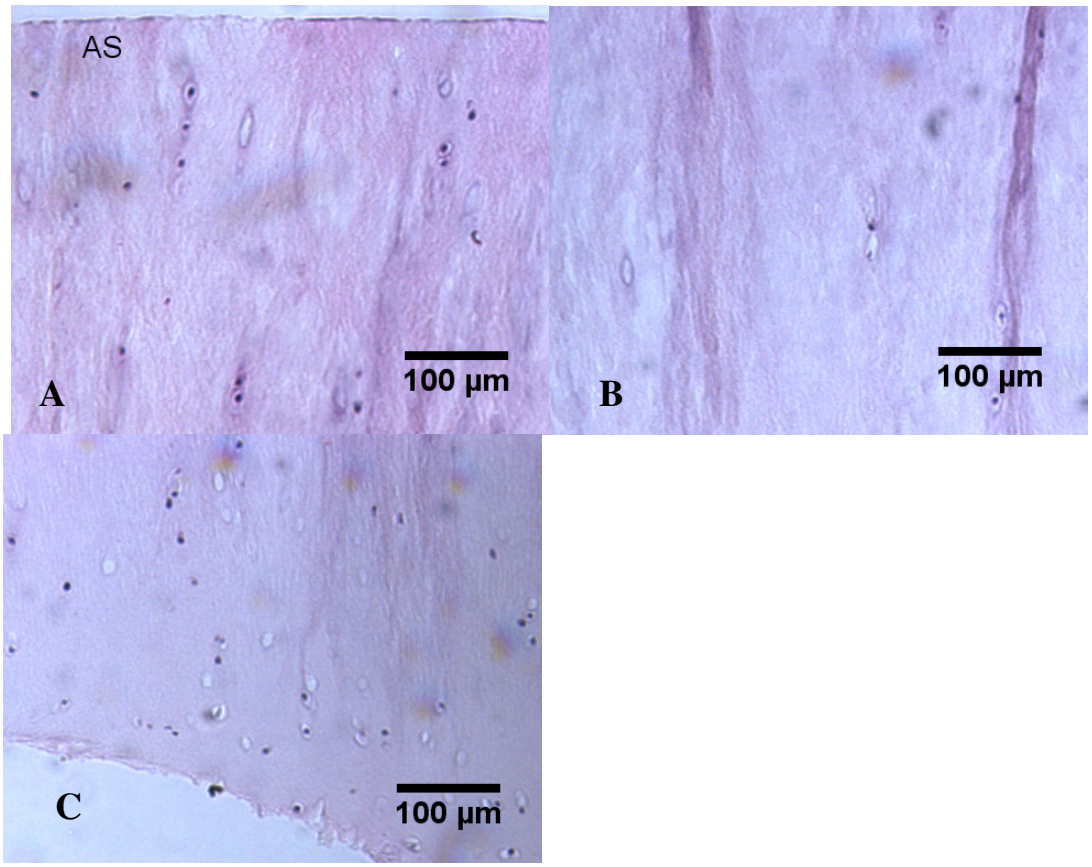

Figure 30: Light micrographs of H&E stained 2 year-old bovine cartilage sample (10X) depicting the various cartilage zones. Depicted are A) Superficial, B) middle and C) deep zones. Nuclei are stained dark blue, matrix is stained purple. In 30A), AS is the articular surface in the superficial zone.

From Figure 30, it is clear that the mature cartilage was relatively acellular although a few cells can be seen in the deep zone. A few striations were also observed in the matrix and these could be evidence of a more fibrous matrix.

5.3.1 Biochemical composition of mature articular cartilage

Measured biochemical components are shown in figures 31-36. In general, trends deviated from what was observed in immature cartilage. Compared to immature cartilage, mature bovine articular cartilage had much lower sulfated glycosaminoglycan (sGAG) content ($p<0.05$). Figure 32 shows the comparison between sGAG contents in immature and mature cartilage. For the mature bovine, the middle zone (MZ) had a lower sGAG content than the superficial zone (SZ) ($p=0.03$) but it was not significantly different from the deep zone (DZ) ($p=0.40$) (Figure 31). The SZ and DZ did not have significantly different sGAG contents ($p>0.05$). In addition, for the 2 year-old bovine, there were no significant differences in collagen content amongst any of the zones ($p>0.1$) (Figure 33). Furthermore, total collagen content did not change with age (Figure 34). Overall, water content was higher in mature cartilage than in immature cartilage (Figure 36). However, there were no significant differences between the water content in any of the zones in the mature bovine cartilage (figure 35). The average water fraction in the adult samples were 85% while in the juvenile samples, it decreased from 82% in the superficial zone to 74% in the deep zone.

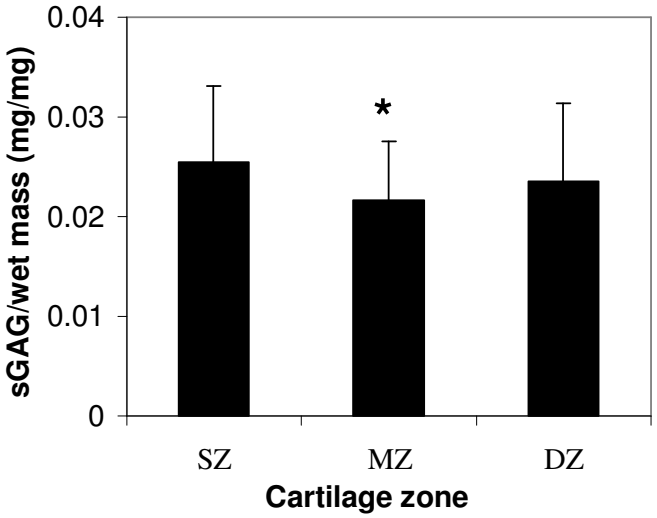

Figure 31: Zonal variation of sGAG (expressed per wet mass) in mature (2 year-old) bovine articular cartilage. * denotes significant difference from the surface zone ($p<0.05$). Values are mean ± standard deviation. n=18 cartilage explants

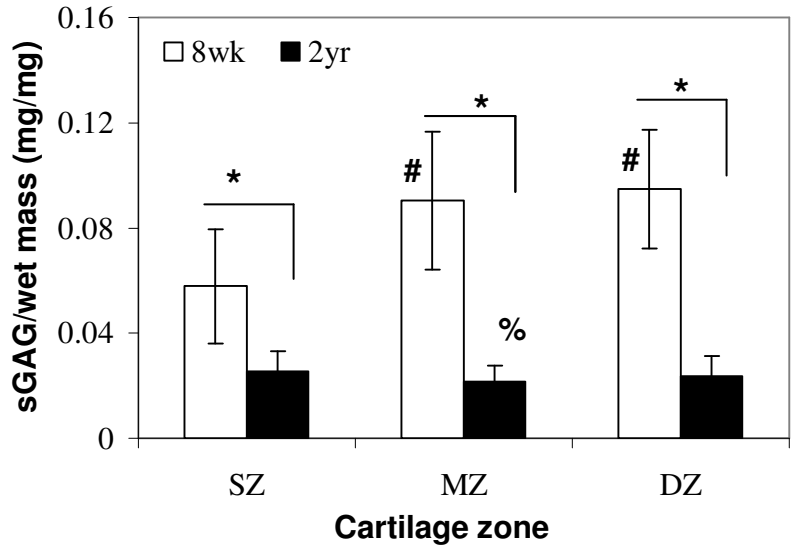

Figure 32: Comparison between sGAG contents in immature (8 week-old) and mature (2year-old) bovine articular cartilage. # indicates significant difference from 8 week-old superficial zone ($p<0.001$). % indicates significant difference from 2 year-old superficial zone. * indicates significant difference ($p<0.05$). Values are mean ± standard deviation. n=18 cartilage explants

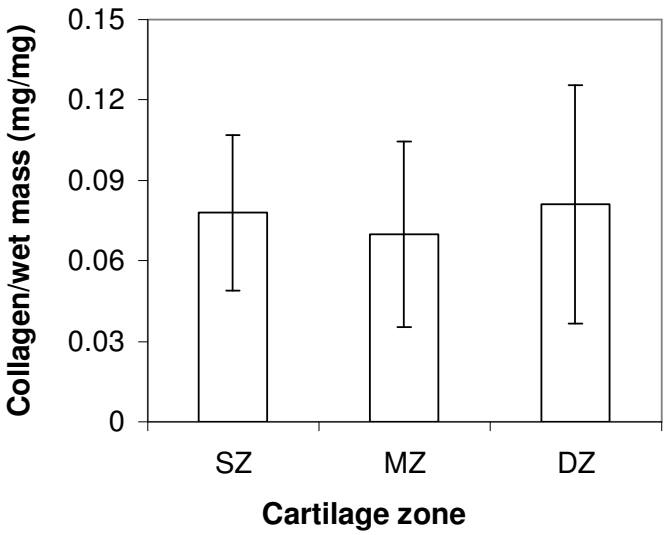

Figure 33: Zonal variation of collagen content (expressed per wet mass) in mature (2 year-old) bovine articular cartilage. **Values are mean ± standard deviation. n=18 cartilage explants**

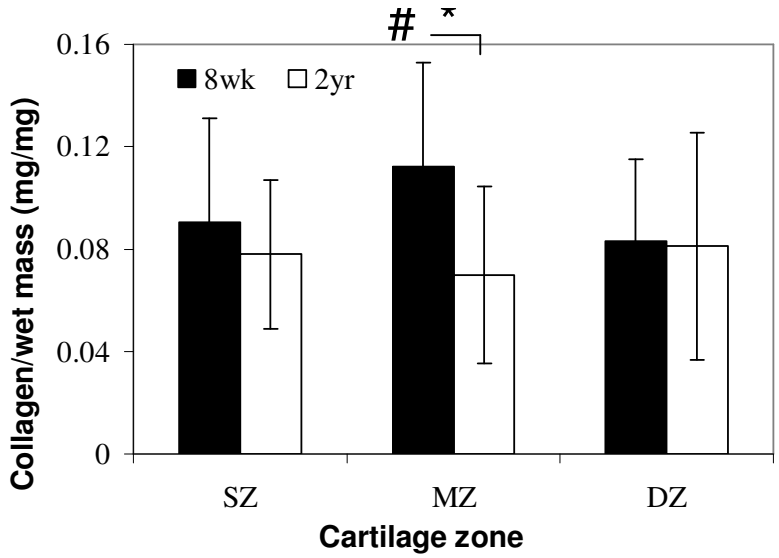

Figure 34: Comparison between collagen contents in immature (8 week-old) and mature (2year-old) bovine articular cartilage. # indicates significant difference from 8 week-old superficial zone; * indicates significant difference ($p<0.05$). Values are mean ± standard deviation. n=24 cartilage explants for 8wk and n=18 for 2yr.

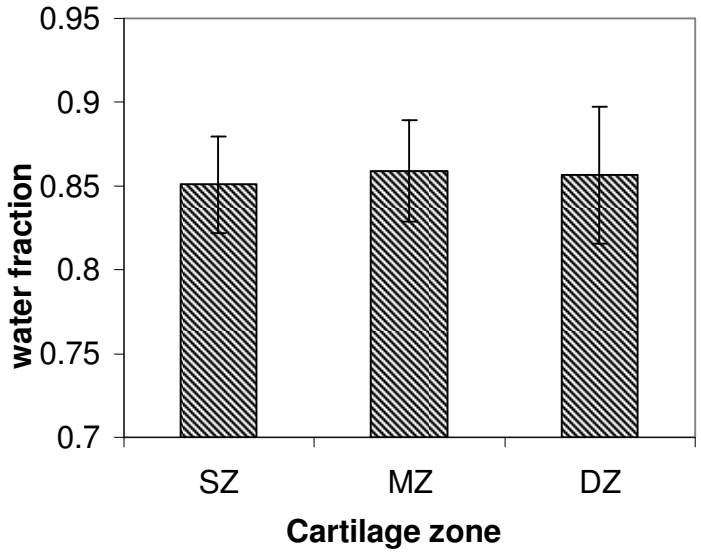

Figure 35: Fractional water content of the different zones (superficial, middle and deep) in mature (2 year-old) bovine articular cartilage. Values are mean ± standard deviation. n=18 cartilage explants

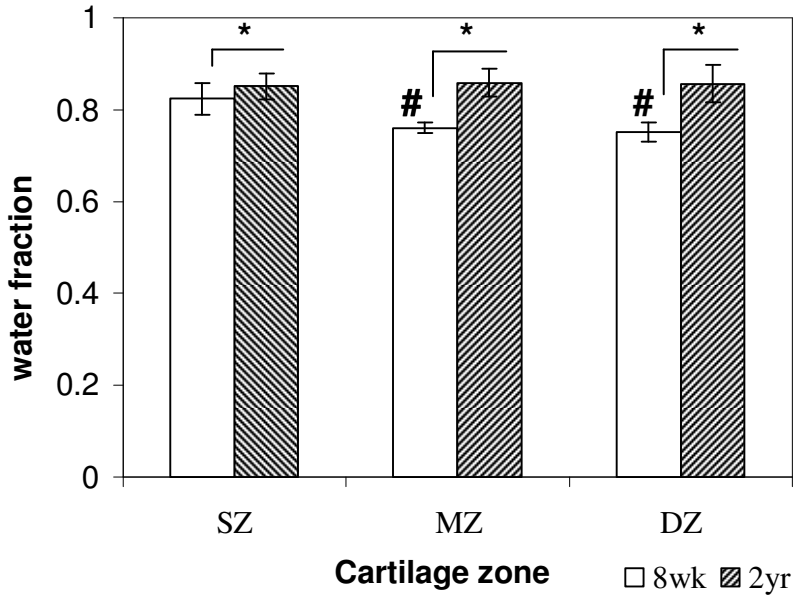

Figure 36: Comparison between water contents in immature (8 week-old) and mature (2year-old) bovine articular cartilage. * indicates significant difference from 8 week-old (p=0.0001). Values are mean ± standard deviation. n=18 for 2yr, n=24 for 8wk.

5.3.2 Diffusivity measurements in mature cartilage superficial zone: Comparison with immature cartilage

Measured radial and transverse diffusivities are shown for superficial zone tissue in figure 37. There was no significant difference between the radial and transverse diffusivities within the mature (2- year old) bovine superficial zone ($p=0.2$). Immature bovine cartilage had higher radial and transverse diffusivities than mature cartilage: radial diffusivity decreased from $34.0\pm1.2\mu m^2/s$ to $9.49\pm0.04\ \mu m^2/s$ ($p<0.001$) while transverse diffusivity decreased slightly from $10.6\pm0.47\mu m^2/s$ to $8.76\pm0.026\mu m^2/s$ ($p=0.005$). The ratio of the radial to transverse diffusivity (diffusional anisotropy) was estimated for each of the 18 cartilage explants and the average DA for mature cartilage was calculated. DA decreased significantly from the immature ($DA= 3.4\pm1.48$) to mature ($DA = 1.2\pm0.61$) superficial zone ($p<0.05$) (Fig. 38).

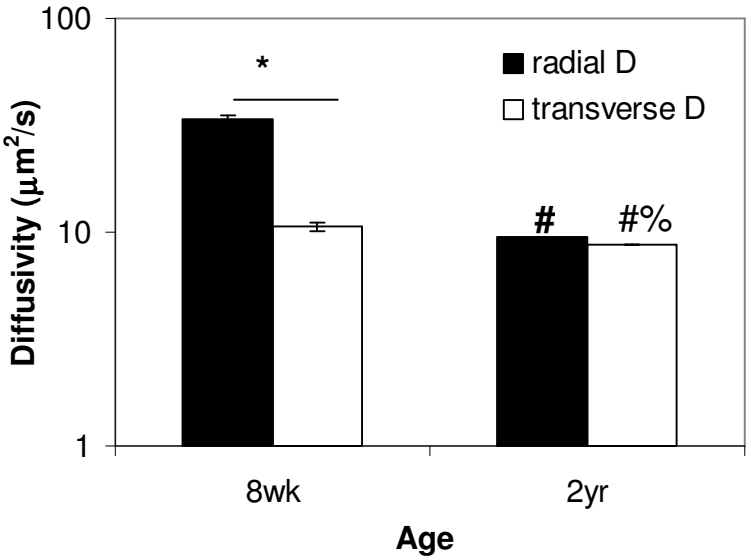

Figure 37: Diffusivity of 4kda fitc-dextran in immature and mature cartilage superficial zone: Effects of tissue orientation and age. Diffusivity values are plotted on a log scale. Radial D and transverse D represent radial and transverse diffusivities respectively.* indicates significant difference ($p<0.05$). # indicates significant difference from 8wk radial diffusivity ($p<0.001$). % indicates significant difference from 8wk transverse diffusivity ($p=0.005$). Values are mean ± SEM

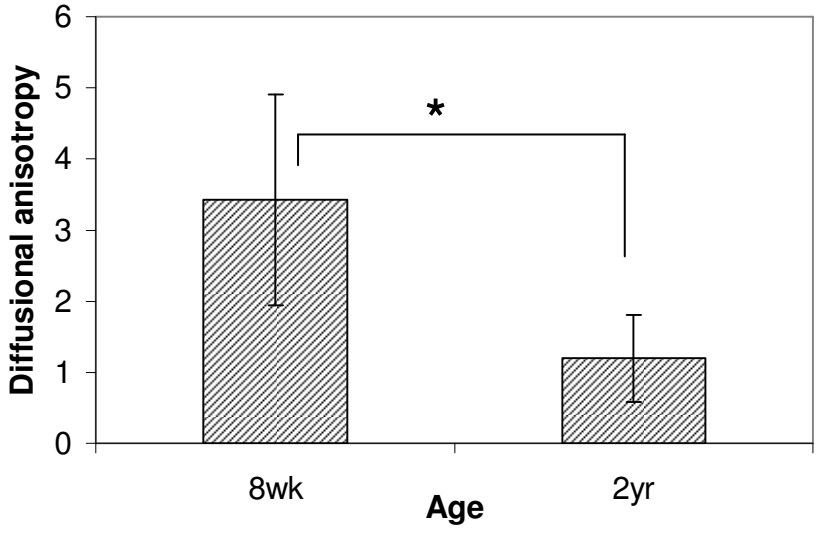

Figure 38: Diffusional anisotropy in the cartilage superficial zone: Influence of age. Mean values of the ratios of estimated radial to transverse diffusivities in each explant. n=23 cartilage

explants for 8 week-old bovines, n=18 cartilage explants for 2 year-old bovines. * indicates significant difference ($p<0.05$). Values are mean ±SD.

5.4 DISCUSSION

Cartilage is known to undergo maturation- and age-dependent changes in matrix structure and composition which may ultimately influence or modify transport of solutes and nutrients within the cartilage ECM. The focus of this study was on the superficial zone because of its importance in the maintenance of cartilage integrity and function *in vivo.*

Total sulfated glycosaminoglycan content decreased significantly in mature cartilage in comparison with the immature cartilage (figures 31-32). Previous research has established that there is a decrease in the quantity and size of cartilage PGs with age as a result of changes in the cells' biosynthetic activity. The zonal variation, however, was different from what has been reported previously. We found that the sGAG content was lowest in the middle zone ($p=0.03$) and the superficial and deep zones were not significantly different from each other ($p>0.05$). In contrast, there was no significant difference in the collagen content of the matrix with increased age ($p=0.076$) nor was there a difference in the collagen contents between zones ($p>0.1$). There was an overall increase in hydration (or water content) with age (figure 35-36) but there were no significant differences in the water content between the different zones in the 2 year old bovines. There have been contradictory reports in the literature about the water contents of young versus adult cartilage. The water content of adult human articular cartilage has been reported to be lower than juvenile cartilage while mature bovine articular cartilage was reported to have higher water content than immature bovine cartilage(35, 37).

In our results, both radial and transverse diffusivities were found to decrease significantly with age but the most drastic decrease in diffusivity was observed in the radial direction (figure 37). Although age-dependent decrease in permeability has been demonstrated in articular cartilage(89), this finding was surprising given the decreased sulfated glycosaminoglycan content and increased water content in the mature animals. It is worthy of mention that the composition of the glycosaminoglycans changes with age: keratin sulphate increases with age while chondroitin sulphate decreases with age(35, 91). In addition, both hyaluronan and core protein have been shown to increase with maturation and age in articular cartilage(92, 93). Hyaluronan is a viscous, high molecular weight non-sulfated GAG molecule and thus could further hinder solute movement within the interstitial space. Removal of hyaluronan from abdominal peritoneum was shown to increase the transport rates of water and other larger solutes(94, 95). Hence, the increase in the proportion of hyaluronan in the tissue could contribute to decrease in diffusivity observed in the superficial zone.

Another possible explanation for this decrease in diffusivity with age is the age-related change in collagen fiber diameter. The diameters of collagen fibrils have been found to increase as articular cartilage matures and ages(96, 97). Larger collagen fibrils, as noted earlier, could well obstruct solute mobility and increase drag force. Indeed, the reported positive correlation of tensile stiffness with age(72) may be as a result of increase in collagen fibril diameters(20).

Although total water content was observed to be higher in the mature cartilage, it could be that increase in water content was mostly an increase in intra-fibrillar water and

less of an increase in extra-fibrillar water. Volpi and Katz reported that both the thickness and the water content of the collagen fibrils of 2 year-old bovine cartilage increased by up to 50% when compared to the fibrils of the older animals (8-14 years)(20). Although, this could be interpreted as only occur after skeletal maturity, it should be noted that diameters of the collagen fibrils in cartilage have been reported to increase from birth to senescence(96). Hence, it is highly probable that the water content within the fibrils of mature bovine cartilage, such as the tissue used in these experiments, is higher than within the immature fibrils. In addition, Maroudas et al reported that a reduction in sGAG concentration within the extra-fibrillar compartment decreases the osmotic pressure exerted on the collagen fibers, thus allowing for a larger intra-fibrillar compartment(98). Thus, there seems to be an age-dependent redistribution of fluid within the cartilage matrix. Therefore, even though the overall water content of the matrix increases, there is no appreciable increase in the water fraction available for diffusion (i.e. the extra-fibrillar water content) since the solute is excluded from the intra-fibrillar compartment. Typically, solutes larger than 1kDa are excluded from intra-fibrillar compartment(43, 98).

In this study, we found that the diffusional anisotropy of the superficial zone decreased significantly with age from a value of 3.4 in the immature to 1.2 in the mature cartilage (Fig. 38). In fact, there was no significant difference found between the measured radial and transverse diffusivities within adult cartilage superficial zone. As reported in the previous chapter, diffusional anisotropy is a measure of the structure or matrix architecture and this evidence strongly suggests that there is a significant age-dependent modification of matrix structure. Even though the collagen content of the

matrix remains relatively constant with increasing age, enzyme-mediated cross-linking between collagen fibrils has been shown to increase with cartilage maturation(99). Moreover, it has been shown that the collagen fiber network undergoes significant remodeling during the maturation process. Type IX collagen, known to be extensively cross-linked to Type II collagen, decreases in abundance with increasing maturity (from 10% in fetal cartilage to 1-2% in mature cartilage). In addition, as PG molecules help stabilize the collagen network via their interactions with the collagen fibrils, the reduction in PG content seen in adult tissue may modulate the alignment of the collagen fibers. These modifications in the structure and composition of the collagen fibrillar network may subtly affect fiber orientation and consequently modulate solute transport and diffusional anisotropy within the cartilage matrix.

Furthermore, MRI and polarized light microscopy measurements have shown that collagen anisotropy is dependent on the age of the cartilage matrix(80, 100, 101). T2 and optical birefringence values are used as measures of collagen fiber orientation (anisotropy) in MRI and polarized light microscopy respectively. In general, zones that have fibers of a preferred orientation yield low T2 values (coinciding with high birefringence on PLM) while regions with a random organization of fibers have high T2 values (low birefringence)(18, 102). A study on the effect of age on collagen birefringence in articular cartilage of immature and mature guinea pigs showed that after physiological loading, the birefringence of the collagen fibers in the superficial zone increased in the juveniles but decreased in the adults. In addition, elevated T2 values have been observed in the articular cartilage of older human subjects and in those with early symptomatic degeneration(100, 103). However, the subjects in the latter study ranged in

age from 18-80 years old. Thus, it is possible that the changes observed does not occur during the maturation process but occurs after maturity and so it is difficult to compare these results with those obtained in this present research work

In general, it should be noted that the water content of the matrix might affect T2 relaxation times so trends might differ from species to species. Nevertheless, from these reports, it might be that changes in the fiber network observed during development and maturation may contrast with those that occur from skeletal maturity to senescence. Thus, the profile of diffusional anisotropy with age might not be monotonic. In order to accurately characterize the effect of age on diffusional anisotropy, it is important to determine the changes in transport properties that occur before and after skeletal maturity (from maturity to senescence). This will also aid in identifying changes that may be indicative of the degenerative process.

Implications of findings and Conclusions

In summary, we found that mature or adult cartilage had much lower surface diffusivities (both radial and transverse) than young cartilage. Although sGAG and water contents could not be implicated for this decrease in diffusivity across ages, these results suggest that there were considerable age-related modifications to the matrix structure. This was further supported by a three-fold decrease in diffusional anisotropy in adult cartilage as compared to immature cartilage. These results suggest that there are substantial differences in the structure of the immature and mature superficial zone

cartilage, thus, reinforcing our inference from the previous chapter that the collagen fiber network plays an important role in the diffusive resistance of the cartilage matrix.

It is worthy of note that much of the decrease in diffusivity was in the radial and not in the transverse direction. As the radial diffusivities are essential for nutrient and fluid exchange, these present results suggest that diffusion of nutrients to the chondrocytes may be hindered with the aging of the matrix. Nutrient deficiency will serve to further alter and reduce the biosynthetic activity of the cells resulting in a matrix that lacks structural and biochemical integrity.

Furthermore, the decreased diffusivity of the adult matrix could be indicative of necessary physiological changes that occur with maturation. Animals get heavier as they mature. The observed decrease in diffusivity could be as a result of a decrease in overall matrix permeability. Decreased permeability may be crucial in increasing fluid pressurization which will aid in maintaining the weight-bearing capacity of the cartilage.

Nevertheless, healthy adult cartilage can still maintain its normal function even with a reduction in solute diffusion rates as nutrient diffusion distances are shorter in mature cartilage. However, any disruption in the mechanical or biological environment could cause an imbalance in tissue homeostasis, which when combined with decreased diffusivities, could trigger catastrophic matrix degeneration. Thus, decreased diffusivity may be a necessary but not a sufficient prerequisite of matrix degeneration. Such a finding could provide insight into the mechanisms and causes of age-related cartilage degeneration.

CHAPTER 6

CONCLUSIONS AND FUTURE WORK

6.1 CONCLUSIONS

Articular cartilage degeneration is both an economic and health burden to any society. Thus, there is need for early intervention strategies to retard its progression.

Nutrient deficiency due to transport limitations is thought to be one of the causes of the pathological degeneration of the cartilage tissue. Thus, it follows that a careful study of diffusion within cartilage as outlined in this project will lead to a better understanding of the causes of cartilage degeneration.

The overall goal of this project was to quantify the influence of ECM composition and ECM orientation on the diffusive resistance of bovine articular cartilage. In order to accomplish this goal, our sub-objectives were to characterize solute diffusivities in immature cartilage, correlate these diffusivities with matrix composition and finally to assess the differences in diffusion within the superficial zone of immature and mature cartilage.

To accurately estimate diffusion coefficients in articular cartilage and other hydrated medium, we developed a finite-element based method, the Direct Diffusion Simulation Parameter Estimation method (DDSPE), as described in chapter 3, to be used for quantitative determination of solute diffusivities from FRAP data. Previous FRAP-

based data analysis has generally been limited by the assumptions that no diffusion occurs during bleaching and that no significant bleaching of the fluorophores occurs during image acquisition. In fact, our preliminary tests showed that these assumptions measurably distort the calculation of the effective diffusivity.

The DDSPE model gives an accurate description of the experimental fluorescence profiles, accounts for time varying boundary conditions and includes a reaction term to account for the confounding effects of low level photobleaching during scanning. Analyses of simulated and experimental FRAP data demonstrated that this method was more accurate than existing analytical methods, including having a low sensitivity to variations in the spot radius.

As an example application, the effects of gel density and dextran size on the diffusivities of fluorescently-labeled-dextrans (10-250kDa) in agarose gels (2-6%) were measured via FRAP. The diffusivities determined by the DDSPE method decreased with increasing solute size and gel density and were in excellent agreement with theoretical predictions based on a recent empirical model in published literature. Furthermore, the DDSPE method is applicable to analysis of any image based experimental data of the general form of pixel intensity as a function of space and time.

In chapter 4, the roles of extracellular matrix composition and ECM orientation in solute diffusion within immature bovine articular cartilage were explored. The diffusivity of the solute (fluorescently-labeled 4kda dextran) in different cartilage zones (at different depths from the articular surface) and in cartilage samples of different orientations (normal and parallel to the articular surface) was measured. Radial and transverse diffusivities exhibited zonal dependence and in general, decreased with

increasing distance from the articular surface. Matrix components also varied with depth: fractional water content decreased with distance from the articular surface while glycosaminoglycan content increased from the surface to deep zone. In the immature cartilage, fractional water content was found to be positively correlated with both radial and transverse diffusivities while sGAG content had negative correlations with diffusivities in both orientations. Further statistical analysis showed that the correlations observed between collagen and both diffusivities were likely because of the inter-correlation of collagen and water fraction.

Of all the matrix components, water content was found to be the best predictor of solute diffusivity in both directions (radial and transverse). sGAG content also had a significant effect on radial diffusivities but not transverse diffusivities. However, the matrix collagen content did not seem to have an appreciable effect on diffusion rates. Although no specific experiments were done to measure the effect of structure, our results suggested that matrix structure did indeed modulate transport. For example, the amount of solvent water available for solute mobility is likely dependent on the inter-fibrillar spacing between the collagen fibers. Hence, matrix water content is not completely an independent parameter and is related to the matrix architecture. As a result, the effects of water and matrix structure on diffusive resistance may not be mutually exclusive.

Anisotropy in cartilage, primarily a consequence of collagen fiber orientation, is thought to be important for normal tissue function. The material/structural anisotropy of articular cartilage is known to have resulted in a tissue with anisotropic mechanical

properties. Thus, we wanted to investigate if diffusion in cartilage was also anisotropic. Diffusional anisotropy (DA) in each cartilage zone was quantified by determining the ratio of the mean radial to the mean transverse diffusivities measured in that particular zone. From our results we found that DA exhibited zonal dependence and was highest in the superficial zone. Diffusional anisotropy was also observed to be significant in the middle and deep layers and these layers had very similar DA values. Indeed, it has been reported that immature articular cartilage has structurally similar middle and deep zones. In addition, the collagen fibers and GAG molecules of the middle zone have been shown to exhibit a preferred spatial orientation. This manifestation of structural properties and anisotropy in measurable transport properties suggest that diffusional anisotropy might play a critical role in the maintenance of matrix integrity. Radial diffusivities were determined to be much higher than transverse diffusivities, supporting previous reports that transport of nutrients and solutes were mostly from the synovial fluid in a direction normal to the articular surface.

In chapter 5, we sought to identify the differences in solute diffusion within the superficial layer of immature and mature bovine articular cartilage. Given the critical role of the superficial layer in the proper functioning of the joint, the effect of maturation on diffusion in the superficial zone was investigated. The greatest changes in matrix composition were in the matrix sGAG and water contents.

Total sulfated glycosaminoglycan content decreased in the mature cartilage while water content was much higher in the older cartilage explants. Collagen content did not change with age. In addition, there was an observable difference in the depth-dependent

variations of the matrix components in the mature cartilage when compared to the immature tissue. The measured decrease in diffusion rates in the older cartilage could not be explained by the changes in sGAG and water contents. It is possible that these alterations in transport rates are the result of other biochemical changes in matrix composition (such as increases in the amount of hyaluronan) and structure (increases in the collagen fibril diameter) that were not investigated in this study. Furthermore, it may be that the increase in hydration was primarily within the collagen fibrils. Thus, the additional amount of water was not available to aid in diffusion within the extra-fibrillar compartments.

Nevertheless, the decrease in diffusivities observed in mature cartilage imply that there may be a reduction in nutrient and growth factor supply to the cells making an imbalance in synthesis and degradation events more likely. Furthermore, animals get heavier as they mature. Thus, the reduction in radial diffusivities might be a consequence of decreased matrix permeability which is required for fluid pressurization, and hence the increased weight-bearing capacity of the older matrix. However, the disadvantages of this event might outweigh the benefits should an imbalance occur in the tissue homeostasis.

In addition, the decreased diffusional anisotropy observed in mature cartilage is strong evidence for age-related modification of matrix structure. Previous studies have shown changes in collagen birefringence during maturation and modifications in collagen organization with aging. Given that collagen birefringence has been observed to decrease in the superficial articular cartilage of mature guinea pigs subjected to physiological loading and in the articular cartilage of older patients and those with asymptomatic

osteoarthritis, diffusional anisotropy may be useful as an index for cartilage health. These results provide a possible mechanism for the role of age in degeneration and will facilitate the design of better diagnostic tools.

6.2 MODELING CHALLENGES

In recent years, medical science has used imaging techniques (such as MRI) that can non-invasively measure the apparent diffusion coefficients of water in tissues such as the brain for diagnosis of injury or disease. Early diagnosis of disease or injury in articular cartilage is critical for the prevention or retardation of joint degenerative disorders such as OA. However, changes in matrix composition or structure due to disease may be localized. Thus, its effect on measurable parameters such as diffusion rates may not be detectable by macroscopic means. Therefore the development of the DDSPE model, as outlined in this research work, as a tool for the analysis of any image-based experimental data is a significant first step in formulation of new diagnostic and treatment protocols.

6.2.1 1-D versus 2-D DDSPE Models

One of the major challenges faced in this investigation was developing a model that could accurately represent the actual, real-life evolution of the concentration profile within a region of interest in this heterogeneous tissue. Since the tissue is three-dimensional, the use of a 3D model for image analysis would have been ideal. However, the development of a 3D model was difficult because of limitations posed by the available equipment. Scanning in x-y plane and in the z axis could not be done simultaneously, thus severely limiting the spatial and temporal information obtained from

the images acquired. Therefore, we assumed that diffusion in any given tissue slice was within the x-y plane and neglected the contribution of diffusion component in the z-direction. It is possible that this may have led to some errors in the estimation of the diffusion coefficients.

As a result of the aforementioned inherent limitations of the experimental apparatus, cartilage was initially modeled as a two-dimensional isotropic material. A variation in the 1-D axisymmetric DDSPE method was developed to be used to perform a two-dimensional quantitative analysis of FRAP diffusion measurements in inhomogeneous tissue. The 2-D model was developed to address certain perceived limitations of the 1-D axisymmetric model such as its inability to account for any angular heterogeneity in fluorophore distribution within the tissue. The 1-D model analysis is based on averaging pixel intensity values which are the same radial distance from the nominal center of the bleached spot resulting in an idealized and homogenized image field with intensity values closest in some global sense to the actual (observed) intensity at a given radial position. In contrast, the 2D model analysis identifies and tracks all values in-situ within the image field and therefore is able to recognize and account for observed angular variations in fluorophore distribution. Both models were used to analyze the FRAP image data. A detailed description of 1D axisymmetric model was given in chapter 3 and a description of the 2D model is given in the next paragraph.

6.2.2 2D Model Development

Each FRAP image represented the concentration profile of a scan region at a specific point in time. The raw pixel values from each FRAP image were read using the '*imread*' function in MATLAB, which reads the pixel intensities from a 2-D image field and produces a 2-D matrix of intensity values. This time-series of images was assembled and represented by a three-dimensional matrix, $C_{exp}(x,y,t)$. The concentration profile of the first post-bleach image (a 2D matrix) was specified as the initial condition, $C(x,y,0)$ while four 2D matrices (of boundary intensity values) were used to define the time-varying boundary conditions – $C(x_o,y,t)$, $C(x_i,y,t)$, $C(x,y_o,t)$, $C(x,y_i,t)$- where the subscripts $_i$ and $_o$ represent the boundaries of the quadrilateral scan region.

A two-dimensional finite element mesh was generated within COMSOL Multiphysics using four-node, quadrilateral elements with equally spaced nodal positions corresponding to the positions with known initial concentrations. The evolution of the concentration profile was thus simulated producing a three-dimensional matrix $c_{sim}(x,y,t)$.

The estimated diffusivity was the value that produced a simulated matrix that best fit the actual spatially and temporally varying concentration field.

<u>2D Model Experimental Results</u>

Below is a graph of the mean radial and transverse diffusivities estimated for immature bovine articular cartilage using the two-dimensional adaptation of the DDSPE method.

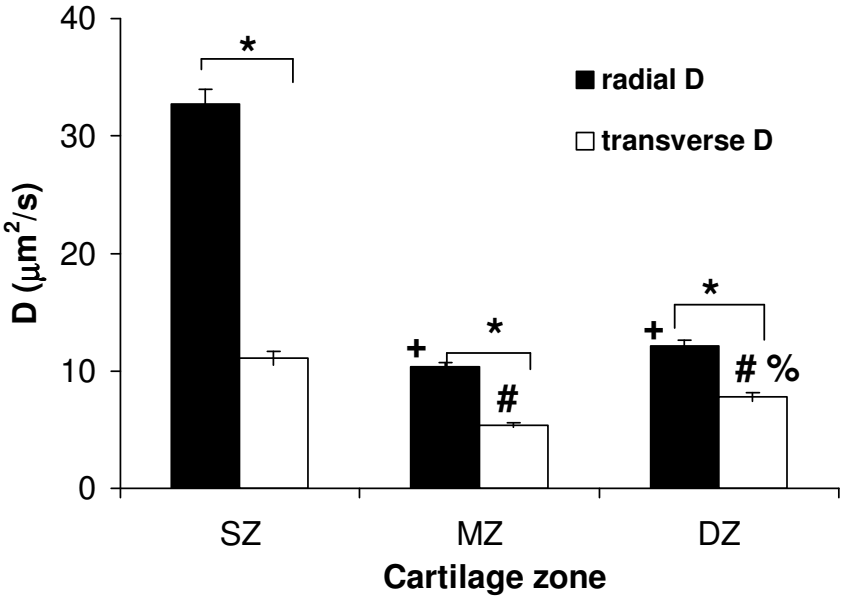

Figure 39: 2D analytical results of the diffusivity of 4kda fitc-dextran in the different cartilage zones (superficial (SZ), middle (MZ) and deep (DZ)) and in radial and transverse orientations. Radial D and transverse D are radial and transverse diffusivities respectively. + indicates significant difference from superficial radial . # indicates significant difference from superficial transverse D. % indicates significant difference from middle transverse D. * indicates significant difference ($p<0.05$).

As in the 1D results (Figure 21), both radial and transverse diffusivities exhibited zonal dependence (Figure 39). As was done with the 1-D results, diffusivities less than 1$\mu m^2/s$ and greater than 65$\mu m^2/s$ were not included in the data analysis. For the 2D analyses, the radial diffusivities of 4kda FITC-dextran measured in superficial, middle and deep zones were 32.7±1.2$\mu m^2/s$, 10.3±0.39$\mu m^2/s$ and 12.1±0.48$\mu m^2/s$ respectively (expressed in mean ± SEM). Measured transverse diffusivities were 11.10±0.58 $\mu m^2/s$, 5.38±0.18 $\mu m^2/s$ and 7.78±0.37 $\mu m^2/s$ in the superficial, middle and deep zones respectively. In comparison to the 1D results, all mean diffusivities (radial and transverse) were 0.9-7% different from the 1D diffusivity estimates except for the deep

zone transverse diffusivity which was 51% higher than its 1D counterpart. Prior to excluding diffusivities that were less than 1$\mu m^2/s$, all 2D diffusivity estimates (radial and transverse) were 10-23% lower than the 1D diffusivity estimates except for the deep zone transverse diffusivity which was 63% lower than its 1D counterpart. Consequently, the trends of the diffusivities in the radial orientation for both models remained the same but the trend of the transverse diffusivity was different between the models.

Based on the data above and on further histogram analysis of the 2D results from individual FRAP images, it became apparent that these underestimations were zone and orientation specific:

Table 1: Zone and orientation dependence of 2D model diffusivity estimates < 1$\mu m^2/s$

Zone-orientation	**% values less than 1$\mu m^2/s$**
Surface zone – radial	1.8
Surface zone – transverse	15.3
Middle zone – radial	19.0
Middle zone – transverse	17.2
Deep zone – radial	26.3
Deep zone – transverse	76.0

As shown above, there is a higher frequency of the low diffusivity measurements in the cartilage deep zone and in the transverse orientation. The values less than 1$\mu m^2/s$ represented about 25% of total number of measurements taken in the cartilage samples. Further inspection of microscope images from the different zones and orientations showed a correlation between the frequency of low estimates and the cell area fraction of the scan regions. Using ImageJ software, cell dimensions and total cell numbers were calculated. Cell density is known to decrease through the cartilage depth while cell surface area increases with depth. In the two-dimensional slices being analyzed in these

experiments, the same pattern was observed: the number of cells observed in the images decreased from the surface zone to the deep zone but the individual and total cell surface area increased through the depth (Table 2). Furthermore, surface areas of the cells were much larger in the transverse slices than in the radial slices especially in the surface and deep zones. Thus, it was apparent that the cells influenced the model's ability to accurately quantify diffusivities.

Table 2: Mean cell number, mean cell radius and % area fraction of cells in zones.

Zone	Mean number of cells	Mean radius (μm)	% area fraction of cells
Superficial zone	16	3.5	2.5
Middle zone	10	5.5	4.5
Deep zone	9	8	8.4

However, in most cases in which the diffusivities were under-estimated, the concentration of the fluorescent dye was much higher in the cells than in the rest of the extracellular matrix often saturating the photomultiplier tube of the microscope. It may be that the fluorescent dye binds to substances (e.g. proteins such as fibronectin) in the cytoplasm and/ its mobility is restricted by membranes and other cytoplasmic structures (e.g. the cytoskeletal filaments).

As a result of the high dye concentrations within the cells, there are very high and localized concentration gradients around most of the cells in the tissue. With high gradients around cell boundaries but very little resultant flux from the cells (when compared to the rest of the matrix), the model incorrectly estimates an unrealistically low diffusivity for the entire scan region. This suggests that the very high levels of

fluorophore concentration seen within cellular regions of the image field were introducing some form of simulation artifact.

Several forms of image filtering were applied to test phantom images and experimental image data in an attempt to better quantify the role played by the cellular component of the image field on the derived estimate of apparent diffusivity.

In particular, we determined the diffusion for test phantom images in which the cells occupied 2.8, 4.4 or 7.4% of the total surface area, and were assumed to represent the surface, middle or deep zones respectively. In all cases, the diffusivity of the cells was set to 0.005$\mu m^2/s$ (i.e. much lower than value to be determined for the matrix). Similarly, in all cases, the extracellular matrix was assumed to have a uniform concentration and a bleached spot was prescribed at the center of the image field. Diffusivities of these simulated matrices were then estimated without accounting for the presence of the cells using the two-dimensional DDSPE method.

Table 3: Influence of cells on the accurate estimation of matrix diffusivities using the 2D DDSPE method: effect of filtering. Superficial, middle and deep zones are represented by images with cells occupying 2.8, 4.4 or 7.4% total surface area.

	SUPERFICIAL ZONE			MIDDLE ZONE (MZ)			DEEP ZONE (DZ)		
Intensity of cells	Dinput ($\mu m^2/s$)	Dpred ($\mu m^2/s$)	%error	Dinput ($\mu m^2/s$)	Dpred ($\mu m^2/s$)	%error	Dinput ($\mu m^2/s$)	Dpred ($\mu m^2/s$)	%error
250	10	8.7	13.0	10	9.0	10.0	10	7.9	21
250	5	1.6	8.2	5	4.5	10.0	5	3.94	21.2
250	1	0.015	98.4	1	0.018	98.1	1	0.014	98.5
250	-	-	-	0.5	0.015	96.8	0.5	0.013	97.2
150	-	-	-	10	9.6	4.0	10	9.1	9.0
150	5	4.93	1.32	5	4.9	2.0	5	4.75	5.0
150	1	0.811	18.9	1	0.75	25.0	1	0.66	33.3
120	5	4.96	0.74	5	4.98	0.4	-		
120	1	0.952	4.8	1	0.93	7.0	-		
100	-	-	-	5	4.98	0.40	5	4.98	0.40

It is important to understand that the number of cells, cell surface area (size) and amount of dye within the cells are not the only factors influencing the accuracy with which the diffusivities will be estimated. The location of the cells in the matrix, more specifically, its distance from the bleached spot, plays a huge role in determining the extent of the influence the cells have on the simulation. The closer the cells are to the bleached area, the greater the influence exerted by the cells on the parameter estimation. Thus, the values estimated from the simulations could differ from one simulation to the other if the positions of the cells change in the “matrix".

Nevertheless, it can be inferred from the data in Table 3 that for tissue with relatively high ECM diffusivity, the presence (or absence) of the cells had relatively little effect on the estimation of apparent diffusivity. In contrast, for tissues with relatively low ECM diffusivity, the presence of even a relatively low concentration of functionally non-permeable cells in the image field could distort the estimate of apparent diffusivity as much as two orders of magnitude (i.e., such that the inferred value was only 1% of the `actual’ ECM value). This was most likely to occur for tissues from the deep zone, where the ECM diffusivity was lowest and the cellular surface area was highest. As was expected, the lower the dye concentration within the cells, the smaller the error of measurement.

Sample FRAP images were selected to quantify the effect of filtering on the estimated diffusivities. The image processing software, ImageJ, was used to filter the images. To filter, lower and upper threshold intensity values were set, using the Multi-

threshold function, to selectively highlight the cells. A much lower intensity value was then prescribed for these highlighted cells to dampen the effect of the high dye concentration within these structures. The filtering was effective in most of the images sampled if the prescribed intensity value was not more than 1.5X the average intensity value of the matrix. Twenty-nine (29) image stacks representing the superficial, middle and deep zones of a cartilage explant were randomly selected and filtered. In this case, the intensity value prescribed on the cells was the average fluorescent intensity value of the matrix. Both 1D and 2D models were used for the analyses of the unfiltered and filtered images (figure 40).

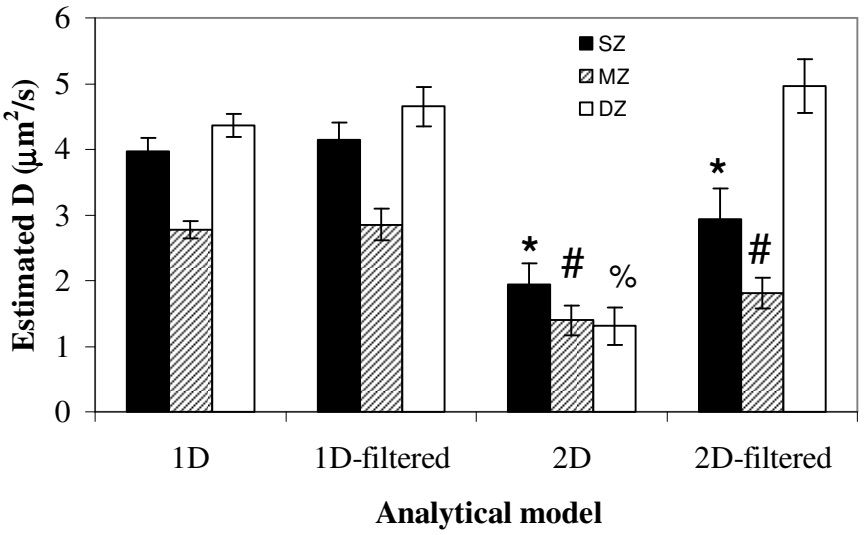

Figure 40: Diffusivity estimates from filtered (f) and unfiltered images from the superficial (SZ), middle (MZ) and deep (DZ) zones using both 1D and 2D DDSPE models. * indicates significant difference from the 1D superficial zone , # indicates significant difference from the 1D middle zone and % indicates significant difference from the 1D deep zone ($p<0.05$). n = 3 samples per zone, 3 measurements per sample. Values are expressed as mean ± SEM.

Certain facts are clear from figure 40: There is no difference in the diffusivities estimated from both filtered and unfiltered image stacks using the 1D model. Mean diffusivities estimated using the 1D model before and after filtering differed by only 2-6% (the filtered values were only slightly higher). Averaging pixel intensity values, as done in the 1D model, diminishes the importance and effect of each individual pixel. Consequently, matrix heterogeneities become less significant. In contrast, both the trends and the absolute values of the 2D model results change with image filtering. For the deep zone, the value estimated by the 2D model prior to image filtering was 73% of the value estimated by the 2D model after filtering. It is important to note that filtering does not completely solve the problems encountered during the 2D model analysis. Within these tissue samples (and any other tissue), there are several structures (pericellular matrix, etc) that may exclude the fluorescent dye. As a result, there were several dark regions in many of the tissue samples that may also distort any simulation of the evolution of the concentration profile. Therefore, it becomes increasingly difficult to keep from tampering with the actual image field if a considerable amount of filtering is done.

Although it was apparent that the 1D model was less influenced by the presence of cells, its accuracy over that of the 2D model was still undetermined as the actual diffusivities in the tissue under investigation were unknown. Therefore, to make a conclusive assessment of the accuracy of one model over the other, test phantom 2D images of cells dispersed within a matrix were simulated using D = 0.5, 0.75, 1.0, and 2.0$\mu m^2/s$. Concentration values of 100 units, 40 units and 250 units were imposed on the matrix, bleach spot and cells respectively. There were a total of 10 circular cells in the

matrix, each with radius of 6μm. Diffusivities were then estimated from the simulated concentration profiles using both 1D and 2D models.

Table 4: Comparison of 1D and 2D DDSPE methods using simulated concentration profiles. Diffusivities were predicted from simulated concentration profiles of 2D phantom images using both models. 1D diffusivity estimates are highlighted

	1-D	**2-D**
D input ($\mu m^2/s$)	**D predicted ($\mu m^2/s$)**	**D predicted ($\mu m^2/s$)**
0.50	**0.46**	0.04
0.75	**0.69**	0.05
1.00	**0.92**	0.05
2.00	**1.82**	1.74

Table 4 shows the diffusivities predicted from the simulated concentration profiles using both 1-D and 2-D models. It should be noted that the accuracy of 1-D is maintained across the diffusivities while the accuracy of the 2D model decreased sharply as the diffusivities decrease. The diffusivities estimated by the 1-D model were approximately 90% of the actual diffusivity values while those estimated by the 2-D model were less than 10% of the actual diffusivity values (for $D<2\mu m^2/s$). Thus, it became evident that local heterogeneities distorted the 2-D parameter estimation approach making it inordinately imprecise for certain data sets. However, it ought to be stressed that in all these simulations, conditions were highly idealized such that the bleached spot, matrix (excluding the cells) and boundary region had uniform concentrations, a situation unlikely to occur in reality. Therefore with realistic

experimental conditions as pertains to the experiments performed in this research work, the accuracy of the 1-D model may diminish, although much less severely than that of the 2-D model.

Despite all these advantages of the 1-D over the 2-D model, it should be emphasized that in reality, diffusion is more likely a two-dimensional (or possibly three-dimensional) rather than an axisymmetric process. However, for some of the experimental data sets considered, the 2-D model was inadequate because of its inability to account for the localized heterogeneities (mostly the cells) in matrix concentration as previously detailed. It was surprising that the 1-D model performed better than the 2-D but on further inspection of the images, it was observed that aside from the cells and a few dark regions, the solute was distributed uniformly throughout the matrix. Thus, with larger solutes, the effect of the heterogeneity of the matrix may be exacerbated, rendering the 1-D model less effective.

Below are graphs of representative integrated fractional fluorescence profiles of the bleached spot in agarose and cartilage samples (Figure 41 and Figure 42). Simulated fractional fluorescence profiles were calculated using the 1-D DDSPE model (similar profiles were obtained using the 2-D DDSPE model). These graphs illustrate that the model excellently predicts the profile in the agarose gels and but deviates at later times in the tissue. It is important to note that calculating a fractional fluorescence profile assumes homogeneity within the bleached spot. It is also worthy of mention the model is optimized to match radial intensity profiles and not integrated fluorescence intensity.

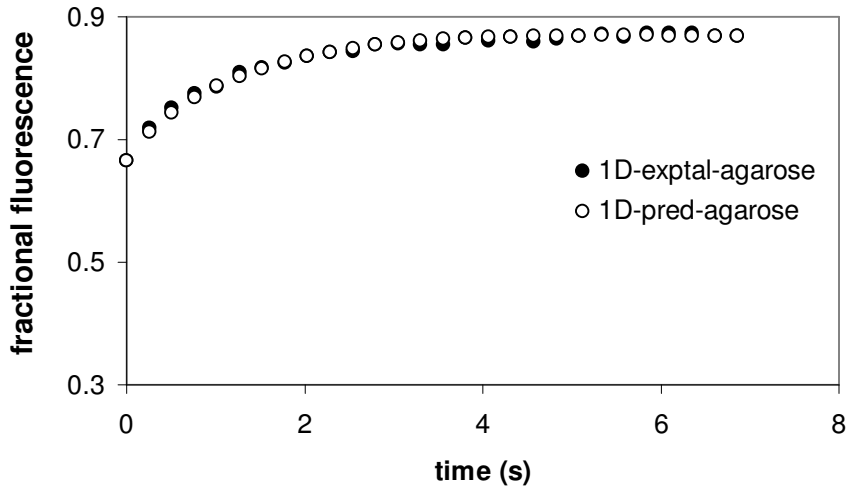

Figure 41: Representative experimental and simulated fractional fluorescence profiles of 10kDa dextran in 2% agarose gels. 1D-exptal and 1D-pred refers to the experimental and simulated fractional fluorescence profiles respectively

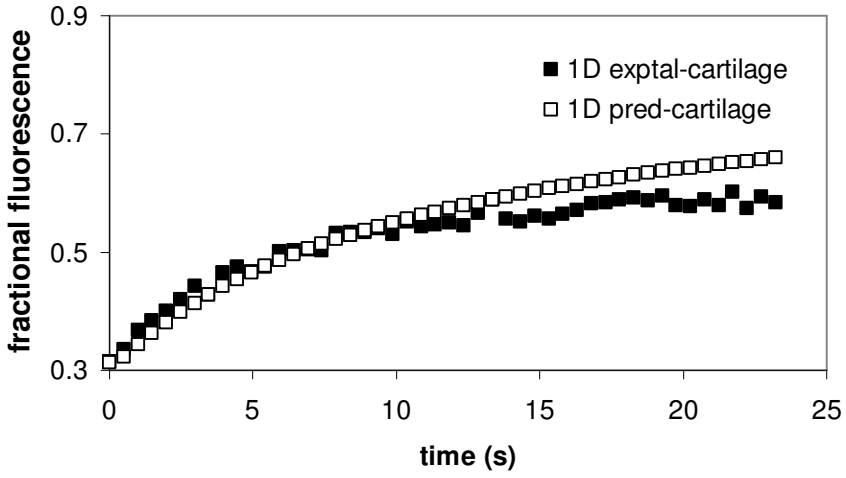

Figure 42: Representative experimental and simulated fractional fluorescence profiles of 4kDa dextran in cartilage. 1D exptal and 1D pred refers to the experimental and simulated (predicted) fractional fluorescence profiles respectively

As can be seen from Figure 42, the simulated (or predicted) curve slightly under-predicts and grossly over-predicts the experimental profiles at early and later time points respectively. This may still be as a result of the high dye concentrations within the cells as explained earlier. Also, as a result of the heterogeneity of the matrix, it is highly

probable that the diffusivity is spatially varying. However the model calculates an effective diffusivity that may be higher and/ lower than the actual diffusivities in different regions.

For future work, the DDSPE model should be extended and modified to account for the contribution of cells and other impermeable structures. The geometry of all the intra-matrix structures should be modeled and boundary conditions explicitly prescribed. This requires modeling sample-specific simulation grids. In addition, both of the models presented in this study assumed that the tissue was isotropic and that diffusivity did not vary with position. Cartilage tissue is known to be anisotropic and highly ordered even in microscopic length scales. Any FE model to be developed should incorporate tissue anisotropy and a spatially-varying diffusion coefficient. Furthermore, for more accurate diffusivity estimates this finite-element model could be adapted to a three-dimensional model. To implement a 3-D model, the FRAP technique could be modified for by bleaching finite and defined volumes within the tissue using a multi-photon confocal microscope. Supplementary parts may have to be purchased for the microscope.

6.3 FUTURE WORK

Only one solute size was used in the diffusivity measurements in this study. There are several physiologically relevant neutral and charged solutes that are within an order of magnitude larger than the 4kDa dextran. It will be interesting to explore the mechanisms by which larger solutes diffuse through cartilage. The effect of solute size and charge on diffusion in cartilage needs to be investigated. Larger solutes may make the contributions of the matrix fiber network more evident. Moreover, as the results of the

present studies suggest that the matrix ultrastructure plays a critical and major role in solute transport, x-ray diffraction studies (and electron microscopy) could be used to further investigate the contribution of the cartilage matrix structure.

Dextrans were used in these studies because they are not metabolized by cells, are water-soluble and do not bind to receptors. As such, we were able to investigate the passive diffusive properties of the cartilage matrix. However, dextrans are flexible, elongated polysaccharide chains which exist as random coils in solution. Consequently dextrans chains can be extended to enable the molecules diffuse through pores with radii smaller than their effective hydrodynamic radii. However, the effective radius of a dextran solute is larger than the radius of a globular protein of similar molecular weight. The nominal molecular weight of a dextran is actually an average molecular weight as the dextran is heterogeneous with higher and lower molecular weight fractions. Therefore, it is difficult to accurately compare the diffusion properties of a dextran with a solute that will behave as a "hard sphere"

In the same vein, the diffusion of physiological solutes should also be examined to determine the relative contribution of solute binding (to matrix, receptors or other proteins) to overall transport. To be able to extend these results to clinically relevant situations, human articular cartilage should be used for some of these studies.

.

Two different ages were used in this study - 8week and 24month old bovines. The changes in diffusivities and matrix composition reported in this study may have been due to maturation and not aging. Further research should be done on several different ages (both younger and older) so that developmental, maturation and aging variations in

matrix transport properties can be fully characterized. In addition, to fully quantify modifications in matrix composition and their relationship to diffusive resistance, extensive biochemical analyses should be performed to measure collagen cross-linking, ECM proteolytic degradation products, and changes in abundance of other matrix components. Also, the intra-fibrillar and extra-fibrillar water contents should be quantified in order to determine the effective proteoglycan concentration and the actual amount of water available for diffusion

Finally in both animal studies, no attempt was made to isolate the possible influence of the sex of the animal on the estimated diffusivity. It is possible that the variability observed amongst the animals may have been lessened if animals were one gender. In addition, diffusivity trends and in broader terms, matrix transport properties may differ between male and female animals. Experiments that discriminate between the genders might unearth results and information that may have been previously obscured.

Moreover, in studies such as this where animals are not laboratory grown, there may be slight variations in the age of the animal subjects. It is possible that there is greater variability in matrix properties between the 6week and 8week old calves than there is between mature bovines that are few months apart in age. Cell proliferation and matrix biosynthesis (matrix remodeling) occurs at a much faster rate in the juvenile than in the adult cartilage. As such, it is likely that the six and eight week–old calves may have matrix properties that are more dissimilar than mature bovines. Future studies should, if possible, investigate the extent of this variability and what effects it might have on the interpretation of the results.

APPENDIX A

MATLAB CODE

Specific Aim I

Develop a numerical technique to accurately estimate diffusivities from data obtained from fluorescence recovery after photobleaching (FRAP) experiments and benchmark the results obtained using this new technique against results obtained using existing analytical methods.

Conversion of FRAP images to intensity matrices (1D axisymmetric model for agarose gels)

readimg.m

```
%This program reads the FRAP image files (a time-series of images) and
%converts them to a concentration matrix which is a function of two
%independent variables, radius and time.

%Inputs are radius(R) and the coordinates of the image center(x1,y1)
%Outputs are Valm, the concentration matrix, and the coefficients of
%the equation used to fit the boundary condition (a1,a2,a3)

[Valm,a1,a2,a3]=readimg(R,x1,y1);

%Define Valm as a global variable
global Valm

%Read FRAP images
for i = 0:67;
X8 = imread(['image filename' num2str(i,'%03i') '.tif']);
k=0;

%Specify 36 line segments all passing through the center(x1,y1)
%from which pixel intensities will be read at 76 equidistant
%points
for theta=0:pi/18:2*pi;
    theta=k*pi/18;
    a=R*cos(theta);
    b=R*sin(theta);
    X1=[x1 x1+a];
    Y1=[y1 y1-b];
    E=improfile(X8,X1,Y1,76);
    k=k+1;
```

```
    [m n]=size(E);
    for j=1:m
    Val(j,k)=E(j,1);
    end
    end
    Valm(:,i+1)=mean(Val,2);
end

%Specify initial condition
%Smooth vector
%Save as text file in current directory

X2=linspace(0,R*.45,76);
Y=Valm(:,1);
Y=smooth(Y,3);
fid=fopen('init.txt','wt');
fprintf(fid, '%%Grid\n');
fprintf(fid,'%6.2f\t',X2);
fprintf(fid,'\n%%Data\n');
fprintf(fid,'%6.2f\t',Y');
fclose (fid);

%Smooth matrix
for i=1:68;
    Valm(:,i)=smooth(Valm(:,i),3);
end

%Specify boundary vector
%Fit to a quadratic equation

YY=mean(Valm(71:76,:));
t=0:0.21:14.07;
z=polyfit(t,YY,2);
a1=z(1);
a2=z(2);
a3=z(3);

%Discard values of the pixel at the image center
Valm(1,:)=[];
```

Simulation of the evolution of the concentration profile

diffd.m

```
%% FEMLAB Model M-file
% Generated by FEMLAB 3.1 (FEMLAB 3.1.0.157, $Date: 2004/11/12 07:39:54
$)

%This program simulates the evolution of concentration profile given
%the initial condition and initial guesses of the diffusivity and
%photobleaching rate constant. Hence it is a two-parameter fit program.

Csim = diffd(D0F)

%Define Valm as a global variable

global Valm
flclear fem

%Define diffusivity and rate constant as elements of the variable, DOF
 D0=D0F(1);
 frac=D0F(2);

% Femlab version
clear vrsn
vrsn.name = 'FEMLAB 3.1';
vrsn.ext = '';
vrsn.major = 0;
vrsn.build = 157;
vrsn.rcs = '$Name:  $';
vrsn.date = '$Date: 2004/11/12 07:39:54 $';
fem.version = vrsn;

%Define geometry of object
g1=solid1([0,63.9]);
clear s
s.objs={g1};
s.name={'I1'};
s.tags={'g1'};

fem.draw=struct('s',s);
fem.geom=geomcsg(fem);

%Initialize mesh, define mesh size
fem.mesh=meshinit(fem, ...
                  'hmax',[0.9]);

%Expressions
fem.equ.expr={'frac', D0F(2)};

% Application mode 1
clear appl
appl.mode.class = 'FlDiffusion';
```

```
appl.mode.type = 'axi';
appl.shape = {'shlag(1,''c'')'};
appl.gporder = 2;
appl.cporder = 1;
appl.assignsuffix = '_di';
clear bnd
bnd.c0 = {0,'bb(t)'};
bnd.type = {'N0','C'};
bnd.ind = [1,2];
appl.bnd = bnd;
clear equ
equ.init = 'interpol(r)';
equ.D = D0;
equ.R = {'-frac*c'};
equ.ind = [1];
appl.equ = equ;
fem.appl{1} = appl;
fem.sdim = {'r'};
fem.border = 1;
fem.outform = 'general';


% Specify functions for initial boundary conditions
clear fcns
fcns{1}.type='interp';
fcns{1}.name='interpol';
fcns{1}.method='linear';
fcns{1}.filename='300test.txt';
fcns{2}.type='interp';
fcns{2}.name='bb';
fcns{2}.method='linear';
fcns{2}.extmethod='extrap';
fcns{2}.filename='B1.txt';
fem.functions = fcns;

% Multiphysics
fem=multiphysics(fem);

% Extend mesh
fem.xmesh=meshextend(fem);

% Solve problem
fem.sol=femtime(fem, ...
                'solcomp',{'c'}, ...
                'outcomp',{'c'}, ...
                'tlist',[0:0.28:59*0.28], ...
                'tout','tlist');

% Save current fem structure for restart purposes
fem0=fem;

% Extract solution (simulated matrix)

  C=fem.sol.u;
  C=C(:,1:60);
```

```
J=C;
I=ones(72,60);
I(1,:)=J(1,:);
I(72,:)=J(2,:);
for i=3:72
    I(i-1,:)=J(i,:);
end
Csim=I;
Csim=Csim(2:72,:);
```

Objective function Calculation for the DDSPE method

differ.m

```
%This program calculates the objective function i.e. the difference
%between the simulated matrix, Csim, and the experimental matrix, Valm.

function [Err1] = differr(D0F);

%Define global variable
global Valm

%To evaluate the simulated matrix
Csim = diffd(D0F);

%Compute least squares error
Err=(Valm-Csim).^2;
Err1=(sum(sum(Err)));
```

Diffusion Coefficient Calculation for the DDSPE method

finalD.m

```
%This program solves for the best fit diffusion coefficient (D0) and
%photobleaching rate constant (frac).

function [newD] = finalD(D0F)

%Define Valm as a global variable
global Valm

%Start saving screen output
diary on
diary('filename');

%Initial guess of D0 and frac;
D0F=[50,0.003];
D0=D0F(1);
frac=D0F(2);

%set lower and upper bounds on D0 and frac
lb=[10,0];
ub=[200,0.01];

%Specify options for the minimization function, fmincon
options=optimset('display','iter','MaxFunEvals',[100000000]);

%Estimate D0 and frac by minimizing objective function
[newD] =fmincon(@differr,D0F,[],[],[],[],lb,ub,[],options);
save('D(3)2%B2e', 'newD', '-ascii');
diary off
```

Calculation of fractional intensity for Axelrod model

exptinteaxelrod.m

```
%This program calculates the fractional fluorescence recovery curve for
%the bleached spot based on the Axelrod model.
%It integrates the fluorescence intensities within the spot and
%normalizes to the pre-bleach intensity

%Specify global variables, Valm and f.
global Valm
global f

%Define radius of bleached spot and integration interval (distance)
R="radius of bleached spot";
dr=integration interval;

%Specify times
t=0:0.28:59*0.28;
t=t';

%Define boundary concentration and initial condition
B=mean(Valm(66:71,1));
Y=Valm(:,1);

%Find length of effective radius vector
r=0.9:0.9:R;
[c]=length(r);

%Specify intensity values to be integrated
Valm2=Valm(1:c,:);

%Calculate the integrated fluorescence intensity over time for the
%bleached spot
for i=1:c;
    for j=1:60;
V(i,j)=(i-1/2)*Valm2(i,j)*dr;
end
end
%Calculate the integrated pre-bleach fluorescence intensity for the
%spot
for i=1:c;
   Vf(i,1)=(i)*M(i,1)*dr;
end
Iavg=(trapz(r,V))/(R^2/2);
Ifin=(trapz(r,Vf))/(R^2/2);

%Calculate fractional fluorescence by normalizing to pre-bleach
%integrated fluorescence
for i=1:60;
    f(i)=(Iavg(i)-Iavg(1))/(Ifin-Iavg(1));

end
f=f';
```

Calculation of experimental fractional intensity for modified Axelrod model

exptintemodaxelrod.m

```
%This program calculates the fractional fluorescence recovery curve for
%the bleached spot based on the modified Axelrod model.
%It integrates the fluorescence intensities within the defined
%effective radius and normalizes to the pre-bleach intensity

%Specify global variables, Valm and f.
global Valm
global f

%Define radius of bleached spot and integration interval (distance)
R=”radius of bleached spot”;
dr=integration interval;

%Specify times
t=0:0.28:59*0.28;
t=t';

%Define boundary concentration and initial condition
B=mean(Valm(66:71,1));
Y=Valm(:,1);


%Find radius at which the bleaching depth falls to e^-2 times the maximum
%bleaching depth at the spot center
Y=B-Y;
k=0.13*Y(1);
ind=find(Y<k);
l=ind(1);
m=Y(l-1);
n=l+((k-Y(l))/(Y(l)-m));
N=n*dr;

%Find length of effective radius vector
r=0.9:0.9:N;
[c]=length(r);

%Specify intensity values to be integrated
Valm2=Valm(1:c,:);

%Calculate the integrated fluorescence intensity over time for the
%bleached spot
for i=1:c;
    for j=1:60;
V(i,j)=(i-1/2)*Valm2(i,j)*dr;
end
end
for i=1:c;
   Vf(i,1)=(i)*M(i,1)*dr;
end
Iavg=(trapz(r,V))/(N^2/2);
Ifin=(trapz(r,Vf))/(N^2/2);
```

```
%Calculate fractional fluorescence by normalizing to pre-bleach
%integrated fluorescence
for i=1:60;
    f(i)=(Iavg(i)-Iavg(1))/(Ifin-Iavg(1));

end
f=f';
```

Calculation of theoretical fractional fluorescence for Axelrod and modified Axelrod models

fracfl.m

```
%This program calculates the theoretical fractional fluorescence for
%both Axelrod and modified Axelrod models

function ft = fracfl(tau);

% Define global variables
global f
global Valm

% Calculate fractional fluorescence
i=0;
for t=0:0.5:50;
    if t==0;
        ft(i+1,1)=0;
    else ft(i+1,1) = exp(-
2*tau./t).*[BESSELI(0,2*tau./t)+BESSELI(1,2*tau./t)];
    end
    i=i+1;
end
```

Calculation of objective function for Axelrod and modified Axelrod models

tauerr.m

```
%This program calculates the objective function (err) i.e. the
%difference between the theoretical and experimentally measured
%fractional fluorescence for the Axelrod and modified Axelrod models.
%The input 'tau' is iteratively adjusted to minimize the output 'err'.

function err = tauerr(tau);

%Define global variables
global f
global Valm

%Calls the program "fracfl.m" inorder to calculate theoretical
%fractional fluorescence
ft = fracfl(tau);

%Defines and calculates the objective function "err"
err=(ft-f).^2;
err=sqrt(sum(sum(err)));
```

Calculation of characteristic diffusion time for Axelrod and modified Axelrod models

fintau.m

```
%This program solves for the best fit characteristic diffusion time,
%tau, that yields a minimum value for the objective function

function tauD = fintau(tau);

%Define global variables
global f
global Valm

%Specify optimset parameters
options=optimset('display','iter','MaxFunEvals',[100000000],
'DiffMaxChange',[1e-3],'TolFun',[1e-1000]);

%Set lower and upper bounds for tau
vlb=0.0001;
vub=20;

%Solve for tau
[tauD] =fminbnd(@tauerr,vlb,vub,options);
```

Fitting initial concentration profile to a 2-D Gaussian (Endress model)

fxnG.m

```
%This program fits the initial post-bleach image field to a two-
%dimensional Gaussian curve.

function C = fxnG(GE)

%Define global variables
global V1
global dd
global S
global Kap
global newGE

%Define Gaussian curve parameters: amplitude (dd), radius at height e^-2
%of Gaussian (S), a measure of the bleaching depth (Kap);
dd=GE(1);
S=GE(2);
Kap=GE(3);

%Define the limit/radius of the region of interest
[uu,vv]=size(V1);
ww=(uu-1)*0.7;

%Fit the initial concentration profile to a 2-D Gaussian curve
i=1;
for xx=-ww/2:0.7:ww/2;
j=1;
for yy=-ww/2:0.7:ww/2;
    if sqrt((xx^2)+(yy^2))<=ww/2
C(i,j)=dd*((1-(Kap*exp(-2*((xx)^2+(yy)^2)/(S^2)))));
    else
    end
j=j+1;
end
i=i+1;
end
```

Calculation of the difference between the theoretical and experimental initial concentration profiles (Endress model)

Gerr.m

```
%This program calculates the difference between the theoretical initial
%concentration profile (2-D Gaussian) and the experimentally measured
%initial concentration matrix

function err = Gerr(GE);

%Define global variables
global V1
global dd
global S
global Kap
global newGE

%Calls the function 'fxnG'
C = fxnG(GE);

%Calculate the difference between the theoretical and experimental
%matrices
err=(C-V1).^2;
err=sqrt(sum(sum(err)));
```

Calculation of the 2-D Gaussian curve parameters

finGE.m

```
%This program iteratively solves for the parameters that best describe
%the two-%dimensional Gaussian distribution of the initial
%concentration field

function newGE = finGE(GE);

%Define global variables
global V1
global dd
global S
global Kap
global newGE

%initial guess of Gaussian parameters
GE=[10,0.5,1];
dd=GE(1);
S=GE(2);
Kap=GE(3);

%Specify optimset parameters
options=optimset('display','iter','MaxFunEvals',[100000000],
'DiffMaxChange',[1e-3],'TolFun',[1e-1000]);

%Set lower and upper bounds
vlb=[1,1,0];
vub=[200,200,40];

%Estimate 2-D Gaussian parameters by minimizing the objective function
[newGE] = fmincon(@Gerr,GE,[],[],[],[],vlb,vub,[],options);
```

Calculation of experimental fractional fluorescence for the Endress model

exptintendress.m

```
%This program calculates the fractional fluorescence recovery curve for
%the bleached spot based on the Endress model.
%It integrates the fluorescence intensities within a specified Gaussian
%radius and normalizes to the pre-bleach intensity


%Define global variables
global Valm
global V1
global S
global MM
global f
global KK
global Kap
global b
global w
global Rg

%Specify size of region of interest, integration intervals and times
[u,v]=size(V1);
w=(u-1)*0.7;
dx=0.7;
dy=0.7;
dt =0.05;
t=0:0.05:2;

%Calculate length of radius vector
Rg=S;
cc=(-Rg:0.7:Rg);
[c]=length(cc);

%Specify the intensity values of the area to be integrated
Valm2=Valm(round((u+2-c)/2):round((u+c)/2),round((u+2-
c)/2):round((u+c)/2),:);
MMM=MM(round((u+2-c)/2):round((u+c)/2),round((u+2-
c)/2):round((u+c)/2));

%Calculate the integrated fluorescence intensity of the specified area
for i=1:c;
    for j=1:c;
        for k=1:41
V(i,j,k)=Valm2(i,j,k)*dx*dy;
end
    end
end
for i=1:c;
    for j=1:c;
   Vf(i,j)=MMM(i,j)*dx*dy;
    end
end
```

```
%Calculate fractional fluorescence
Iavg=0.7*trapz(0.7*trapz(V))/(Rg^2);
Ifin=0.7*trapz(0.7*trapz(Vf))/(Rg^2);
for i=1:41;
    f(i)=(Iavg(i))/(Ifin);

end
f=f';

%Calculate bleaching depth parameter
KK=-log(1-(2/(1-exp(-2)))*((Ifin-Iavg(1))/Ifin));
```

Calculation of theoretical fractional fluorescence for the Endress model

fracfl2.m

```
%This program calculates the theoretical fraction fluorescence within
%the specified radius based on the Endress model

function ft = fracfl2(D);

%Define global variables
global f
global Valm
global Rg
global KK
global b

%Calculate theoretical fractional fluorescence
 i=0;
for t=0:0.05:2;
  ft(i+1,1) = exp(-b*t)*(((1-exp(-KK)))*(exp(-
(2*Rg^2)./((Rg^2)+8*D*t))-1)+2)*(0.5);
    i=i+1;
end
```

Calculation of the objective function for the estimation of diffusivity (Endress model)

Derr2.m

```
%This program calculates the objective function which is the difference
%between the theoretical and experimentally measured fractional
%fluorescence

function err = Derr2(D);

%Define global variables
global f
global Valm
global Rg
global KK
global b

%Call the function "fracfl2"
ft = fracfl2(D);


%Calculate the difference between the theoretical and experimental
%fractional fluorescence (objective function)
err=(ft-f).^2;
err=sqrt(sum(sum(err)));
```

Estimation of the diffusion coefficient for the Endress model

finD2.m

```
%This program iteratively solves for the diffusion coefficient by
%minimizing the %difference between the experimental and theoretical
%fractional intensity curves

function D = finD2(D);

%Define global variables
global f
global Valm
global Rg
global KK
global b

%Specify optimset parameters
options=optimset('display','iter','MaxFunEvals',[100000000],
'DiffMaxChange',[1e-3],'TolFun',[1e-1000]);

%Specify lower and upper bounds
vlb=0.0001;
vub=500;

%Estimate diffusion coefficient using minimization function
[D] =fminbnd(@Derr2,vlb,vub,options);
```

Conversion of FRAP images to intensity matrices (1D axisymmetric model used for tissue samples)

readimg1D.m

```
function [Valm]=readimg1D;
global Valm
dt=0.494;
nbins=73;

%Read images and determine center of image, rad
for i = 0:67;
    X8 = imread(['tr4b' num2str(i,'%03i') '.tif']);
    M=size(X8,1);
    rad = M/2 + (mod(M,2)-1)/2;
    dr = rad/nbins;

[xx, yy] = meshgrid(-rad:rad,rad:-1:-rad);
R = sqrt(xx.^2 + yy.^2);

for k = 0:(nbins-1);
    indices{k+1} = find( (R > (k*dr)) .* (R < ((k+1)*dr)) );
end

indices{1} = [indices{1} find(R == 0)];
for k=1:length(indices);
    E(k)=mean(X8(indices{k}));
end
Valm(:,i+1)=E;
end
X2=linspace(0,256*.29,73);
t=0:0.494:67*0.494;
Y=Valm(:,1);
Y=smooth(Y,3);
fid=fopen('init.txt','wt');
fprintf(fid, '%%Grid\n');
fprintf(fid,'%6.2f\t',X2);
fprintf(fid,'\n%%Data\n');
fprintf(fid,'%6.2f\t',Y');
fclose (fid);
for i=1:68;
    Valm(:,i)=smooth(Valm(:,i),3);
end
Inx2=Valm(73,:);
fid=fopen('bb.txt','wt');
fprintf(fid, '%%Grid\n');
fprintf(fid,'%6.2f\t',t);
fprintf(fid,'\n%%Data\n');
fprintf(fid,'%6.2f\t',Inx2');
fclose (fid);
Valm(1,:)=[];
```

Conversion of FRAP images to intensity matrices (2D model used for tissue samples)

readimg.m

```
function [Valm]=readimg(r,x,y);
global Valm
global Xi
global Yi
dt=0.494;
r=255;
x=256;
y=256;

%Read the images
for i = 0:67;
    X8 = imread(['tr6b' num2str(i,'%03i') '.tif']);
    E2(1:2*r+1,1:2*r+1)=X8(y-r:y+r,x-r:x+r);

[m,n]=size(E2);
k=1;

%Downsize the image
for ii=1:7:m-6;
  l=1;
  for jj=1:7:n-6;
        E3(k,l)=((mean2(E2(ii:ii+6,jj:jj+6))));

  l=l+1;
  end
 k=k+1;

end
Valm(:,:,i+1)=E3;
end

%Specify initial and boundary conditions
Xi=0:2.03:146.16;
Yi=0:2.03:146.16;
t=0:0.494:67*0.494;
In(:,:,:)=Valm(:,:,1);
Inx1(:,:)=Valm(1,:,:);
Inx2(:,:)=Valm(73,:,:);
Iny1(:,:)=Valm(:,1,:);
Iny2(:,:)=Valm(:,73,:);
fid=fopen('A1.txt', 'wt');
fprintf(fid,'%%Grid\n');
fprintf(fid,'%6.2f\t',Xi);
fprintf(fid,'\n');
fprintf(fid,'%6.2f\t',Yi);
fprintf(fid,'\n%%Data\n');
fprintf(fid,'%6.2f\t',In);
fclose(fid);
fid=fopen('A2.txt', 'wt');
fprintf(fid,'%%Grid\n');
```

```
fprintf(fid,'%6.2f\t',Yi);
fprintf(fid,'\n');
fprintf(fid,'%6.2f\t',t);
fprintf(fid,'\n%%Data\n');
fprintf(fid,'%6.2f\t',Inx1);
fclose(fid);
fid=fopen('A3.txt', 'wt');
fprintf(fid,'%%Grid\n');
fprintf(fid,'%6.2f\t',Yi);
fprintf(fid,'\n');
fprintf(fid,'%6.2f\t',t);
fprintf(fid,'\n%%Data\n');
fprintf(fid,'%6.2f\t',Inx2);
fclose(fid);
fid=fopen('A4.txt', 'wt');
fprintf(fid,'%%Grid\n');
fprintf(fid,'%6.2f\t',Xi);
fprintf(fid,'\n');
fprintf(fid,'%6.2f\t',t);
fprintf(fid,'\n%%Data\n');
fprintf(fid,'%6.2f\t',Iny1);
fclose(fid);
fid=fopen('A5.txt', 'wt');
fprintf(fid,'%%Grid\n');
fprintf(fid,'%6.2f\t',Xi);
fprintf(fid,'\n');
fprintf(fid,'%6.2f\t',t);
fprintf(fid,'\n%%Data\n');
fprintf(fid,'%6.2f\t',Iny2);
fclose(fid);
```

Calculation of the simulated concentration profile

diffd2.m

```
function Csim = diffd2(D0F)
global Valm
global Xi
global Yi
flclear fem
D0=D0F(1);
frac=D0F(2);


% COMSOL version
clear vrsn
vrsn.name = 'COMSOL 3.2';
vrsn.ext = '';
vrsn.major = 0;
vrsn.build = 222;
vrsn.rcs = '$Name:  $';
vrsn.date = '$Date: 2005/09/01 18:02:30 $';
fem.version = vrsn;

% Geometry
g1=square2('146.16','base','corner','pos',{'0','0'},'rot','0');
clear s
s.objs={g1};
s.name={'SQ1'};
s.tags={'g1'};

fem.draw=struct('s',s);
fem.geom=geomcsg(fem);

% Create mapped quad mesh
fem.mesh=meshmap(fem, ...
                 'edgegroups',{{[2],[4],[3],[1]}}, ...
                 'edgelem',{1,[72],2,[72],3,[72],4,[72]});


% (Default values are not included)
%expressions
fem.equ.expr={'frac', D0F(2)};

% Application mode 1
clear appl
appl.mode.class = 'FlDiffusion';
appl.assignsuffix = '_di';
clear bnd
bnd.type = 'C';
bnd.c0 = {'bb4(y,t)','bb1(y,t)','bb2(x,t)','bb3(x,t)'};
bnd.ind = [2,3,4,1];
appl.bnd = bnd;
clear equ
equ.D = D0;
```

```
equ.init = 'In(x,y)';
equ.R = '-frac*c';
%equ.R=0;
equ.ind = [1];
appl.equ = equ;
fem.appl{1} = appl;
fem.border = 1;
fem.outform = 'general';
fem.units = 'SI';

% Functions
clear fcns
fcns{1}.type='interp';
fcns{1}.name='In';
fcns{1}.method='linear';
fcns{1}.extmethod='extrap';
fcns{1}.filename='A1.txt';
fcns{2}.type='interp';
fcns{2}.name='bb1';
fcns{2}.method='linear';
fcns{2}.extmethod='extrap';
fcns{2}.filename='A2.txt';
fcns{3}.type='interp';
fcns{3}.name='bb2';
fcns{3}.method='linear';
fcns{3}.extmethod='extrap';
fcns{3}.filename='A4.txt';
fcns{4}.type='interp';
fcns{4}.name='bb3';
fcns{4}.method='linear';
fcns{4}.extmethod='extrap';
fcns{4}.filename='A5.txt';
fcns{5}.type='interp';
fcns{5}.name='bb4';
fcns{5}.method='linear';
fcns{5}.extmethod='extrap';
fcns{5}.filename='A3.txt';
fem.functions = fcns;

% Multiphysics
fem=multiphysics(fem);

% Extend mesh
fem.xmesh=meshextend(fem);

% Solve problem
fem.sol=femtime(fem, ...
                'solcomp',{'c'}, ...
                'outcomp',{'c'}, ...
                'tlist',[0:0.494:67*0.494], ...
                'tout','tlist');

% Save current fem structure for restart purposes
fem0=fem;
```

```
% Extract solution
x=0:2.03:146.16;
y=0:2.03:146.16;
[x,y]=meshgrid(x,y);
XX=[x(:),y(:)]';
W = postinterp(fem,'c',XX,'solnum',1:68);
W=W';
for i=1:68;
CCC(:,:,i) = reshape(W(:,i), size(x));
i=i+1;
end
for i=1:68;
Csim(:,:,i)=[CCC(:,:,i)]';
i=i+1;
end
```

Calculation of Objective function for 2D DDSPE model

Differ.m

```
%This program calculates the objective i.e. the difference between the
%simulated and experimental concentration profiles

function [Err2] = differr(D0F);
global Valm
global Xi
global Yi
[m,n,o]=size(Valm);

%Call the diffd2 function which produces the simulated concentration
%profile
Csim = diffd2(D0F);

%Need to apply a weight to the objective function to hasten convergence
and to minimize %the contribution of points farthest away from the
%center of the image
%Determine the center of the image field
Xc=(Xi(1)+Xi(m))/2;
Yc=(Yi(1)+Yi(n))/2;
for i=1:m
 for j=1:n
    r=((Xi(i)-Xc)^2+(Yi(j)-Yc)^2)^(1/2);
    if (r>0)
       w(i,j)=1./r^2;
    else
        w(i,j)=2;
    end
    end
    end

%Calculate the least square error
Err=(Valm-Csim).^2;
for i=1:o
Err1(:,:,i)=w.*Err(:,:,i);
  i=i+1;
 end
Err2=sum(sum(sum(Err1)));
```

Estimation of diffusion coefficient for the 2D DDSPE model

finalD.m

```
%This program solve for the best fit diffusivity (D0) and
%photobleaching rate constant (frac) by iteratively adjusting their
%values using a MATLAB minimization function

function [newD] = finalD(D0F)
global Valm
global Xi
global Yi
diary on
diary('tr6b');
%Specify an initial guess for D0 and frac
D0F=[10,0.0003];
D0=D0F(1);
frac=D0F(2);

%Define lower and upper bounds on D0 and frac
lb=[1e-20,0];
ub=[100,0.1];

%Specify optimset parameters
option=optimset('display','iter','MaxFunEvals',[100000000]);

%Estimate D0 and frac by iteratively adjusting their values using the
%minimization function, fmincon
[newD] =fmincon(@differr,D0F,[],[],[],[],lb,ub,[],option);
save('Dtr6b', 'newD', '-ascii');
diary off
```

APPENDIX B

B.1 HISTOGRAM OF NORMALIZED LEAST SQUARE ERRORS FOR 1-D DDSPE METHOD

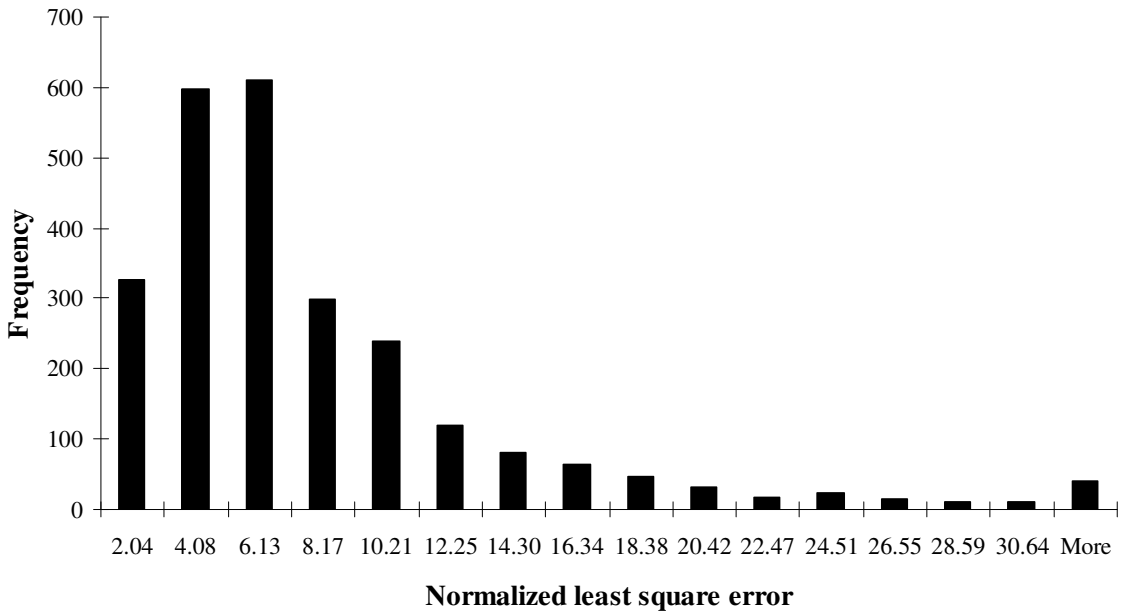

Figure 43: Histogram of the normalized least square error values obtained during from the analyses of the FRAP experimental data using the 1D-DDSPE method. The normalized least square error was obtained by the dividing the value of the objective function (ϕ) with the total number of elements within the matrix (either experimental or simulated). Diffusivity estimates with values greater than 20.42 were discarded.

REFERENCES

1. Buckwalter, J. A., and J. A. Martin. 2006. Osteoarthritis. Advanced drug delivery reviews 58:150-167.

2. Buckwalter, J. A., and D. R. Lappin. 2000. The disproportionate impact of chronic arthralgia and arthritis among women. Clin Orthop Relat Res:159-168.

3. Jacobs, J. J., N. J. Hallab, R. M. Urban, and M. A. Wimmer. 2006. Wear particles. J Bone Joint Surg Am 88 Suppl 2:99-102.

4. Gerwin, N., C. Hops, and A. Lucke. 2006. Intraarticular drug delivery in osteoarthritis. Adv Drug Deliv Rev 58:226-242.

5. Klein, T. J., M. Chaudhry, W. C. Bae, and R. L. Sah. 2007. Depth-dependent biomechanical and biochemical properties of fetal, newborn, and tissue-engineered articular cartilage. J Biomech 40:182-190.

6. Keren Keinan-Adamsky, H. S. G. N. 2006. Multinuclear NMR and MRI studies of the maturation of pig articular cartilage. 532-540.

7. Shinar, H., and G. Navon. 2006. Multinuclear NMR and microscopic MRI studies of the articular cartilage nanostructure. NMR Biomed 19:877-893.

8. Setton, L. A., W. Zhu, and V. C. Mow. 1993. The biphasic poroviscoelastic behavior of articular cartilage: role of the surface zone in governing the compressive behavior. J Biomech 26:581-592.

9. Mow, V. C. a. R., A. 1997. Structure and Function of Articular Cartilage and Meniscus. In Basic Orthopedic Biomechanics. Lippincott-Raven Publishers, Philadelphia. 113-177.

10. Poole, A. R., T. Kojima, T. Yasuda, F. Mwale, M. Kobayashi, and S. Laverty. 2001. Composition and structure of articular cartilage: a template for tissue repair. Clin Orthop Relat Res:S26-33.

11. Speight, G., C. J. Handley, and D. A. Lowther. 1978. Extracellular matrix metabolism by chondrocytes. 4. Role of glutamine in glycosaminoglycan synthesis in vitro by chondrocytes. Biochim Biophys Acta 540:238-245.

12. Dimicco, M. A., J. D. Kisiday, H. Gong, and A. J. Grodzinsky. 2007. Structure of pericellular matrix around agarose-embedded chondrocytes. Osteoarthritis Cartilage.

13. Alexopoulos, L. G., L. A. Setton, and F. Guilak. 2005. The biomechanical role of the chondrocyte pericellular matrix in articular cartilage. Acta Biomater 1:317-325.

14. Verkman, A. S. 2003. Diffusion in cells measured by fluorescence recovery after photobleaching. Methods Enzymol 360:635-648.

15. Chahine, N. O., C. T. Hung, and G. A. Ateshian. 2007. In-situ measurements of chondrocyte deformation under transient loading. Eur Cell Mater 13:100-111; discussion 111.

16. Cohen, N. P., R. J. Foster, and V. C. Mow. 1998. Composition and dynamics of articular cartilage: structure, function, and maintaining healthy state. J Orthop Sports Phys Ther 28:203-215.

17. McGowan, K. B., and R. L. Sah. 2005. Treatment of cartilage with beta-aminopropionitrile accelerates subsequent collagen maturation and modulates integrative repair. J Orthop Res 23:594-601.

18. Xia, Y., J. B. Moody, N. Burton-Wurster, and G. Lust. 2001. Quantitative in situ correlation between microscopic MRI and polarized light microscopy studies of articular cartilage. Osteoarthritis Cartilage 9:393-406.

19. Muir, H., P. Bullough, and A. Maroudas. 1970. The distribution of collagen in human articular cartilage with some of its physiological implications. J Bone Joint Surg Br 52:554-563.

20. Volpi, M., and E. P. Katz. 1991. On the adaptive structures of the collagen fibrils of bone and cartilage. J Biomech 24 Suppl 1:67-77.

21. Maroudas, A. 1970. Distribution and diffusion of solutes in articular cartilage. Biophys J 10:365-379.

22. Mow, V. C., and X. E. Guo. 2002. Mechano-electrochemical properties of articular cartilage: their inhomogeneities and anisotropies. Annu Rev Biomed Eng 4:175-209.

23. Maroudas, A. 1975. Biophysical chemistry of cartilaginous tissues with special reference to solute and fluid transport. Biorheology 12:233-248.

24. Von den Hoff, H. W., G. P. van Kampen, and J. K. van der Korst. 1993. Proteoglycan depletion of intact articular cartilage by retinoic acid is irreversible and involves loss of hyaluronate. Osteoarthritis Cartilage 1:157-166.

25. Silver, F. H., G. Bradica, and A. Tria. 2001. Relationship among biomechanical, biochemical, and cellular changes associated with osteoarthritis. Crit Rev Biomed Eng 29:373-391.

26. Holland, T. A., and A. G. Mikos. 2003. Advances in drug delivery for articular cartilage. J Control Release 86:1-14.

27. Rieppo, J., J. Toyras, M. T. Nieminen, V. Kovanen, M. M. Hyttinen, R. K. Korhonen, J. S. Jurvelin, and H. J. Helminen. 2003. Structure-function relationships in enzymatically modified articular cartilage. Cells Tissues Organs 175:121-132.

28. Bonassar, L. J., J. D. Sandy, M. W. Lark, A. H. Plaas, E. H. Frank, and A. J. Grodzinsky. 1997. Inhibition of cartilage degradation and changes in physical properties induced by IL-1beta and retinoic acid using matrix metalloproteinase inhibitors. Arch Biochem Biophys 344:404-412.

29. Aigner, T., J. Rose, J. Martin, and J. Buckwalter. 2004. Aging theories of primary osteoarthritis: from epidemiology to molecular biology. Rejuvenation Res 7:134-145.

30. Bank, R. A., M. T. Bayliss, F. P. Lafeber, A. Maroudas, and J. M. Tekoppele. 1998. Ageing and zonal variation in post-translational modification of collagen in normal human articular cartilage. The age-related increase in non-enzymatic glycation affects biomechanical properties of cartilage. Biochem J 330 (Pt 1):345-351.

31. L'Hermette, M. F., C. Tourny-Chollet, G. Polle, and F. H. Dujardin. 2006. Articular cartilage, degenerative process, and repair: current progress. International journal of sports medicine 27:738-744.

32. Carrington, J. L. 2005. Aging bone and cartilage: cross-cutting issues. Biochem Biophys Res Commun 328:700-708.

33. Bonassar, L. J., E. H. Frank, J. C. Murray, C. G. Paguio, V. L. Moore, M. W. Lark, J. D. Sandy, J. J. Wu, D. R. Eyre, and A. J. Grodzinsky. 1995. Changes in cartilage composition and physical properties due to stromelysin degradation. Arthritis Rheum 38:173-183.

34. Magnussen, R. A., F. Guilak, and T. P. Vail. 2005. Cartilage degeneration in post-collapse cases of osteonecrosis of the human femoral head: altered mechanical properties in tension, compression, and shear. J Orthop Res 23:576-583.

35. Meachim, G. 2001. Age changes in articular cartilage. 1969. Clin Orthop Relat Res:S6-13.

36. Martin, J. A., and J. A. Buckwalter. 2001. Roles of articular cartilage aging and chondrocyte senescence in the pathogenesis of osteoarthritis. The Iowa orthopaedic journal 21:1-7.

37. Lemperg, R. K., S. E. Larsson, and S. O. Hjertquist. 1971. Distribution of water and glycosaminoglycans in different layers of cattle articular cartilage. Isr J Med Sci 7:419-421.

38. Maroudas, A., and P. Bullough. 1968. Permeability of articular cartilage. Nature 219:1260-1261.

39. Roughley, P. J. 2001. Age-associated changes in cartilage matrix: implications for tissue repair. Clin Orthop Relat Res:S153-160.

40. Torzilli, P. A., J. M. Arduino, J. D. Gregory, and M. Bansal. 1997. Effect of proteoglycan removal on solute mobility in articular cartilage. J Biomech 30:895-902.

41. Uesugi, M., and H. E. Jasin. 2000. Macromolecular transport across the superficial layer of articular cartilage. Osteoarthritis Cartilage 8:13-16.

42. Swabb, E. A., J. Wei, and P. M. Gullino. 1974. Diffusion and convection in normal and neoplastic tissues. Cancer research 34:2814-2822.

43. Nimer, E., R. Schneiderman, and A. Maroudas. 2003. Diffusion and partition of solutes in cartilage under static load. Biophys Chem 106:125-146.

44. Leddy, H. A., and F. Guilak. 2003. Site-specific molecular diffusion in articular cartilage measured using fluorescence recovery after photobleaching. Ann Biomed Eng 31:753-760.

45. Aigner, T., and N. Gerwin. 2006. Drug delivery in degenerative joint disease. Advanced drug delivery reviews 58:123-124.

46. Foy, B. D., and J. Blake. 2001. Diffusion of paramagnetically labeled proteins in cartilage: enhancement of the 1-D NMR imaging technique. J Magn Reson 148:126-134.

47. Garcia, A. M., E. H. Frank, P. E. Grimshaw, and A. J. Grodzinsky. 1996. Contributions of fluid convection and electrical migration to transport in cartilage: relevance to loading. Arch Biochem Biophys 333:317-325.

48. Quinn, T. M., V. Morel, and J. J. Meister. 2001. Static compression of articular cartilage can reduce solute diffusivity and partitioning: implications for the chondrocyte biological response. J Biomech 34:1463-1469.

49. Bonassar, L. J., A. J. Grodzinsky, E. H. Frank, S. G. Davila, N. R. Bhaktav, and S. B. Trippel. 2001. The effect of dynamic compression on the response of articular cartilage to insulin-like growth factor-I. J Orthop Res 19:11-17.

50. Torzilli, P. A. 1993. Effects of temperature, concentration and articular surface removal on transient solute diffusion in articular cartilage. Medical & biological engineering & computing 31 Suppl:S93-98.

51. Fischer, A. E., T. A. Carpenter, J. A. Tyler, and L. D. Hall. 1995. Visualisation of mass transport of small organic molecules and metal ions through articular cartilage by magnetic resonance imaging. Magn Reson Imaging 13:819-826.

52. Nguyen-minh, C., L. Riley, 3rd, K. C. Ho, R. Xu, H. An, and V. M. Haughton. 1997. Effect of degeneration of the intervertebral disk on the process of diffusion. Am. J Neuroradiol 18:435-442.

53. Roberts, S., J. P. Urban, H. Evans, and S. M. Eisenstein. 1996. Transport properties of the human cartilage endplate in relation to its composition and calcification. Spine 21:415-420.

54. Meyvis, T. K., S. C. De Smedt, P. Van Oostveldt, and J. Demeester. 1999. Fluorescence recovery after photobleaching: a versatile tool for mobility and interaction measurements in pharmaceutical research. Pharm Res 16:1153-1162.

55. Braeckmans, K., L. Peeters, N. N. Sanders, S. C. De Smedt, and J. Demeester. 2003. Three-dimensional fluorescence recovery after photobleaching with the confocal scanning laser microscope. Biophys J 85:2240-2252.

56. Weiss, M. 2004. Challenges and artifacts in quantitative photobleaching experiments. Traffic 5:662-671.

57. Pluen, A., P. A. Netti, R. K. Jain, and D. A. Berk. 1999. Diffusion of macromolecules in agarose gels: comparison of linear and globular configurations. Biophys J 77:542-552.

58. Axelrod, D., D. E. Koppel, J. Schlessinger, E. Elson, and W. W. Webb. 1976. Mobility measurement by analysis of fluorescence photobleaching recovery kinetics. Biophys J 16:1055-1069.

59. Soumpasis, D. M. 1983. Theoretical analysis of fluorescence photobleaching recovery experiments. Biophys J 41:95-97.

60. Lardner, T. J. 1977. The measurement of cell membrane diffusion coefficients. J Biomech 10:167-170.

61. Teissie, J., J. F. Tocanne, and A. Baudras. 1978. A fluorescence approach of the determination of translational diffusion coefficients of lipids in phospholipid monolayer at the air-water interface. Eur J Biochem 83:77-85.

62. Endress E, W. S., Reents G, Bayerl TM. 2005. Derivation of a closed form analytical expression for fluorescence recovery after photo bleaching in the case of continuous bleaching during read out. Eur Phys J E Soft Matter 16:81-87.

63. Lopez, A., L. Dupou, A. Altibelli, J. Trotard, and J. F. Tocanne. 1988. Fluorescence recovery after photobleaching (FRAP) experiments under conditions of uniform disk illumination. Critical comparison of analytical solutions, and a new mathematical method for calculation of diffusion coefficient D. Biophys J 53:963-970.

64. Kubitscheck, U., P. Wedekind, and R. Peters. 1994. Lateral diffusion measurement at high spatial resolution by scanning microphotolysis in a confocal microscope. Biophys J 67:948-956.

65. Sniekers, Y. H., and C. C. van Donkelaar. 2005. Determining diffusion coefficients in inhomogeneous tissues using fluorescence recovery after photobleaching. Biophys J 89:1302-1307.

66. Gu, W. Y., H. Yao, A. L. Vega, and D. Flagler. 2004. Diffusivity of ions in agarose gels and intervertebral disc: effect of porosity. Ann Biomed Eng 32:1710-1717.

67. Bert, J. L., R. H. Pearce, J. M. Mathieson, and S. J. Warner. 1980. Characterization of collagenous meshworks by volume exclusion of dextrans. Biochem J 191:761-768.

68. Armstrong, J. K., R. B. Wenby, H. J. Meiselman, and T. C. Fisher. 2004. The hydrodynamic radii of macromolecules and their effect on red blood cell aggregation. Biophys J 87:4259-4270.

69. Gu, W. Y., H. Yao, C. Y. Huang, and H. S. Cheung. 2003. New insight into deformation-dependent hydraulic permeability of gels and cartilage, and dynamic behavior of agarose gels in confined compression. J Biomech 36:593-598.

70. Venn, M. F. 1978. Variation of chemical composition with age in human femoral head cartilage. Ann Rheum Dis 37:168-174.

71. Korhonen, R. K., P. Julkunen, J. Rieppo, R. Lappalainen, Y. T. Konttinen, and J. S. Jurvelin. 2006. Collagen network of articular cartilage modulates fluid flow and mechanical stresses in chondrocyte. Biomech Model Mechanobiol 5:150-159.

72. Charlebois, M., M. D. McKee, and M. D. Buschmann. 2004. Nonlinear tensile properties of bovine articular cartilage and their variation with age and depth. J Biomech Eng 126:129-137.

73. Deng, X., M. Farley, M. T. Nieminen, M. Gray, and D. Burstein. 2007. Diffusion tensor imaging of native and degenerated human articular cartilage. Magn Reson Imaging 25:168-171.

74. Filidoro, L., O. Dietrich, J. Weber, E. Rauch, T. Oerther, M. Wick, M. F. Reiser, and C. Glaser. 2005. High-resolution diffusion tensor imaging of human patellar cartilage: feasibility and preliminary findings. Magn Reson Med 53:993-998.

75. Farndale, R. W., D. J. Buttle, and A. J. Barrett. 1986. Improved quantitation and discrimination of sulphated glycosaminoglycans by use of dimethylmethylene blue. Biochim Biophys Acta 883:173-177.

76. Cao, M., M. Stefanovic-Racic, H. I. Georgescu, L. A. Miller, and C. H. Evans. 1998. Generation of nitric oxide by lapine meniscal cells and its effect on matrix metabolism: stimulation of collagen production by arginine. J Orthop Res 16:104-111.

77. Brower, T. D., Y. Akahoshi and P. Orlic. 1962. The Diffusion of Dyes Through Articular Cartilage in Vivo. J Bone Joint Surg Am. 44:456-463.

78. Torzilli, P. A., D. A. Grande, and J. M. Arduino. 1998. Diffusive properties of immature articular cartilage. J Biomed Mater Res 40:132-138.

79. Xia, Y., T. Farquhar, N. Burton-Wurster, M. Vernier-Singer, G. Lust, and L. W. Jelinski. 1995. Self-diffusion monitors degraded cartilage. Arch Biochem Biophys 323:323-328.

80. Xia, Y., T. Farquhar, N. Burton-Wurster, E. Ray, and L. W. Jelinski. 1994. Diffusion and relaxation mapping of cartilage-bone plugs and excised disks using microscopic magnetic resonance imaging. Magn Reson Med 31:273-282.

81. Xia, Y. 2007. Averaged and Depth-Dependent Anisotropy of Articular Cartilage by Microscopic Imaging. Semin Arthritis Rheum (Article In Press).

82. Reynaud, B., and T. M. Quinn. 2006. Anisotropic hydraulic permeability in compressed articular cartilage. J Biomech 39:131-137.

83. Quinn, T. M., P. Dierickx, and A. J. Grodzinsky. 2001. Glycosaminoglycan network geometry may contribute to anisotropic hydraulic permeability in cartilage under compression. J Biomech 34:1483-1490.

84. Maroudas, A. 1976. Transport of solutes through cartilage: permeability to large molecules. J Anat 122:335-347.

85. Burstein, D., M. L. Gray, A. L. Hartman, R. Gipe, and B. D. Foy. 1993. Diffusion of small solutes in cartilage as measured by nuclear magnetic resonance (NMR) spectroscopy and imaging. J Orthop Res 11:465-478.

86. Jadin, K. D., B. L. Wong, W. C. Bae, K. W. Li, A. K. Williamson, B. L. Schumacher, J. H. Price, and R. L. Sah. 2005. Depth-varying density and organization of chondrocytes in immature and mature bovine articular cartilage assessed by 3d imaging and analysis. J Histochem Cytochem 53:1109-1119.

87. Owen, J. R., and J. S. Wayne. 2006. Influence of a superficial tangential zone over repairing cartilage defects: implications for tissue engineering. Biomech Model Mechanobiol 5:102-110.

88. Kumar, P., M. Oka, J. Toguchida, M. Kobayashi, E. Uchida, T. Nakamura, and K. Tanaka. 2001. Role of uppermost superficial surface layer of articular cartilage in the lubrication mechanism of joints. J Anat 199:241-250.

89. Stockwell, R. A., and C. H. Barnett. 1964. Changes in Permeability of Articular Cartilage with Age. Nature 201:835-836.

90. Wang, L., D. N. Kalu, J. Banu, J. B. Thomas, N. Gabriel, and K. Athanasiou. 2006. Effects of ageing on the biomechanical properties of rat articular cartilage. Proc Inst Mech Eng [H] 220:573-578.

91. Kaplan, D., and K. Meyer. 1959. Ageing of human cartilage. Nature 183:1267-1268.

92. Bayliss, M. T., and S. Y. Ali. 1978. Age-related changes in the composition and structure of human articular-cartilage proteoglycans. Biochem J 176:683-693.

93. Inerot, S., D. Heinegard, L. Audell, and S. E. Olsson. 1978. Articular-cartilage proteoglycans in aging and osteoarthritis. Biochem J 169:143-156.

94. Flessner, M. F. 2001. The role of extracellular matrix in transperitoneal transport of water and solutes. S24-29.

95. Maroudas, A., P. D. Weinberg, K. H. Parker, and C. P. Winlove. 1988. The distributions and diffusivities of small ions in chondroitin sulphate, hyaluronate and some proteoglycan solutions. Biophysical chemistry 32:257-270.

96. Parry, D. A., G. R. Barnes, and A. S. Craig. 1978. A comparison of the size distribution of collagen fibrils in connective tissues as a function of age and a

possible relation between fibril size distribution and mechanical properties. Proc R Soc Lond B Biol Sci 203:305-321.

97. Bhatnagar, R., R. G. Christian, T. Nakano, F. X. Aherne, and J. R. Thompson. 1981. Age related changes and osteochondrosis in swine articular and epiphyseal cartilage: light ane electron microscopy. Can J Comp Med 45:188-195.

98. Maroudas, A., Schneiderman, R. and Popper, O. 1992. The Role of Water, Proteoglycans, and Collagen in Solute Transport in Cartilage. In Articular Cartilage and Osteoarthritis. K. E. kuettner, Schleyerbach, R., Peyron, J. G. and Hascall, V. C., editor. Raven Press, New York. 355-369.

99. Hollander, A. P., I. Pidoux, A. Reiner, C. Rorabeck, R. Bourne, and A. R. Poole. 1995. Damage to type II collagen in aging and osteoarthritis starts at the articular surface, originates around chondrocytes, and extends into the cartilage with progressive degeneration. J Clin Invest 96:2859-2869.

100. Mosher, T. J., Y. Liu, Q. X. Yang, J. Yao, R. Smith, B. J. Dardzinski, and M. B. Smith. 2004. Age dependency of cartilage magnetic resonance imaging T2 relaxation times in asymptomatic women. Arthritis Rheum 50:2820-2828.

101. Dunn, T. C., Y. Lu, H. Jin, M. D. Ries, and S. Majumdar. 2004. T2 Relaxation Time of Cartilage at MR Imaging: Comparison with Severity of Knee Osteoarthritis. 592-598.

102. Alhadlaq, H. A., Y. Xia, J. B. Moody, and J. R. Matyas. 2004. Detecting structural changes in early experimental osteoarthritis of tibial cartilage by microscopic magnetic resonance imaging and polarised light microscopy. Annals of the rheumatic diseases 63:709-717.

103. Mosher, T. J., B. J. Dardzinski, and M. B. Smith. 2000. Human Articular Cartilage: Influence of Aging and Early Symptomatic Degeneration on the Spatial Variation of T2-Preliminary Findings at 3 T1. 259-266.

VITA

Onyi Irrechukwu was born on May 31 in Owerri, Nigeria. Her parents knew she was special from the day she was born as her name literally means “gift from God”. One could say that she was born with a silver spoon in her mouth because she was chauffeur-driven most of her life in Nigeria, had never taken public transportation and lived in rather large houses until she came to the States. Her parents always thought she was a rather silent child. In elementary and secondary schools, she excelled in both sciences and arts: she won first place in a National Essay competition and she represented her country in a Girls’ Science Workshop held in Ghana. She finished secondary school at the tender age of 16 and spent one year in medical school in Nigeria where she had all round A’s before coming to the States. The political changes in the country forced her entire family to immigrate to the US with almost nothing to their name. The girl who had everything did not have anything at all anymore. Not easily discouraged, she set out again in search of fame and fortune when she enrolled in the University of Maryland, Baltimore County. Working almost 40hours a week while enrolled full-time, she was able to graduate from the Chemical Engineering department with a Summa cum laude in May 2001. Actually she had only one B during her entire time at the school. She also was able to do 3 summer internships at McCormick & Co and was active in many student organizations. She surprised quite a few of her teachers as they did not expect that level of excellence from a little African girl. Her love for medicine drove her to pursue a Doctorate degree in Biomedical Engineering at Georgia Institute of Technology. Graduate school life left her little time to pursue some of her passions which included playing the piano and learning foreign languages (she is also an avid reader of historical

genre). During her tenure at Georgia Tech, her love for research and adventure propelled her to do a summer research internship at the University of Keele in England. However, after six years at Tech and a PhD in hand, she is off yet again to conquer hitherto untamed terrain for she is one that loves “the road less traveled”.